The lysosomotropic agent siramesine induces cell death in prostate cancer cells and synergizes with the tyrosine kinase inhibitor lapatinib

by

Ilsa Bhatti

A thesis submitted in partial fulfillment of the requirements for the degree of

Master of Science

in

Cancer Sciences

Department of Oncology
University of Alberta

Abstract

Prostate cancer is the most diagnosed cancer affecting Canadian men. Prostate tumors that progress from localized disease to advanced stages show resistance to standard therapy, a major problem that requires alternative treatments. One new treatment possibility is targeting lysosomal membrane disruption with lysosomotropic agents, leading to lysosome membrane permeabilization (LMP) and triggering pathways that result in cell death. Lysosomotropic agents can also be combined with other targeted agents to increase the efficacy of cell death induction in different types of cancer. Previous research has shown that the most effective lysosomotropic agent for inducing ROS generation, lysosome membrane permeabilization, and cell death in prostate cancer cell lines is siramesine which inhibits acidic sphingomyelinase. My results indicate that combining siramesine with lapatinib, a tyrosine kinase inhibitor for EGFR and HER2, synergistically increased prostate cancer cell death. This combination induced cell death to a greater extent in an aggressive castration-resistant prostate cell line compared to an androgen-sensitive prostate cancer cell line or non-malignant cell line. The synergistic increase in cell death with the combination treatment is mediated by increased ROS levels following lysosome membrane permeabilization but is independent of the actions of Cathepsin D released after LMP and caspase activation. The combination also failed to result in BID cleavage. Combining siramesine and lapatinib resulted in decreased expression of MCL-1, a BCL-2 family member, and increased cellular and mitochondrial ROS. Treating cells with the antioxidant alpha-tocopherol attenuated the cell death resulting from siramesine alone or the combination treatment, suggesting a role for ROS in the caspase-independent cell death. In other cancer cells, siramesine induces autophagy (self-eating). I found that siramesine and lapatinib caused

accumulation of the autophagic markers LC3-II and p62 and combining the combination treatment with chloroquine administration did not further increase expression indicating that siramesine and lapatinib fail to increase autophagic flux. This suggests the combination treatment inhibits autophagy and damage to the lysosome through siramesine prevents the progression of the autophagic pathway and subsequent degradation of the autophagic markers. These results indicate that combination treatments between lysosomotropic agents such as siramesine and targeted inhibitors such as the tyrosine kinase inhibitor lapatinib induce ROS driven cell death in prostate cancer cell lines, but that further work is needed to determine approved treatment options to target these pathways and provide an alternative treatment strategy in the management of drug resistant aggressive prostate cancers.

Preface

A portion of this research in Chapter 4 was used in the publication, E. Garcia, I. Bhatti, E. Henson, and S. Gibson, "Prostate Cancer Cells Are Sensitive to Lysosomotropic Agent Siramesine through Generation Reactive Oxygen Species and in Combination with Tyrosine Kinase Inhibitors," *Cancers*, vol. 14, issue 22, 5478. E. Garcia was responsible for the experimental design, data collection, and data analysis of the majority of experiments in the publication, except for those noted below. I was responsible for experimental design, data collection, and data analysis of the western blot experiment to determine PARP and caspase-3 cleavage in Figure 5 of the publication, the Trypan blue experiment to determine cell death with the siramesine lapatinib combination with α-tocopherol in Figure 8b, the MTS assay experiment to determine cell death in Supplemental Figure S1, the western blot experiment to determine MCL1 expression in Supplemental Figure S4, the microscopy experiment to determine lysosome disruption with Lysotracker Red in Supplemental Figure S6, the flow cytometry experiment to determine ROS expression in Supplemental Figure S7. E. Henson was responsible for experimental design, data collection, and data analysis of the flow cytometry experiments determining ROS and assisted in analyzing other data. S. Gibson was the research supervisor, and responsible for experimental design, data analysis, and manuscript writing. The remainder of the data collection and analysis in Chapter 4 is my own original work.

Acknowledgements

I would like to acknowledge the contributions of my funding sources, the NSERC CGS M scholarship, the Walter H Johns Graduate Fellowship, the Antoine Noujaim award, and the University Hospital Foundation for supporting my research.

Thank you to Dr. Spencer Gibson, my supervisor, for his guidance and understanding throughout my degree. Dr. Gibson has supported me greatly throughout my program, and I owe my current progress to the resources and insights he has provided. I appreciate every time he provided his expertise in planning experiments, clarified any questions I had, kept me motivated to experiment with and explore everything research has to offer, and patiently helped fill in the gaps of my knowledge on the project. Thank you for giving me the opportunity to learn and grow in the Gibson lab under your mentorship.

I would also like to express my appreciation for the members of my committee: Dr. Kristi Baker, Dr. Roseline Godbout, and Dr. Richard Fahlman. I thank them for giving me their time during our committee meetings. Their efforts in highlighting the gaps of my research, prompting me to think and respond critically, and pushing my work in the right direction are invaluable, and I will keep all the advice they provided in my mind throughout my career.

The members of the Gibson lab all have my appreciation for the great deal of assistance they have given me. Whether it be sharing their knowledge, having a meal together in the lunchroom, or chatting in the hallways or lab, I am grateful for them being by my side during my time in this program. I extend my deep gratitude to Yan Yang for being a brilliant mentor, role model, and someone I could always turn to.

Thank you to Dr. Xuejun Sun and Dr. Guobin Sun for their microscope training and assistance in microscopy-based experiments. Thank you as well to the members of the Flow Core facility at the University of Alberta. I would also like to thank Nathanael Lee for guiding me in creating scripts for analysis done with ImageJ on the microscopy experiments to validate cell counting.

I also greatly appreciate the work of Ronald Mariñas and Jen Freund for their help, and for responding to all my emails alongside my various inquiries and requests for them.

I would also like to thank my family for their unwavering support and encouragement, their love kept me going and gave me the drive to pursue my potential. Thank you to my friends for always being there for me during all the ups and downs, I could not ask to be surrounded by better people who I will always aspire to match up to. Finally, thank you to the members of HOLOSTARS for being stars that shine brightly to light my path forward.

Table of Contents

List of Tables

List of Figures

List of Abbreviations

ABC	ATP-binding cassette
ADT	Androgen deprivation therapy
AMP	Adenosine monophosphate
APS	Ammonium persulfate
AR	Androgen receptor
ARL8B	ADP ribosylation factor like GTPase 8B
aSMase	Acidic sphingomyelinase
Atg-9	Autophagy related 9
BAK	BCL-2 homologous antagonist/killer
BAX	BCL2 Associated X
BCA	Bicinchoninic acid
BCL-2	B-cell leukemia/lymphoma 2
BID/tBID	BH3 interacting-domain death agonist/truncated BH3 interacting-domain death agonist
BRAF	Serine/threonine-protein kinase B-Raf
BRCA1/2	Breast cancer gene 1/2
BSA	Bovine serum albumin

CAD	Cationic amphiphilic drug
CD20	B-lymphocyte antigen CD20
CI	Combination index
CLL	Chronic lymphocytic leukemia
CQ	Chloroquine
CRPC	Castration resistance prostate cancer
CTLA4	Cytotoxic T-lymphocyte associated protein 4
CYP17A1	Cytochrome P450 family 17 subfamily A member 1
DAPI	4′,6-diamidino-2-phenylindole
DEGS1	Dihydroceramide desaturase 1
DHE	Dihydroethidium
DHT	Dihydrotestosterone
DMEM	Dulbecco's Modified Eagle Medium
DMSO	Dimethyl sulfoxide
DNA	Deoxyribonucleic acid
ECL	Enhanced chemiluminescence
EDTA	Ethylenediaminetetraacetic acid

EGF	Epidermal growth factor
EGFR/HER1	Epidermal growth factor receptor
EPG5	Ectopic P-granules 5 autophagy tethering factor
FBS	Fetal bovine serum
FDA	Food and Drug Administration
FIJI	Fiji is just ImageJ
FITC	Fluorescein isothiocyanate
FOXA1	Forkhead box protein A1
HCQ	Hydroxychloroquine
HEK293	Human embryonic kidney 293
HER2	Human epidermal growth factor receptor 2
HOPS	Homotypic fusion and protein sorting
HRP	Horseradish peroxidase
IC50	Inhibitory concentration 50
IL-1	Interleukin 1
LBD	Ligand binding domain
LC3I/II	Microtubule-associated proteins 1A/1B light chain 3B I/II

LDL	Low-density lipoprotein
LMP	Lysosome membrane permeabilization
MAPK	Mitogen-activated protein kinase
MCL-1	Induced myeloid leukemia cell differentiation
MMP/$\Delta\psi m$	Mitochondrial membrane potential
MOMP	Mitochondrial outer membrane permeabilization
MRI	Magnetic resonance imaging
MRP2/3	Multidrug resistance-associated protein 2/3
mTORC1	Mammalian target of rapamycin complex 1
MTS	3-(4,5-dimethylthiazol-2-yl)-5-(3-carboxymethoxyphenyl)-2-(4-sulfophenyl)-2H-tetrazolium, inner salt
NH_4Cl	Ammonium chloride
NKX3.1	NK3 homeobox 1
NLRP3	NLR family pyrin domain containing 3
p53	Tumor protein P53
p62/SQSTM1	Sequestosome-1
PAGE	Polyacrylamide gel electrophoresis
PARP-1	Poly(ADP-ribose) polymerase 1

PBS	Phosphate-buffered saline
PD1	Programmed cell death protein 1
PD-L1	Programmed death-ligand 1
PE	Phycoerythrin
PerCP	Peridinin-Chlorophyll-Protein
PI3K	Phosphoinositide 3-kinase
PIN	Prostatic intraepithelial neoplasia
PLEKHM1	Pleckstrin homology and RUN domain containing M1
PSA	Prostate specific antigen
PTEN	Phosphatase and tensin homolog
RB1	Retinoblastoma 1
ROS	Reactive Oxygen Species
RPMI 1640	Roswell Park Memorial Institute 1640
SDS	Sodium dodecyl sulfate
SMAD4	SMAD family member 4
SMPD1	Sphingomyelin phosphodiesterase
SNARE	Soluble N-ethylmaleimide-sensitive factor attachment protein receptor

TBS(T)	Tris-buffered saline (Tween® 20)
TEMED	Tetramethylethylenediamine
TFEB	Transcription factor EB
TLR	Toll-like receptor
TMPRSS2-ERG	Transmembrane protease serine 2:v-ets erythroblastosis virus E26 oncogene homolog
ULK1	Unc-51 like autophagy activating kinase 1

Chapter 1: Introduction

1.1 Prostate Cancer

Prostate cancer is the most diagnosed and third leading cause of cancer-related death, accounting for about 10% of deaths, in Canadian men as of 2023[1]. There are several risk factors that may elevate the chances of prostate cancer diagnosis or mortality such as family history, age, hereditary mutations, race, and lifestyle and environmental factors such as smoking and obesity[2,3]. In their lifetime, 1 in 8 Canadian men are predicted to develop prostate cancer[1]. The majority of cases develops in men older than 50, and screening for prostate cancer can be done with methods such as digital rectal examination, prostate-specific antigen (PSA) screening, prostate tissue biopsy, or magnetic resonance imaging (MRI)[1,4]. When diagnosed early, 5-year survival in stages I to III are nearly 100%, but survival rate sharply declines for stage IV patients[5]. Prostate cancers that progress to these advanced stages of the disease are fatal, and currently existing treatments only extend patient survival and palliate some effects of treatment on quality of life[6].

The prostate gland is an organ that is responsible for producing seminal fluid, which contains many compounds and enzymes such as PSA. Prostate cancer can develop when prostate cells mutate in ways that result in them growing and reproducing excessively, exhibiting what are known as the hallmarks of cancer[7–9]. Hallmarks of cancer include increased cell proliferation, avoiding cell growth suppressors and cell death signals, increased genomic instability, metabolic adaptations, and increased angiogenesis. Typically, the genes mutated in cancer regulate these hallmarks of cancer involved in cell proliferation, metabolism, death or survival, and cell

differentiation. Mutations in genes such as loss of PTEN or NKX3.1, MYC overexpression, and chromosomal alterations like TMPRSS2-ERG gene fusion can turn normal prostate epithelial cells into a prostate intraepithelial neoplasia (PIN) lesion[10–16]. In this pre-malignant state, the prostate epithelial cells gain more mutations and lead to inflammation in the lesion area. PIN lesions can progress to adenocarcinoma through more mutations like FOXA1 mutation, loss of RB1, and activation of telomerase[17–20]. These can further progress to metastatic cancer from loss of the tumor suppressor SMAD4, mutations in BRCA 1 and 2, and mutations in the androgen receptor[21–28].

Androgen receptor (AR) is a critical receptor for normal prostate development, but this also enables it to contribute to prostate cancer carcinogenesis as its activation can be used by cancer cells to resist cell death and continue replicating[22,29–33]. Its main ligands are testosterone and dihydrotestosterone (DHT), which are steroidal androgens primarily produced in the testes, with DHT having a greater affinity for the AR[34,35]. In response to ligand binding, the AR translocates from the cytoplasm to the nucleus and binds to the androgen response elements of its target genes which are responsible for promoting cell growth and proliferation. There are also connections between AR signaling and cell migration through complexes between AR and the cell cytoskeleton, which could impact cell motility and metastasis[36,37]. The progression of prostate cancer and the development of castration resistance in prostate cancer is strongly correlated with AR expression and activity and presents a challenge for therapies against more aggressive tumors.

1.2 Prostate Cancer Treatment and Challenges

Over the years, treatments for prostate cancer have changed, resulting in longer survival times for patients. Since 1994 and until 2012, the mortality rate for prostate cancer decreased by about 2.8% annually, and by 1.6% annually following 2012 until the present[1]. Some standard treatments for prostate cancer include anti-hormonal therapies and radiation therapy[3]. The treatment used for prostate cancer patients depends on the severity and spread of the cancer. Prostate cancer is scored based on a set of criteria known as the Gleason score[38–40]. The Gleason score correlates with the severity of the disease and whether it has metastasized and informs the treatments given to the patient. Two tissue samples from different areas are taken and graded from 1 through 5, with lower grades corresponding to well-differentiated tissue that does not differ significantly from non-malignant tissue, and higher grades for more abnormal tissue. These two grades are added up from representative tissue samples to give the Gleason score, and a score of less than 6 is low grade, 7 is intermediate grade, and 8 to 10 is high grade disease. The combination of Gleason score, PSA level and clinical stage can be used to further categorize prostate cancer to determine the course of treatment. In the earlier stages of the disease with a localized, slow growing tumor, the first strategy is keeping watch over tumor progression through regular surveillance of PSA levels and tissue biopsies[41]. This is done to ensure that the tumor is not progressing, and to maintain patient quality of life, especially in older patients with low-risk cancer where aggressive treatment would not bring significant benefits. For growing cancers with a higher Gleason score, surgery or radiotherapy might be used to ablate the tumor instead. These strategies, however, run the risk of recurrence if tumor cells are left behind to proliferate once more. Prostate cancer can advance to metastatic prostate cancer and spread to other organs, typically the bones or lymph nodes[42,43]. In the case of recurrence after surgery or

radiation and in more advanced metastatic prostate cancer, the mainline treatment involves using chemotherapy with taxanes such as docetaxel, combined with hormone manipulation[44]. The hormonal-based treatment can involve agents such as luteinizing hormone-releasing hormone agonists and antagonists, abiraterone which inhibits CYP17A1 and blocks androgen production, or enzalutamide which inhibits AR in combination with other therapies to inhibit the production of androgens or the activation of the AR, one of the key players in this disease's progression[45,46]. This is known as Androgen Deprivation Therapy (ADT)[29]. ADT is used against prostate cancer that is metastasized beyond the prostate gland, but which remains androgen sensitive. Ninety percent of patients find benefit with ADT, but eventually most of them become resistant to the therapy, resulting in a highly aggressive cancer and poor patient outcomes[47].

Some tumors may become resistant to ADT and other commonly used treatments, and progress to a more advanced and aggressive phenotype that no longer responds to standard treatments. There are several different ways the cancer become drug resistant: cell death pathway inhibition, DNA damage repair, drugs being removed from the cell by membrane transporters and therefore unable to act upon their targets, alterations in the immune system, epigenetic modifications, and changes in the tumor microenvironment[47–56]. Prostate cancer cells could become resistant to its main chemotherapeutic taxane docetaxel by overexpressing the ATP-binding cassette (ABC) transporters such as MRP2, MRP3, and p-glycoprotein, as these transporters are able to pump certain drugs out of the cell preventing them from exerting their therapeutic effects[48,49]. For androgen-based therapies, prostate cancer can become resistant to ADT when androgen receptor signalling function is restored, which could be through but is not limited to AR mutations, AR splice variants that remain active constitutively, AR overexpression,

or androgens are synthesized in the prostate[57–68]. Once this occurs, the cancer is referred to as castration-resistant prostate cancer[45,46]. Most point mutations in the AR in prostate cancer are in the ligand binding domain, and this makes AR antagonists behave as agonists instead, activating the receptor and promoting tumor progression and castration resistance[34,67,69,70]. For example, the mutation F876L/T878A causes a change in the conformation of the AR LBD and switches enzalutamide into an AR agonist[71]. Even in environments with low levels of androgens, AR overexpression can develop by gene amplification, or the cancer cells can show increased expression of co-regulators for AR allowing the cells to respond to androgens despite their depletion. This gene amplification is present in 20-33% of castration resistant prostate cancers[31,72,73]. As a result of prostate cancers receiving ADT, the cancer can alternatively bypass the need for the AR axis entirely and upregulate pathways like the glucocorticoid receptors which shares some of the same gene targets as AR signaling, causing treatment resistance[65]. In addition, using these drugs in sequence with one another can lower their effectiveness due to cross-resistance, as one study demonstrated that following up abiraterone treatment with enzalutamide only shows a response rate between 15-30%[48,74]. Inappropriate activation of AR can be detected by increased levels of PSA detected in the serum[75–77].

Other treatment strategies for prostate cancer have been under investigation in recent years, such as sipuleucel-T, an immunotherapeutic cancer vaccine that has shown a 4.1-month median survival increase in phase 3 studies against metastatic castration resistant prostate cancer[48,78]. Studies on immune checkpoint inhibitors that have shown effects in other types of cancer like ipilimumab which inhibits CTLA4, nivolumab which is an antibody against PD-1,

and pembrolizumab which is an anti-PD-1 monoclonal antibody fail to show the same efficacy in prostate cancer[79–81].

Despite available treatments, there is no definitive cure for aggressive prostate cancer. Thus, there is a need for developing alternative therapy strategies that are effective and carry less toxic side effects compared to typical chemotherapy regimens to overcome the development of drug resistance in these prostate cancers.

1.3 Targeting the EGFR with Lapatinib in Prostate Cancer Therapy

In metastatic prostate cancer, there is increased expression of the epidermal growth factor 1 receptor (EGFR) and its ligand epidermal growth factor (EGF)[82–84]. The expression of the receptor correlates with a higher Gleason score, and it has been predicted that it may be involved in the switch from hormone sensitive to hormone resistant prostate cancer. In addition, activation of the receptor by EGF causes activation of the MAPK pathway, responsible for supporting cell growth and promoting tumor progression[31,85,86]. In addition, literature has shown that there is cross talk between AR and EGFR pathways, as activating EGFR in an AR-negative prostate cancer cell line resulted in transcription of an AR-mediated reporter gene indicating that stimulation of EGFR can activate AR pathways and gene targets despite the lack of AR in the cells[87]. EGFR mediated pathways can be targeted with tyrosine kinase inhibitors such as Gefetinib, which has shown an effect in both androgen sensitive and insensitive prostate cancer xenograft models but failed to show the same effects in phase II studies on patients[88–91]. Lapatinib (GW572016) inhibits tyrosine kinases such as EGFR and HER2, both of which are altered in cancers such as breast cancer and prostate cancer, and which overexpression can lead

to worse patient outcomes[92]. Phase II studies on lapatinib show effects in breast cancer, and the drug is well tolerated, and FDA approved for breast cancer treatment[93,94]. In phase II studies on prostate cancer however, lapatinib treatment alone has minimal effect in advanced prostate cancer that has not been treated with hormone-based therapies and a moderate effect on androgen-dependent prostate cancer that has relapsed after primary treatment or some castration-resistant prostate cancer patients[92,95,96]. In *in vitro* studies, lapatinib alone has shown apoptosis induction and migration inhibition in the hormone-sensitive LNCaP cells, but not in the castration-resistant PC3 cell lines[97]. Lapatinib was also able to enhance apoptosis induced by navitoclax in prostate cancer cells[98]. Previous research has shown the combination of siramesine (a lysosome disrupting agent) and lapatinib induced synergistic cell death in breast cancer cell lines[99]. Using lapatinib in combination with other anti-cancer drugs such as lysosome disrupting agents might be an effective strategy to treat prostate cancer cells.

1.4 Lysosomes as a Target for Prostate Cancer Therapy

One method of developing new therapies is to investigate targeting cellular machinery such as the lysosome[100]. The lysosome is an acidic organelle often located near the nucleus or cell membrane that is responsible for degrading cellular components and macromolecules, as it contains enzymes such as cathepsins, hydrolases, proteinases to degrade proteins, and other degradative enzymes[44,101]. It is responsible for a variety of cellular functions, such as protein degradation, nutrient recycling, and disposing of cellular waste and damaged organelles[44,102–104]. In addition, it also has functions in signalling, immune responses, and exocytosis[105–111]. The lysosome can receive substances for degradation through autophagy or endocytosis[102,107,112–116]. Lysosomes can be classified into two categories, the first being the endolysosome which is the

fusion of a late endosome with a lysosome, and the second being a classic dense lysosome[44]. The biogenesis of lysosomes needs to be carefully controlled depending on the nutritional status of the cell. When there is an abundance of nutritionally relevant biomarkers such as amino acids present, signalling pathways in the cell result in the activation of mTORC1 kinase complex on the lysosomal membrane which inhibits the translocation of the transcription factor controlling lysosome biogenesis, Transcription Factor EB (TFEB), to the nucleus through phosphorylating TFEB ensuring it remains bound to a regulatory protein, thereby preventing more lysosomes from being synthesized[117]. Conversely, in conditions such as starvation, where the cells do not have sufficient levels of nutrients and other macromolecules, mTORC1 is not able to activate and the inhibition on TFEB is released, allowing more lysosome biogenesis and the ability for them to carry out their function of degrading organelles and other cellular components and the process of autophagy to recycle nutrients and sustain normal cellular function[118].

Lysosomes are involved in antigen presentation for immune cell communication. Lysosomes degrade proteins that are then displayed as antigens on MHC type II molecules in antigen-presenting cells, which can be presented to immune cells such as T cells[110,119]. Lysosome-related organelles in leukocytes can release granules through exocytosis for damaging pathogens[119]. Some Toll-like receptors that respond to double stranded RNA from pathogens are located within the lysosome, and TLRs 7, 8, and 9 need proteolytic processing for their activation. Lysosomes can also release exosomes to release cellular contents into the extracellular space or for repairing the membrane[107]. Exocytosis enables lysosomes to clear cellular substances, which benefits the cells as accumulation of these unwanted molecules can result in detrimental effects on the cells, as seen in pathologies like lysosomal storage disorders

[120,121]. After damage to the cell membrane, lysosomes can join and fuse at the site of injury, helping to seal the insult. Exosomes also contribute to the creation of pseudopods in the process of phagocytosis[107,122]. Molecules engulfed by phagocytosis can be subjected to autophagy by the lysosomes, another one of its key functions in the cell. Given the lysosomes' myriad uses in the cell including autophagy in maintaining cellular homeostasis, this makes the lysosome a target for therapies that disrupt these processes, which can result in cell death.

As lysosomes are critical to healthy metabolic functioning of the cell, cancer cells may upregulate the number of lysosomes to keep up with the high demands of tumor proliferation[123,124]. Cancer cells initially have high metabolic needs that benefit from the macromolecule recycling capabilities of the lysosome[44,118,125]. Cancer cells often have a greater number of lysosomes near the plasma membrane compared to the nucleus as opposed to non-cancerous cells, and this is so the lysosomes can assist in invasion and adhesion of the cancer cells[44,126]. The lysosomes in cancer cells are also larger and more fragile than the lysosomes of non-cancerous cells[127]. Previous literature has shown that inhibiting lysosome biogenesis through siRNAs acting against TFEB causes a reduced metastatic potential in cancer cells[128]. Lysosomes, which are involved in autophagy, can be either tumor suppressive or tumor promoting through autophagy function[129]. This is because autophagy is tumor promoting in that it prevents ROS build up which would lead to cell death in conditions like stress and hypoxia, something cancer cells might experience in larger more aggressive tumors. In prostate cancer mouse models that have autophagy deficiency through deletion of the autophagy related gene *Atg7*, tumor progression is slowed in both castration-naïve and castration resistant cancer[130]. Increased expression of cathepsin B is correlated with tumor invasion[131]. In addition, lysosome function

can contribute to cancer cells acquiring resistance to first line therapies, as they can sequester some drugs to the lysosome instead of to their action sites[132]. Therefore, the contribution of lysosomes in maintaining the homeostasis of cancer cells makes it a target for combination therapies, by inducing autophagy or cell death through disruption of lysosomal function.

1.5 Lysosomes and Autophagy

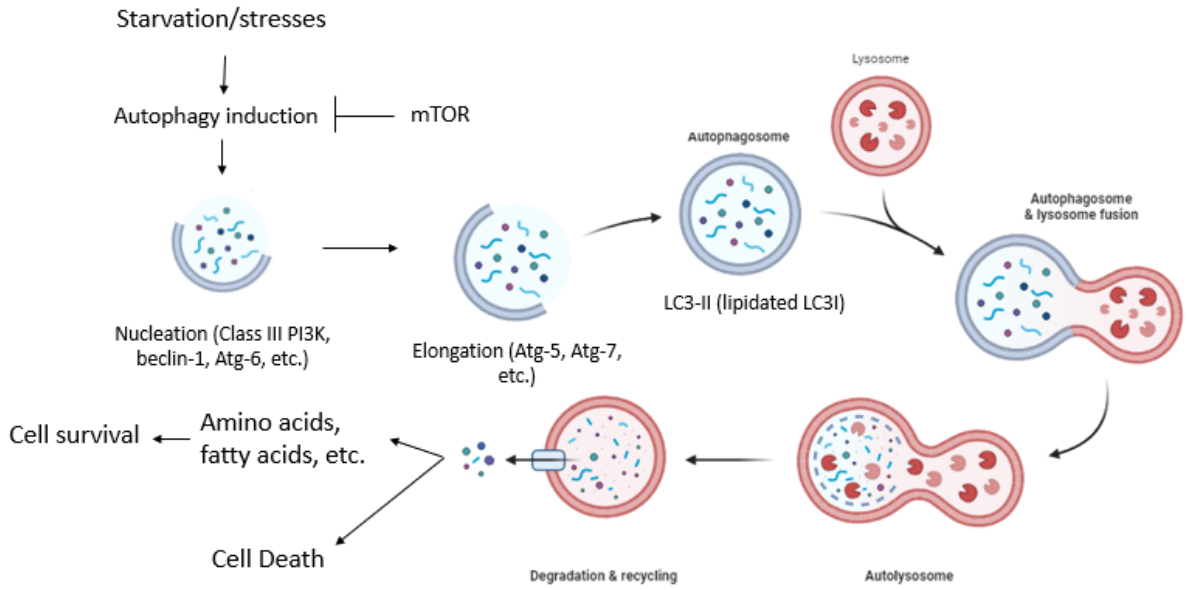

Figure 1.1. The process of autophagy. Autophagy is blocked by mTOR, but this inhibition is released and autophagy is initiated when the cell experiences stressors such as starvation. This causes the creation of a vesicle by enzymes such as PI3K class III, beclin-1, and Atg-6 in a process known as nucleation. Following this, the vesicle undergoes elongation and eventually forms the autophagosome. The autophagosome-bound protein LC3I is lipidated to become LC3II. Lysosomes fuse with the autophagosome to form the autolysosome, which is the organelle that carries out the degradative functions of autophagy. Autophagic degradation can

free macromolecules such as amino acids and fatty acids to help facilitate protein synthesis, ATP generation, and ultimately promote cell survival. However, an overabundance of autophagy activation and degradation can also lead to cell death. This figure is adapted from: Levine, B., & Yuan, J. (2005)[133].

Lysosomes are involved in autophagy. Autophagy is a process by which cells degrade cellular components to promote survival during adverse conditions[102]. Autophagy is inhibited during times where the cell has access to sufficient nutrient levels, as GTPases on the lysosome activate mTORC1 which phosphorylates and inhibits proteins in the autophagy initiation complex[134,135]. When nutrient levels drop, mTORC1 is no longer activated, and autophagy can initiate. During the process, lysosomes fuse with the autophagosome to form the autolysosome, leading to degrading cellular components such as damaged organelles to promote nutrient recycling in the cell[136]. For fusion between the autophagosome and the lysosome, SNARE complexes are formed along with assistance from proteins such as HOPS complex, PLEKHM1, and EPG5, which interact with Arl8b and RAB7 on the lysosome, and LC3 on the autophagosome[111,137–140]. This fusion allows for the components of each organelle to occupy the interior of the newly formed autolysosome, including hydrolases from inside the lysosome, which can degrade the autophagic substrates present. The lysosomal degradation pathway involves several steps: initiation, nucleation, elongation, fusion, and finally degradation[141]. Upon initiation, cellular stress and AMP kinase can set off a chain of events that results in mTORC1 downregulation, releasing mTORC1 inhibition of autophagy proteins in the Atg family and the ULK1 complex[141–143]. Nucleation involves activation of the PI3K III complex and recruitment of vesicles that contain Atg-9[144,145]. During elongation, two conjugation systems are activated with

one containing the protein LC3I[146–148]. LC3I is lipidated by several enzymes to become LC3II and is bound to the autophagosome membrane. The lysosome fuses with the autophagosome to form the autolysosome which is what carries out the degradative function of autophagy[149]. Autophagy can carry out bulk degradation, but proteins such as p62 can transport cargo to the autophagosome for more selective degradation[150,151].

Previous literature has shown that cancers including prostate cancer have altered levels of autophagic flux compared to normal cells as well as higher lysosomal content with altered activity and responses to metabolic changes[8]. Autophagy can play a role in modulating cell survival or cell death. Under stressful conditions such as hypoxia, cancer cells have been shown to use autophagy to promote cell survival[129]. However, autophagy has also been shown to have a tumor suppressive effect when exposing cells to more prolonged stress, as autophagy is induced. Autophagy can prevent tumor progression, as it prevents cells from being damaged leading to genetic problems and the initial trigger for cancer[129]. In addition, through degradation of cellular components, it contributes to nutrient recycling and freeing up building blocks for cancer cells to synthesize new proteins and continue tumor growth and proliferation[152]. The mechanism responsible for the switch between the tumor promoting and tumor suppressing effects is not completely understood.

1.6 Lysosomal Cell Death

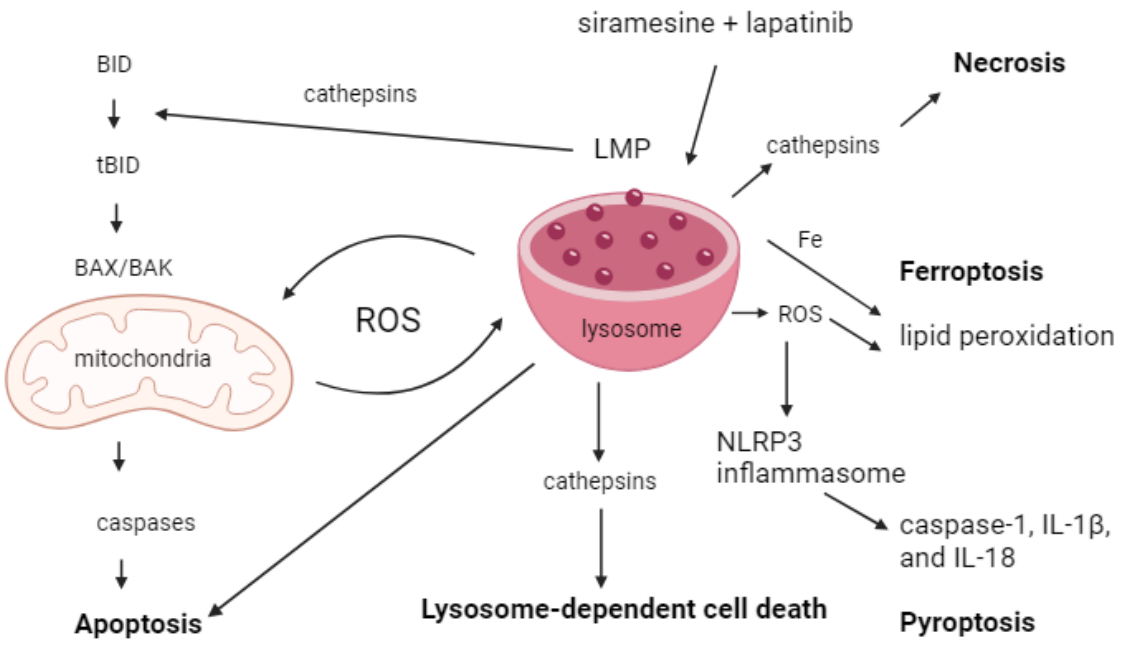

Figure 1.2. Outcomes of lysosome membrane permeabilization. Various triggers such as calpain activation by increased calcium concentration can cause the permeabilization of the lysosome membrane, resulting in the release of cathepsins, iron, and ROS generation. This can lead to several types of cell death through different mechanisms. Release of cathepsins leads to lysosome-dependent cell death and to necrosis. The released cathepsins can also cause activation of the NLRP3 inflammasome, activating A, which lead to cell death by pyroptosis. Cathepsins have also been implicated in causing apoptosis by cleaving BID which activates BAX/BAK on the mitochondrial membrane leading to release of cytochrome c, ROS generation, and the start of the caspase cascade. Iron and ROS release can result in an iron-dependent form of cell death known as ferroptosis. This figure is adapted from: Wang, F., Gómez-Sintes, R., & Boya, P. (2018).[153]

Disruption of the lysosomal membrane, or lysosomal membrane permeabilization (LMP) can lead to lipid peroxidation, generation of ROS, release of lysosomal contents, and cell death in a caspase-dependent or independent manner [154].

In caspase-dependent apoptosis, membrane disruption results in the release of lysosomal molecules such as cathepsins, which triggers the caspase cascade indirectly resulting in the induction of apoptosis[155,156]. The intrinsic pathway for apoptosis involves permeabilization of the mitochondrial outer membrane (MOMP), which results in the release of cytochrome c and the rest of the caspase cleavage pathway[157,158]. Lysosome disruption can initiate this pathway as Cathepsins B and D have been shown to cleave the proapoptotic protein BID. The cleaved BID then interacts with BAX and BAK, which when activated form a pore in the mitochondrial membrane which leads to MOMP[159]. Due to the links between lysosomes and mitochondria, antiapoptotic BCL-2 family members have been shown to inhibit LMP as well[160,161]. LMP can also cause other forms of cell death independent of caspase activation mediated by reactive oxygen species (ROS)[126,162]. Reactive oxygen species are highly reactive oxygen-based molecules which can be generated inside cells through exogenous or endogenous means[141]. Some examples include the hydroxyl radical, superoxide, and hydrogen peroxide[141,163]. Endogenously, the main source of ROS generation is the mitochondrial electron transport chain, including superoxide production at complexes I and III[164]. External factors such as drugs and stressors such as hypoxia or starvation can also cause cells to increase ROS production[141,165–167]. Cancer cells have altered metabolism and increased ROS compared to normal cells[118]. After mitochondrial dysfunction and membrane destabilization, ROS is produced which can lead to lipid peroxidation that results in LMP and further mitochondrial destablization[118]. If the redox

balance is sufficiently disrupted, this causes oxidative stress that when combined with the damage to organelles results in cell death[168–171]. Antioxidants and ROS scavengers including vitamin E (α-tocopherol) can protect against toxic accumulation of ROS [156]. Siramesine-induced cell death in CLL has been shown to be blocked by α-tocopherol, and despite not preventing LMP, it prevented changes in mitochondrial membrane potential and inhibited lipid peroxidation. This indicated that following LMP, ROS production led to cell death through disruption of the mitochondria. The effect of lysosome disruption in prostate cancer is not completely understood.

Necrosis is a less frequent type of cell death induced after excessive mechanical and/or chemical damage events[172,173]. This type of cell death is known to be triggered and regulated in a more uncontrollable manner. An excessive mechanical damage and significant concentrations of certain drugs can lead to the rupture of the plasma membrane and DNA damage. This is the more primitive type of cell death where cellular damage cannot sustain the process of finalizing signaling cascades or programmed cell death. When lysosome membrane permeabilization (LMP) occurs rapidly necrotic cell death occurs.

Ferroptosis is the most newly discovered type of cell death that relies on the increased availability of labile iron through altered iron transport or storage and inhibition of the Xc-cysteine pathway that imports cysteine as an antioxidant[99,172,174–177]. In cells, where these pathways are upregulated or altered, an increase in labile iron can potentially lead to an increase in reactive oxygen species which can target oxidation of lipids more specifically than other cellular processes. An increase in lipid peroxidation rapidly leads to cell death since membrane integrity becomes unstable and can no longer sustain cell and organelle structure. In breast

cancer cells, lysosome disruption leads to increased labile iron and ferroptosis[99,177]. The role of ferroptosis in prostate cancer is unclear.

Pyroptosis is an inflammatory form of cell death involving the inflammasome[172,178–183]. The inflammasome contains NLPR3 and caspase 1 in complex that is induced by ROS from lysosomes. This leads to cleavage of IL1 leading to cell death. In prostate cancer cells, the type of lysosome mediated cell death is unclear.

1.7 Lysosome Targeting Drugs

Targeting the lysosome or the autophagy pathway with drugs is undergoing investigation. Some antimalarial agents such as chloroquine, hydroxychloroquine, and quinacrine have also been found to inhibit autophagy in cells, and studies have shown these agents can induce cell death of cancer cells in vitro[127,184–190]. Other drugs currently under investigation have the goal of inducing LMP leading to cancer cell cytotoxicity[127]. These include lysosomotropic agents. These agents are typically cationic amphiphilic drugs (CADs) which are weak bases. At a neutral pH, such as in the cytosol, these drugs can cross the lipid membrane of the lysosome due to their lipophilic or amphiphilic nature, but because the inside of the lysosome is acidic due to the action of proton pumps, the drugs can become charged through protonation, preventing them from leaving the lysosome. When these drugs accumulate, they disrupt the lysosomal membrane. Some lysosomotropic agents also use different methods to induce LMP. Lysosomal membranes are enriched with sphingolipids and glycerophospholipids compared to other membranes in the cell[191]. Therefore, disrupting the balance of these sphingolipids can lead to membrane fragility

and LMP induction which cancer cells are more sensitive to than normal cells[192]. This can be done with drugs like siramesine.

1.8 Lysosome Disrupting Agent Siramesine

To induce lysosomal membrane permeabilization (LMP), lysosomotropic agents such as siramesine can be used[99,177,193–196]. Other lysosomotropic agents include nortriptyline, amlodipine, terfenadine, mefloquine, desipramine, loratadine, desloratadine, and clemastine, which have been tested in various cancers such as chronic lymphocytic leukemia (CLL) or prostate cancer[192,197–206]. Of the agents tested in prostate cancer, previous literature suggests that the acidic sphingomyelinase inhibitor siramesine is the most effective LMP inducing agent[196]. Within the lysosome is an enzyme called acidic sphingomyelinase (aSMase) that hydrolyses sphingomyelin into ceramide. Cancer cells have lower aSMase activity than normal cells, and further inhibiting this enzyme can lead to an increase in sphingomyelin levels, which eventually results in the disruption of the lysosome membrane and LMP[207]. Siramesine is an inhibitor of aSMase which acts as a lipase that converts sphingomyelin to ceramide[208]. By inhibiting aSMase from binding to one of its essential co-factors, the inability for aSMase to carry out its function results in LMP. The subsequent LMP induction can also cause the release and prevent the further accumulation of other cancer killing drugs that would otherwise be sequestered within the lysosome, enabling them to go to their active sites and carry out their therapeutic functions, presenting an avenue for drug combinations with siramesine to re-sensitize cancer cells to these drugs[209]. Literature has shown siramesine is able to cause cell death in glioblastoma *in vitro*, in breast cancer xenografts, in primary CLL cells, and in breast cancer cells *in vitro*[99,156,177,194]. The influence of cathepsin release or the involvement of caspases in cell death was cell type

dependent. Siramesine has demonstrated promotion of autophagosome accumulation in cancer cells[193]. In prostate cancers, siramesine re-sensitized multidrug resistant PC3 prostate cancer cells to docetaxel in vitro and in a xenograft model[192]. When combined with the tyrosine kinase inhibitor lapatinib, siramesine caused synergistic cell death through ferroptosis in breast cancer cells, but this combination has not been investigated in prostate cancer[99,177]. Based on these findings, I will investigate targeting the lysosome to induce cell death in prostate cancer cells, and since the lysosome is involved in autophagy, whether disruption of the lysosome and its impact on autophagy plays a role in promoting or preventing cell death of cancer cells. In addition, using targeted therapy lapatinib in combination with siramesine, I will determine whether this combination acts synergistically in prostate cancer cells.

1.9. Rationale

Prostate cancer is the most commonly diagnosed cancer in Canadian men, and if detected and diagnosed early, shows good survival rates. However, prostate cancer can develop resistance to commonly used treatments, and this advanced stage of cancer is fatal. A strategy to overcome the drug resistance developed by prostate cancer is targeting organelles such as the lysosome. The lysosome is responsible for a variety of cellular functions in cancer cells but has a weaker lysosomal membrane in cancer due to altered sphingolipid biology, enabling it to act as a target for drugs that induce lysosome membrane permeabilization. Lysosome disrupting agents, such as the aSMase inhibitor siramesine, induce cell death in cancer cells such as glioblastoma, CLL, and breast cancer. Prostate cancers also show elevated levels of EGFR and HER2, receptors which are responsible for cell proliferation, growth, and can contribute to metastasis in cancer. The tyrosine kinase inhibitor lapatinib can inhibit both receptors. The combination of lysosome disrupting agent siramesine and tyrosine kinase inhibitor lapatinib induces synergistic cell death in breast cancer cells. The role of lysosome disrupting agents alone or in combination with lapatinib in prostate cancer cells is unknown.

1.10. Hypothesis and Aims

Hypothesis: Targeting lysosomal mediated cell death through siramesine alone or in combination with lapatinib will be effective in inducing killing prostate cancer cells

Aim 1: Determining whether lysosome disrupting agent siramesine and tyrosine kinase inhibitor lapatinib increase cell death in prostate cancer cell line PC3.

Aim 2: Determine the mechanism of action for synergy between siramesine and lapatinib.

Aim 3: Define the role of autophagy in siramesine and lapatinib induced cell death.

Chapter 2: Methods and Materials

2.1 Cell Culture

2.1.1 Cell Culture

There were four cell lines utilized, PC3, LNCaP, RWPE-1, and HEK293 cells. The cell lines were obtained from the University of Manitoba. PC3 cells were cultured in Dulbecco's Modified Eagle Medium F12 (DMEM F12) (12800-082, Gibco) with 5% FBS (12483-020, Gibco) and 1% Penicillin-Streptomycin (15070-063, Gibco). LNCaP cells were cultured in RPMI Medium 1640 (31800-089, Gibco) with 10% FBS (12483-020, Gibco) and 1% Penicillin-Streptomycin (15070-063, Gibco). RWPE-1 cells were cultured in Keratinocyte-Serum Free Medium (1X) (10724-011, Gibco) with 1% Penicillin-Streptomycin. HEK293 cells were cultured in Dulbecco's Modified Eagle Medium Low Glucose (DMEM Low-Glucose) with 5% FBS and 1% Penicillin-Streptomycin. All cell lines were grown in 10cm plates with 7-10mL of media in a tissue culture incubator at 5% CO_2 and 37ºC.

2.1.2 Cell Passaging

Cells were passaged upon reaching 70-90% confluency and media was changed every 3 days. For passaging PC3, LNCaP, and HEK293 cells, media was aspirated off and 10mL of PBS was added to plates before aspirating once more. For PC3 cells, cells were trypsinized with 0.25% w/v Trypsin-EDTA (25200-072, Gibco) for 5 minutes, while LNCaP and HEK293 cells were trypsinized for 3 minutes. A minimum of 10mL of media was added to neutralize the Trypsin-EDTA on cells after trypsinization, and cells were diluted by a ratio of 1:3 or 1:4 and

redistributed into 100mm plates. For passaging RWPE-1 cells, media was aspirated off and 200µL of PBS was added to plates before aspirating once more. Cells were trypsinized with 0.05% w/v Trypsin-EDTA for 5-8 minutes and observed under microscope periodically to ensure cell detachment.

2.1.3 Cell Collection

For collecting PC3, LNCaP, and HEK293 cells, media was aspirated off and 500µL of PBS was added to plates before aspirating once more. For PC3 and HEK293 cells, cells were trypsinized with 500µL (100mm plates) or 200µL (60mm plates) 0.25% w/v Trypsin-EDTA for 5 minutes, while LNCaP cells were trypsinized for 3 minutes. A minimum of 500µL of media was added to neutralize the Trypsin-EDTA on cells after trypsinization, and cells were collected into 15mL Falcon tubes before centrifuging at 1500rpm for 5 minutes. Media was aspirated off and cells were resuspended in 500µL of PBS and moved into Eppendorf tubes on ice. Tubes were centrifuged at 1200xG for 5 minutes at room temperature and PBS was aspirated off to obtain cell pellets for protein isolation or flow cytometry or stored temporarily at -80ºC for later use.

2.1.4 Cell Cryopreservation and Thawing

Cells were collected into 15mL Falcon tubes before being counted and centrifuged at 1200rpm for 5 minutes. Media was aspirated off and cells were resuspended in freezing media containing 50% of their growth media, 40% FBS and 10% DMSO (D2650-100ML, Sigma). $5x10^5$ up to $1.2x10^6$ cells were placed per vial and were initially frozen at -80ºC and transferred to liquid

nitrogen for storage. For thawing, cell vials were removed from liquid nitrogen and placed in a 37ºC water bath until contents were liquid, after which the thawed cells were added to Falcon tubes containing pre-warmed media and centrifuged at 120rpm for 5 minutes. Media was aspirated off from tubes and cells were resuspended and redistributed into 10cm plates.

2.1.5 Cell Counting

Cells were collected using the steps described in Cell Collection. Cells were resuspended in 500µL of PBS and transferred to Eppendorf tubes, where 10µL of cells were taken and mixed with 10µL 0.4% Trypan Blue (T8154-100ML, Sigma). 10µL of the mixture was added to each chamber of a hemocytometer before counting under microscope. The four corner grids on each chamber of the hemocytometer were counted, averaged, and multiplied by the dilution factors to get the number of cells per mL. Cells were seeded based on cells per mL, by calculating the volume of cells to seed the required number of cells. The equations used are as follows:

$$average\ number\ of\ cells\ in\ 8\ grids\ of\ hemocytometer\ \times 2\ \times 10^4 = cells/mL$$

$$number\ of\ required\ cells \div cells/mL\ =\ volume\ in\ mL\ to\ seed$$

2.2 Cell Treatment and Inhibition

2.2.1 Drug Treatments

Siramesine fumarate salt (#SML0976, Sigma) stock was diluted in DMSO to a concentration of 10mM. This stock siramesine solution was diluted and used at a concentration of 10µM in the

cell line's respective culturing media for all experiments involving PC3, LNCaP, or HEK293 cells excluding the MTS assay (see MTS Assay). Lapatinib (L-4899, LC Laboratories) stock was diluted in DMSO to a stock concentration of 10mM, which was then further diluted into aliquots with a concentration of 0.5mM. The 0.5mM stock lapatinib solution was diluted and used at a concentration of 0.5µM in for all experiments involving PC3, LNCaP, or HEK293 cells excluding the MTS assay (see MTS Assay). Both siramesine and lapatinib were stored at -20ºC.

2.2.2 Inhibitors

Antioxidant α-tocopherol (#258024, Sigma) was prepared as a stock solution of 0.95g/mL in ethanol and used at a final concentration of 200µg/mL for 1 hour prior to treatment. z-vad fmk (#219007, Sigma) stock was prepared at a concentration of 10mM in DMSO and used at a final concentration of 10µM z-vad for 1 hour prior to treatment. E-64 (#AAJ62933LB0, Thermo) was prepared at a stock concentration of 5mM in DMSO and used at a final concentration of 10µM E-64 for 1 hour prior to treatment. Chloroquine (#C6628-25G, Sigma) stock solution was prepared at a concentration of 10mM in distilled, autoclaved water. In experiments, 10 or 20µM of chloroquine in media was added with the siramesine and lapatinib treatments for 24 hours. z-vad fmk, E-64, and chloroquine were all stored at -20ºC. α-tocopherol as stored at 4ºC.

2.2.3 Starvation

Cell starvation was done using the same conditions as all other treatments, but serum-free media was used in substitute of culturing media.

2.3 Cell Death and Viability

2.3.1 Cell Death

Cell death was measured using the Trypan Blue cell exclusion assay, following the steps described in "Cell Counting" above. The average number of dead cells dyed by Trypan blue was divided by the average total number of cells across all counted chambers to get the cell death percentage. The equations used are as follows:

$$total\ number\ of\ live\ cells\ in\ 8\ grids + total\ number\ of\ dead\ cells\ in\ 8\ grids = total\ number\ of\ cells\ overall$$

$$\frac{average\ dead\ cells\ across\ 3\ experiments}{total\ number\ of\ cells\ overall\ across\ 3\ experiments} = percentage\ of\ dead\ cells$$

2.3.2 MTS Assay for Cell Viability

PC3 cells were seeded at 1.5 x 10^4 cells per well in 96-well plates and treated with 0.5, 1, 2, 3, 4, 5, 6, 7, 8, 9, or 10μM of lapatinib, and 5, 10, 15, 20, 25, or 30μM of siramesine for 24 hours, with DMSO-only treated wells as a negative control. MTS assay was performed using the CellTiter 96 Aqueous Non-Radioactive Cell Proliferation Assay kit (G5421, Promega). 10μL of MTS assay solution was added to each well, and plates were incubated for 4.5 hours before being analyzed on the FLUOstar Omega microplate reader (BMG Labtech) at 490nm.

2.3.3 Combination Index

An MTS assay was performed (see MTS Assay for Cell Viability) on PC3 cells treated with a range of lapatinib or siramesine concentrations for 24 hours, and the IC50 was determined for each drug. The IC50 for each drug was inputted into Chou and Talalay's formula: $Combination\ Index = \frac{(D)1}{(Dx)1} + \frac{(D)2}{(Dx)2}$ where the numerators are the concentrations of the individual drugs and the denominators are the concentrations of the drugs used in the combination treatment, with the subscript 1 corresponding to siramesine and the subscript 2 corresponding to lapatinib.

2.4 Flow cytometry

2.4.1 Dihydroethidium ROS Detection Assay

PC3 cells were seeded at 5 x 10^5 cells per 60mm plate and treated with DMSO as a negative control, 0.5µM lapatinib, 10µM siramesine, or a combination of siramesine and lapatinib for 24 hours with or without the addition of 200µg/mL α-tocopherol for 1 hour prior to treatment. Cells were washed with PBS and stained with 3.2µM Dihydroethidium (DHE) for 30 minutes at 37ºC in the dark before collecting cells into pellets (see Cell Collection). Cells were resuspended in 220uL PBS and run through an Attune NxT flow cytometer (ThermoFisher Scientific) or CytoFlex S flow cytometer (Beckman Coulter). ROS detection was determined by gating for DHE-positive cells, indicated with the PerCP channel. Data was analyzed using the FlowJo software (BD Biosciences).

2.4.2 Lysotracker Red DND-99 Assay

LNCaP cells were seeded at 5 x 10^5 cells per 60mm plate and treated with DMSO as a negative control, 0.5 μM lapatinib, 10 μM siramesine or a combination of siramesine and lapatinib for 24 hours and stained with 100nM Lysotracker Red DND-99 (excitation/emission maxima 577/590nm) in PBS for 1 hour at 37ºC in the dark. Cells were collected into pellets. Cell pellets were resuspended in 220uL PBS and run through an Attune NxT flow cytometer (ThermoFisher Scientific) or CytoFlex S flow cytometer (Beckman Coulter). The change in the loss of fluorescence of Lysotracker in the cells was determined by gating with the PE channel, as PE has an emission wavelength of ~575nm. Data was analyzed using the FlowJo software (BD Biosciences).

2.4.3 MitoSOX Red Assay

PC3 cells were seeded at 5 x 10^5 cells per 60mm plate and treated with DMSO as a negative control, 0.5 μM lapatinib, 10 μM siramesine or a combination of siramesine and lapatinib for 6 hours (A), 24 hours (B), or 48 hours (C). Cells were stained with 50 nM MitoSOX Red (absorption/emission maxima of ~396/610 nm) (Thermofisher Scientific) for 45 minutes at 37ºC in the dark. Cells were collected into pellets (see Cell Collection). Cell pellets were resuspended in 220uL PBS and run through an Attune NxT flow cytometer (ThermoFisher Scientific) or CytoFlex S flow cytometer (Beckman Coulter). MitoSOX Red was detected using the PE channel (CytoFlex S flow cytometer (Beckman Coulter)) or with the BL-2 emission filter

(590/40nm) (Attune NxT flow cytometer (ThermoFisher Scientific)). Gating of the flow cytometry assay was done on live cells and MitoSOX Red positive cells. Data was analyzed using the FlowJo software (BD Biosciences).

2.5 Western Blot

2.5.1 Cell Lysis

Cells were treated for 6, 18, or 24 hours and collected. After collection (see Cell Collection), cell pellets were lysed with 50µL NP-40 Lysis Buffer (30mL 5M NaCl (BP358-212, Fisher Scientific), 100mL 10% NP-40 (74385, Sigma), 50mL 1M Tris (pH 8.0) (T2694, Sigma), 820mL water) containing 1% Halt Protease Inhibitor Cocktail (100X) (#1862209, Thermofisher). Cells in lysis buffer were placed on ice for 10 minutes, vortexed for 10 seconds, and placed back on ice for a total of 3 repeats. Cells were centrifuged at 13,000xG for 15 minutes at 4ºC. The supernatant containing the cellular lysate was transferred to Eppendorf tubes, of which 5 µL was taken aside for use in BCA assays (see BCA Assay). Tubes containing lysate were stored at -20ºC initially and then transferred to -80 ºC for longer term storage.

2.5.2 BCA Assay

To measure protein concentration, 5µL of cell lysate from each sample (see Protein Isolation) were combined with 15uL of NP-40 Lysis Buffer to use in the BCA assay. Using the Pierce BCA Protein Assay Kit (#23225, Thermofisher) and following the manufacturer's instructions to create

a standard curve with BSA standard from the kit ranging from 0-2000µg/mL BSA, 10µL from each standard or sample was placed into 2 wells each on a 96-well flat bottom plate. Reagent A and Reagent B from the kit were combined in a 1:50 ratio of B:A, and 200 µL of this solution was added to each well. The plate was tapped to mix and eliminate air bubbles and sealed and stored at 37C for 30 minutes before reading the plate with the FLUOstar Omega microplate reader (BMG Labtech). The readings from each well of standard and/or sample were averaged and compared to the standard curve, and the amount of protein was calculated.

2.5.3 Western Blot

Based on the results of the BCA Assay (see BCA Assay), 5-30µg of protein for each sample was taken and diluted to the correct volume for loading using 4X Laemmli Sample Buffer (#1610747, Bio-Rad) with 10% β-mercaptoethanol (#1610710, Bio-Rad), and mili-Q water to reach a 1X concentration of Sample Buffer. The samples were heated at 90ºC for 10 minutes. 12% SDS-PAGE gels were made using 8mL of resolving gel stock solution composed of 30mL 40% Acrylamide/Bis (#161-0146, Bio-Rad), 25mL of 1.5M Tris-HCl pH 8.8 (#1610798, Bio-Rad), 1mL 10% SDS (#1610301, Bio-Rad), and 43.5mL mili-Q water, as well as 2mL of stacking gel buffer composed of 2.5mL 40% Acrylamide/Bis (#161-0146, Bio-Rad), 6.3mL of 0.5M Tris-HCl pH 6.8 (#1610799, Bio-Rad), 0.25mL of 10% SDS, and 15.9mL of milli-Q water. To the 8mL of resolving gel stock solution, 4µL of TEMED (#161-0800, Bio-Rad) and 40µL of 10% Ammonium Persulfate (APS) (#1610700, Bio-Rad) was added. To the 2mL of stacking gel stock solution, 2µL of TEMED (#161-0800, Bio-Rad) and 10µL of 10% Ammonium Persulfate (APS)

(#1610700, Bio-Rad) was added. For 1.5mm gels, 30µL (15-well) or 40µL (10-well) of the protein samples was added to each well, while 3µL of Precision Plus Protein All Blue Standard ladder (#1610373, Bio-Rad) was loaded as a marker for protein molecular weights. The gel was run at 100V for around 1.5 hours with 1X Running buffer (250.1mM Tris base, 1918.2mM glycine, 34.7mM SDS) diluted by 1:100 in mili-Q water. After the gels were finished running, the gel was transferred using 0.22µm nitrocellulose membranes on the Trans-Blot Turbo transfer system (1704150, Bio-Rad) for 10 minutes using the Bio-Rad defined 1.5mm gel protocol for 1-minigel or 2-minigels depending on how many blots were being transferred at one time in each chamber and transfer buffer composed of 10mL mili-Q water, 10mL methanol and 30mL Trans Blot Turbo 5x Transfer Buffer (#10026938, Bio-Rad). After transferring, the nitrocellulluose membrane was rinsed once with 1X TBST with 1% Tween-20 (BP337-500, Fisher) and blocked with 5% milk in 1X TBST for 1 hour, before rinsing with 1X TBST three times and adding primary antibody dissolved in 1X TBST (see Table 2.1) at 4C overnight. Membranes were washed three times with 1X TBST before adding secondary antibody dissolved in 1X TBST at room temperature for 1 hour, before rinsing with 1X TBST three times. Western blot images were taken using a scanner (Licor) using 200-500µL of a solution of equal parts Clarity western luminol/enhancer solution and peroxide solution from the Clarity Western ECL Substrate kit (#170-5060, Bio-Rad) per membrane. Images were analyzed with the Fiji is just ImageJ (FIJI) software or Image Studio software (Licor). Band intensities with backgrounds subtracted were normalized to β-Actin or α-Tubulin, as well as to negative controls.

2.5.4 Western Blot Antibodies

Name	Molecular Weight (kDa)	Secondary Required	Concentration Used	Storage Condition	Source
Cathepsin D	30, 50	Rabbit	1:1,000	-20ºC	Thermofisher
MCL-1	37	Rabbit	1:1,000	-20ºC	Cell Signaling
BCL-2	26	Mouse	1:1,000	-20ºC	Cell Signaling
capsase-3	35	Rabbit	1:1,000	-20ºC	Cell Signaling
Cleaved capsase-3	17	Rabbit	1:1,000	-20ºC	Cell Signaling
PARP-1	86, 113	Rabbit	1:1,000	-20ºC	Thermofisher
LC3A/B	14, 16	Rabbit	1:1,000	-20ºC	Cell Signaling
p62	62	Rabbit	1:1,000	-20ºC	Cell Signaling
β-Actin	42	Mouse	1:10,000	-20ºC	Thermofisher
α-Tubulin	52	Rabbit	1:10,000	-20ºC	Cell Signalling
HRP Goat-anti-Rabbit	N/A	N/A	1:5,000	4ºC	LiCor
HRP Goat-anti-Mouse	N/A	N/A	1:5,000	4ºC	LiCor

Alexa Fluor 488	N/A	N/A	1:2,000	4ºC	Thermofisher

Table 2.1. List of Antibodies Used.

2.6 Acid Spingomyelinase (aSMase) Activity Assay

The Acid Sphingomyelinase Assay Kit is an enzyme assay that determines acid sphingomyelinase activity in biological samples through the direct hydrolysis of a fluorogenic substrate. Steps are adapted from the manufacturers protocol for Echelon Biosciences Acid Spingomyelinase (aSMase) Activity Assay kit catalogue number K-3200. PC3 cells were seeded at $5x10^5$ cells per plate and treated with 10 μM siramesine for 24 hours. DMSO was used as a negative control. Cells were collected into pellets (see Cell Collection) and resuspended with 100μL of Substrate buffer from the aSMase kit and were then sonicated for three 10 second pulses on ice. The sonicated cells were centrifuged at 13,000xG for 15 minutes at 4ºC and the supernatant was collected. The assay kit Substrate and Stop buffers were brought to room temperature, and the Standard and aSMase Substrate were placed on ice. 150μL of Substrate buffer was added to the full vial of Standard, and then diluted through a standard dilution series using 50μL of the previous Standard solution mixed with 50μL of Substrate buffer. 20μL of each standard solution or sample was added to the 96-well round bottom plate included in the kit, and 30μL of Substrate buffer was then added to each well. The plate was tapped for 5 minutes. aSMase Substrate was thawed at 70ºC on a heat block for 1 minute and diluted at 1:40 aSMase Substrate to Substrate Buffer at room temperature. 50μL of the diluted aSMase Substrate was

added to each well. The plate was sealed and incubated at 37ºC for 3 hours. After incubation, 50µL of Stop Buffer was added to each well and incubated at room temperature for 10 minutes. The plate was read using FLUOstar Omega microplate reader (BMG Labtech) at 360nm excitation and 460nm emission to determine the aSMase activity in each well, calculated against the standard curve.

2.7 Microscopy

2.7.1 Lysotracker Microscopy

PC3 cells were seeded at 3 x 10^5 cells per 60mm plate on flame-sterilized glass coverslips and treated for 4 hours with DMSO as a negative control, 0.5 µM lapatinib, 10 µM siramesine or a combination of siramesine and lapatinib. Media was aspirated and cells were stained for 30 mins at 37ºC in the dark with 100nM Lysotracker DND-99 (#L75298, Thermofisher), and fixed for 20 minutes with 1mL 4% paraformaldehyde at room temperature. Cells were washed with PBS and mounted with mounting media made with Mowiol (#475904, Calbiochem) containing DAPI (#D9542, Sigma). Images were obtained by confocal microscopy using Cy3 (Lysotracker) and DAPI channels and the Metamorph software (Molecular Devices). The number of cells with no punctation and/or weak staining were counted and divided by the total number of cells per image.

2.7.2 Cathepsin D Immunofluorescence

PC3 or HEK293 cells were seeded at 3 x 10^5 cells per 60mm plate on flame-sterilized glass coverslips and treated for 4 hours with DMSO as a negative control, 0.5 μM lapatinib, 10 μM siramesine or a combination of siramesine and lapatinib. Media was aspirated and cells were fixed with 4% paraformaldehyde, then permeabilized with methanol and quenched with ammonium chloride (NH_4Cl) (A661-500, Fisher) in PBS before blocking for 1 hour, incubating with a primary Cathepsin D antibody (#PA572182, Thermofisher) for 1 hour, and incubating in the dark for 1 hour with a secondary Alexa Fluor 488 antibody (#A11008, Thermofisher). Cells were mounted with media containing DAPI (#D9542, Sigma). Images were obtained by confocal microscopy using FITC-50 (Cathepsin D) and DAPI-5 channels using the Metamorph software (Molecular Devices). The number of cells with no punctation and/or weak staining were counted and divided by the total number of cells per image.

2.8 Statistical Analysis

Statistical analysis on all data was done using a Student's T-Test with Welch's correction. T-test was done on the replicates (N=3 independent experiments) of each treatment group compared to the replicates of the vehicle control, and between each treatment group. $p<0.05$*, $p<0.01$**, $p< 0.001$***, $p< 0.0001$****.

Chapter 3: Results

3.1 Lysosome disrupting agent siramesine inhibits acid sphingomyelinase (aSMase) in prostate cancer cell line PC3.

It has been previously shown that siramesine is a lysosomotropic agent that accumulates in lysosomes and disrupts the balance of phospholipids in the lysosomal membrane by inhibiting the enzyme acid sphingomyelinase (aSMase), leading to lysosome membrane disruption, the release of lysosomal contents into the cell, and cell death in other cancer types, such as breast cancer[99,177]. To determine whether siramesine inhibits aSMase in prostate cancer cells, I conducted an assay that detects aSMase activity. I treated prostate cancer cell line PC3 with 10 μM siramesine for 24 hours. The cells were lysed and aSMase activity determined (Figure 3.1.). The results showed an approximately 80% reduction which was statistically significant in the aSMase activity in the cells after the treatment. This indicates that siramesine inhibits aSMase activation in prostate cancer cells similar to other cancer cells.

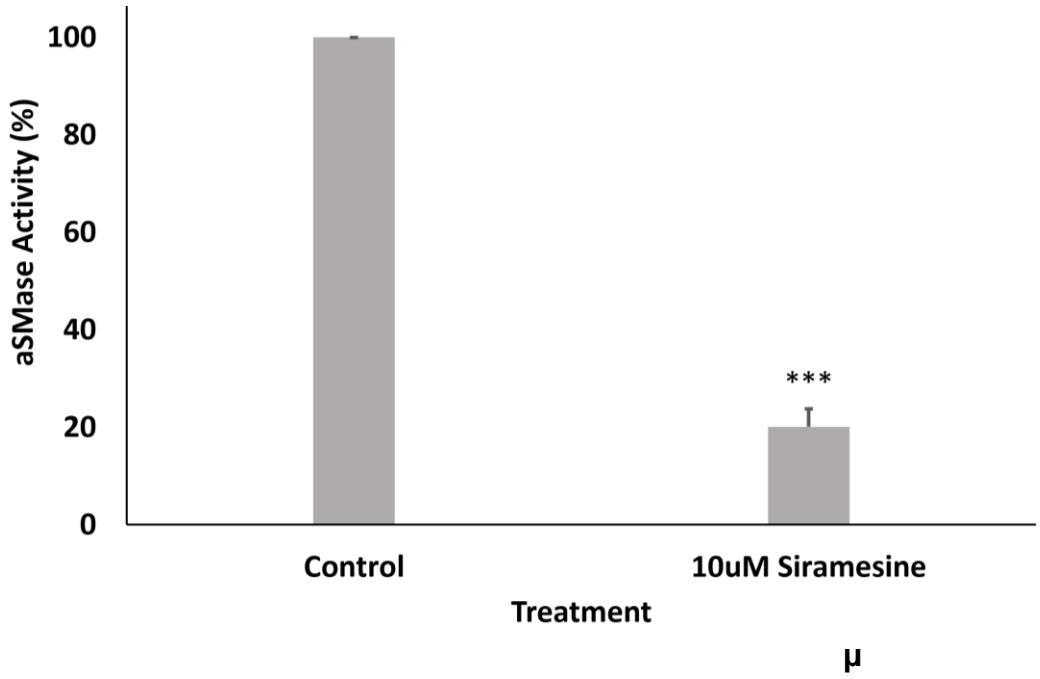

Figure 3.1. PC3 cells treated with 10 μM siramesine for 24 hours show a decrease in aSMase activity as shown by an aSMase activity assay. PC3 cells were seeded at $5x10^5$ cells per plate and grown overnight. DMSO was used as a negative control. $p<0.05$*, $p<0.01$**, $p< 0.001$***, $p< 0.0001$****. N=3 independent experiments.

3.2 Siramesine and lapatinib in combination cause synergistic cell death in prostate cancer cells.

Since the siramesine can inhibit aSMase in prostate cancer cells, and previously it was demonstrated that siramesine in combination with lapatinib induces cell death in other cancer cell lines, I then determined whether siramesine and lapatinib combined increased cell death in prostate cancer cells[177,208]. I treated PC3 cells with 10 μM siramesine, 0.5 μM lapatinib, or in combination for 24 hours and the amount of cell death was determined by Trypan Blue assay. An

increase in the number of Trypan Blue-stained cells compared to the total number of cells corresponds to the amount of cell death, as the Trypan Blue dye enters dead cells with disrupted cell membranes. The combination treatment was able to significantly increase the cell death from 8.7% with siramesine alone and 6.0% with lapatinib alone to 24% in combination (Figure 3.2.). This suggests that the combination of siramesine and lapatinib increased cell death in prostate cancer cells.

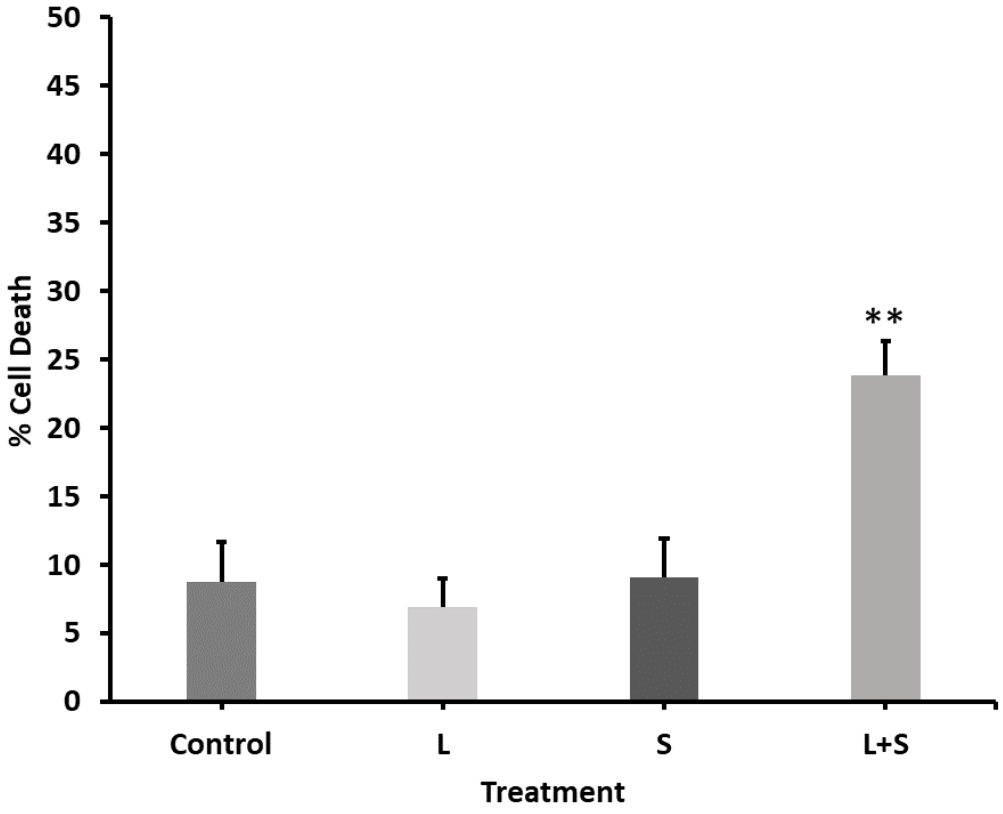

Figure 3.2. PC3 cells treated with a combination of 10 µM siramesine and 0.5 µM lapatinib for 24 hours show significantly higher cell death as determined by Trypan Blue cell exclusion assay. 5 x 10^5 PC3 cells were seeded and treated with DMSO as a negative control (CTRL), 0.5 µM lapatinib (L), 10 µM siramesine (S) or a combination of siramesine and

lapatinib (S+L) for 24 hours after which a Trypan Blue cell exclusion assay was performed. $p<0.05$*, $p<0.01$**, $p< 0.001$***, $p< 0.0001$****. N=3 independent experiments.

To confirm if siramesine and lapatinib treatment increases cell death, cell viability was determined by MTS assay. PC3 cells were treated with10 μM siramesine, 0.5 μM lapatinib, or in combination for 24 hours. I found that cell viability decreased to 88% with siramesine treatment and 80% with lapatinib treatment alone and further decreased to 35% viable cells relative to the negative control condition with the combination treatment (Figure 3.3.). The reduction in cell viability from the control to the combination was statistically significant. These results are similar to the total cell death following treatment and suggest that the combination treatment is increase cell death compared to either drug alone.

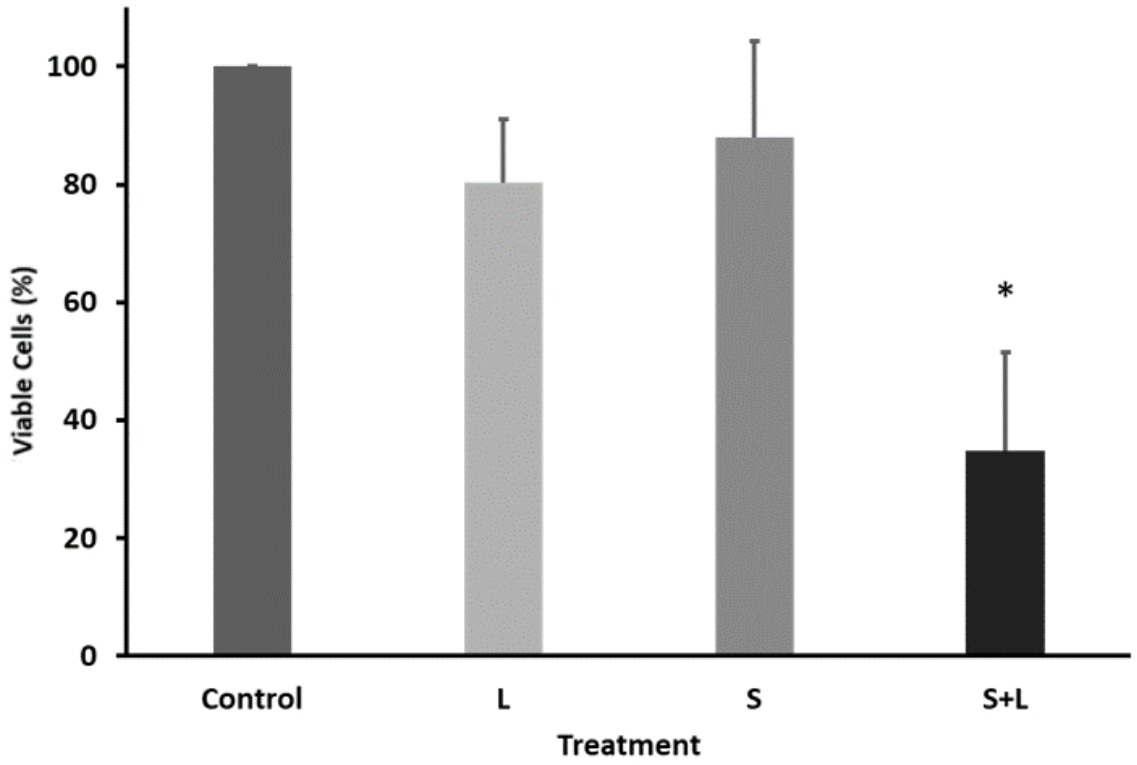

Figure 3.3. PC3 cells treated with a combination of 10 µM siramesine and 0.5 µM lapatinib for 24 hours show significantly decreased cell viability as determined by MTS assay. 5 x 10^5 PC3 cells were seeded and treated with DMSO as a negative control (CTRL), 0.5 µM lapatinib (L), 10 µM siramesine (S) or a combination of siramesine and lapatinib (S+L) for 24 hours after which an MTS assay was performed. $p<0.05$*, $p<0.01$**, $p< 0.001$***, $p< 0.0001$****. N=3 independent experiments.

Since the drug combination increased cell death in PC3 cells, I determined whether this combination treatment gave synergistic cell death. I performed a series of MTS assays on a range of concentrations of siramesine alone and lapatinib alone that would produce the same effect as

the combination treatment of 10μM siramesine and 0.5μM lapatinib. PC3 cells were treated with 0.5, 1, 2, 3, 4, 5, 6, 7, 8, 9, or 10μM of lapatinib, and 5, 10, 15, 20, 25, or 30μM of siramesine for 24 hours, with DMSO-only treated wells as a negative control. After determining these where the IC50 lies based on the concentrations of the individual drugs alone, I inputted them into Chou and Talalay's formula: $Combination\ Index = \frac{(D)1}{(Dx)1} + \frac{(D)2}{(Dx)2}$ where the numerators are the concentrations of the drugs used in the combination treatment and the denominators are the concentrations of the individual drugs required to produce the same effect as the combination, with the subscript 1 assigned to siramesine and the subscript 2 assigned to lapatinib[210]. The combination index determined was 0.7, and as this is less than 1, this indicates that the two treatments are synergistic when combined at the concentrations used (Figure 3.4.).

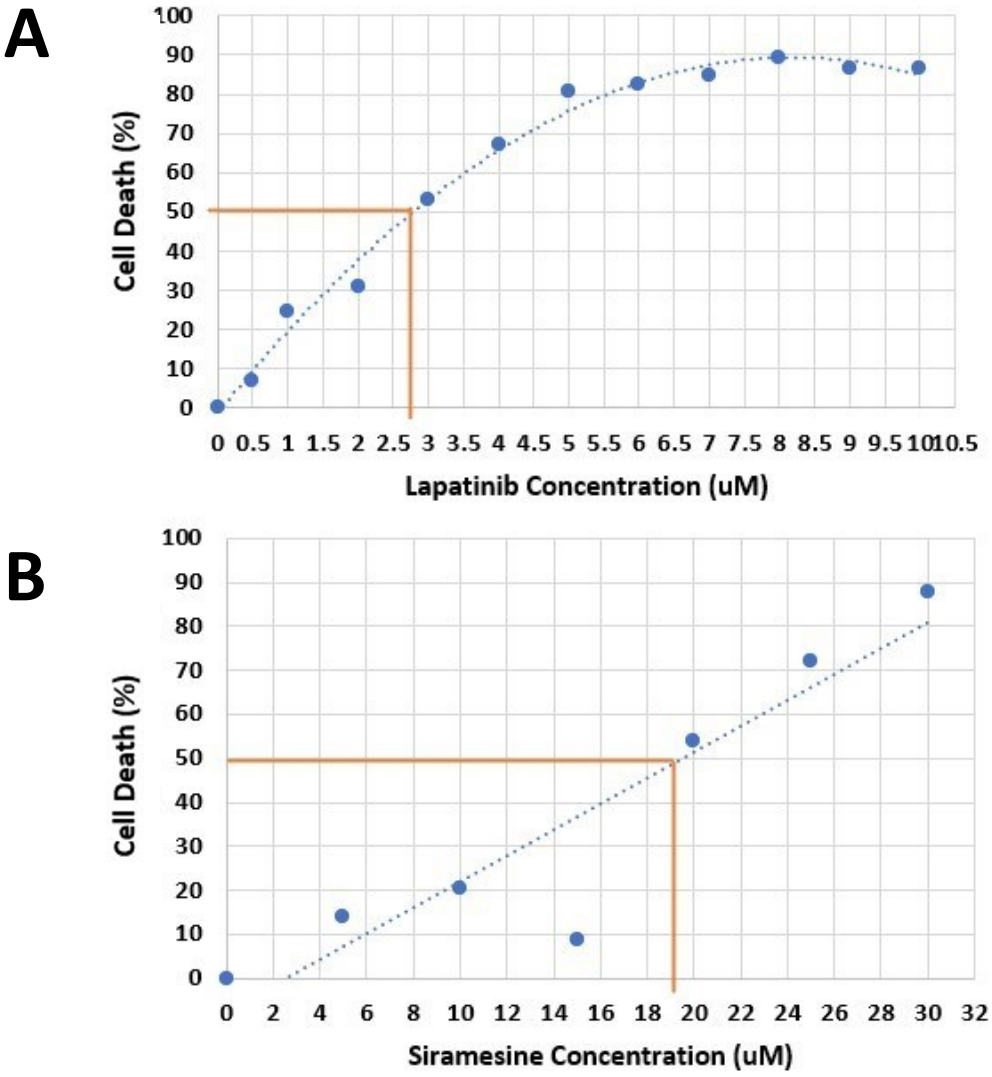

Figure 3.4. Siramesine and lapatinib act synergistically on PC3 cells treated for 24 hours as determined by MTS assay and the combination index. An MTS assay was performed on PC3 cells treated with a range of lapatinib or siramesine concentrations for 24 hours, and the IC50 was determined. N=3 independent experiments.

Next, I determined if the cytotoxicity of the combination of siramesine and lapatinib differs between different cell lines, comparing the effects of the combination on the cancerous PC3 cells with the non-tumorigenic RWPE-1 cell line[211]. The goal of therapy with drugs is to selectively target cancer cells while minimizing the impact on surrounding normal tissue, so the two cell lines were utilized to model this. The metastatic, androgen resistant PC3 cells represent an aggressive form of prostate cancer and this cell line synergistically responded to the siramesine and lapatinib combination treatment (Figure 3.2.). To evaluate whether the combination of siramesine and lapatinib treatment increased cell death in non-transformed prostate epithelial cells, I used RWPE-1 cells as a model a non-cancerous cell type. RWPE-1 and PC3 cells were switched to serum-free medium 2 hours before being treated with 5μM siramesine and 0.1μM lapatinib for 24 hours in serum-free medium. With a background cell death of 22.4% in the RWPE-1 cells, siramesine alone increased cell death to 33.4% percent and the combination further increased the cell death to 52.5%, a statistically significant increase of about 30% from the negative control (Figure 3.5A.). In the PC3 cells, the cell death in the negative control was 9.8%, which was increased to 42.5% with the siramesine and lapatinib combination (Figure 3.5B.). Only the combination had this effect in the PC3 cells, as siramesine and lapatinib alone did not induce a significant increase in cell death, being within 10% of the negative control. This suggests that the combination of siramesine and lapatinib induces cell death to a greater extent in PC3 cells compared to RWPE-1 cells.

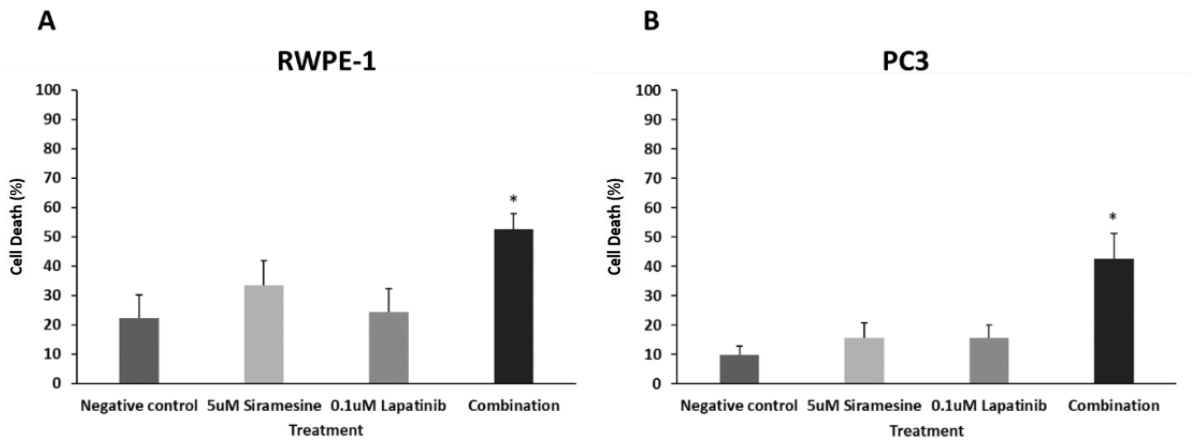

Figure 3.5. Siramesine and lapatinib treatment of RWPE cells compared with PC3 cells. A. 5 x 10^5 RWPE cells were seeded and starved in serum-free media for 2 hours before being treated with DMSO as a negative control (CTRL), 0.1μM lapatinib (L), 5μM siramesine (S) or a combination of siramesine and lapatinib (S+L) in serum-free media for 24 hours after which a Trypan Blue cell exclusion assay was performed. **B**. 5 x 10^5 PC3 cells were seeded and starved in serum-free media for 2 hours before being treated with DMSO (CTRL), 0.1μM lapatinib (L), 5μM siramesine (S) or a combination of siramesine and lapatinib (S+L) in serum-free media for 24 hours after which a Trypan Blue cell exclusion assay was performed. $p<0.05$*, $p<0.01$**, $p< 0.001$***, $p< 0.0001$****. N=3 independent experiments.

I also compared the effects of the siramesine and lapatinib treatment on a less aggressive prostate cancer cell line LNCaP. LNCaP is not castration-resistant, unlike PC3[212,213]. I conducted a Trypan Blue cell exclusion assay for cell death. In the Trypan Blue assay, the LNCaP cells showed a high background cell death of 28% and following lapatinib, siramesine, and combination treatments cell death failed to significantly increase with 24.6%, 32.6%, and 38.7%

cell death respectively (Figure 3.6.). This suggests that siramesine and lapatinib affects aggressive, androgen-resistant prostate cancer more strongly than the androgen-sensitive prostate cancer cells modelled by LNCaP.

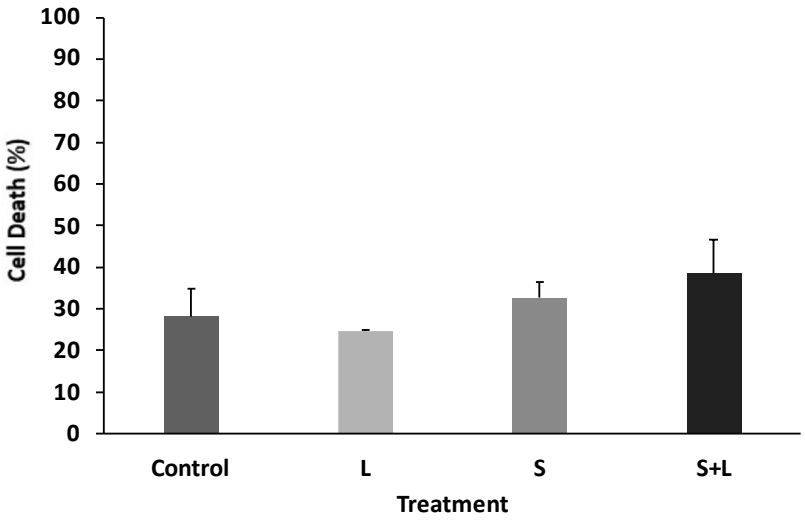

Figure 3.6. 0.5 µM Lapatinib and 10 µM siramesine fail to increase cell death in LNCaP cells after 24 hours. 5 x 10^5 LNCaP cells were seeded and treated with DMSO as a negative control (Control), 0.5 µM lapatinib (L), 10 µM siramesine (S) or a combination of siramesine and lapatinib (S+L) for 24 hours. The cells were then stained with 100nM Lysotracker Red DND-99 for 1 hour at 37ºC in the dark. A Trypan Blue exclusion assay was performed for cell death of LNCaP cells after treatment. $p<0.05$*, $p<0.01$**, $p< 0.001$***, $p< 0.0001$****. N=3 independent experiments.

3.3 The cell death induced by siramesine and lapatinib on prostate cancer cells is caspase independent.

Since siramesine and lapatinib interact synergistically to induce cell death, our next question was what mechanism was mediating this death. To investigate the contribution of apoptosis on the level of cell death observed, PC3 cells were treated with 10 µM siramesine and 0.5 µM lapatinib for 6 hours, 18 hours (Figure 3.7A.) or for 24 hours (Figure 3.7B.). A western blot was performed for common markers of apoptosis such as PARP cleavage or caspase-3 expression and cleavage. At all 3 time points, the treatments did not cause a significant increase in PARP and caspase-3 cleavage. This indicates that the cleavage of caspase-3, an early step in apoptosis, is not induced by the treatment.

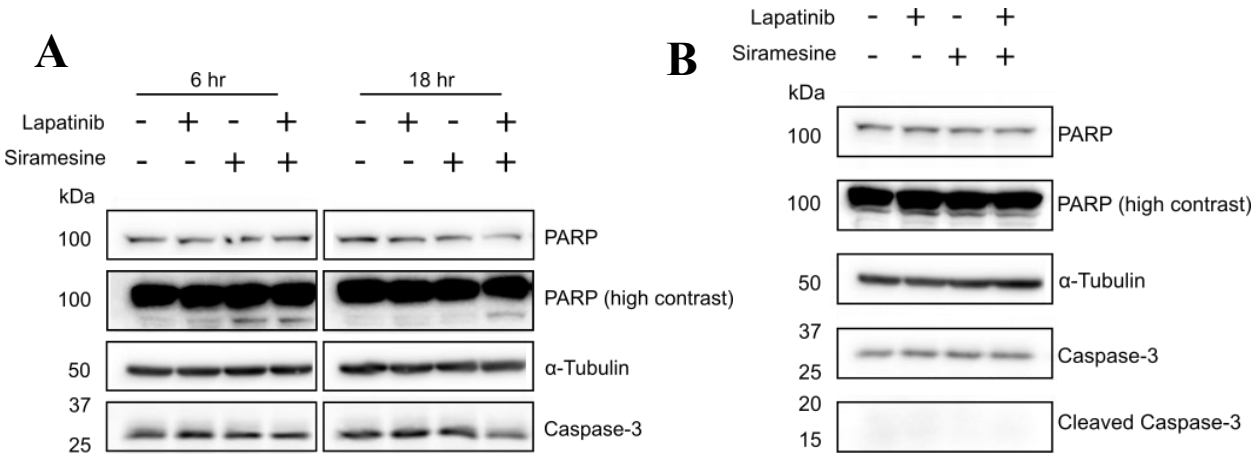

Figure 3.7. PC3 cells treated with a combination of 10 µM siramesine and 0.5 µM lapatinib for 6, 18, and 24 hours do not show increased PARP or caspase-3 cleavage as determined by western blot. Western blot of 5 x 10^5 PC3 cells treated with DMSO as a negative control, 0.5 µM lapatinib, 10 µM siramesine or a combination of siramesine and lapatinib for 6, 18 (Panel A) or 24 hours (Panel B). N=1 independent experiment for A, N=3 independent experiments for B.

To further expand on whether the cell death induced by the drugs is apoptotic and involves the cleavage of caspases, I performed a western blot on PC3 cells treated with 10 µM siramesine, 0.5 µM lapatinib, or both for 24 hours with or without the presence of the caspase inhibitor z-vad. There is a lack of caspase-3 cleavage and PARP cleavage observed after treatment, and the addition of z-vad did not change this observation. Using trypan blue exclusion assay, we found the increased in cell death following treatment with combination was not changed by the presence of z-vad (Figure 3.8.). The combination treatment with and without z-vad had a cell death around 47.5 and 47.3% respectively, indicating that the cell death observed is not affected by inhibition of caspases by the inhibitor, and so a caspase independent form of cell death is occurring.

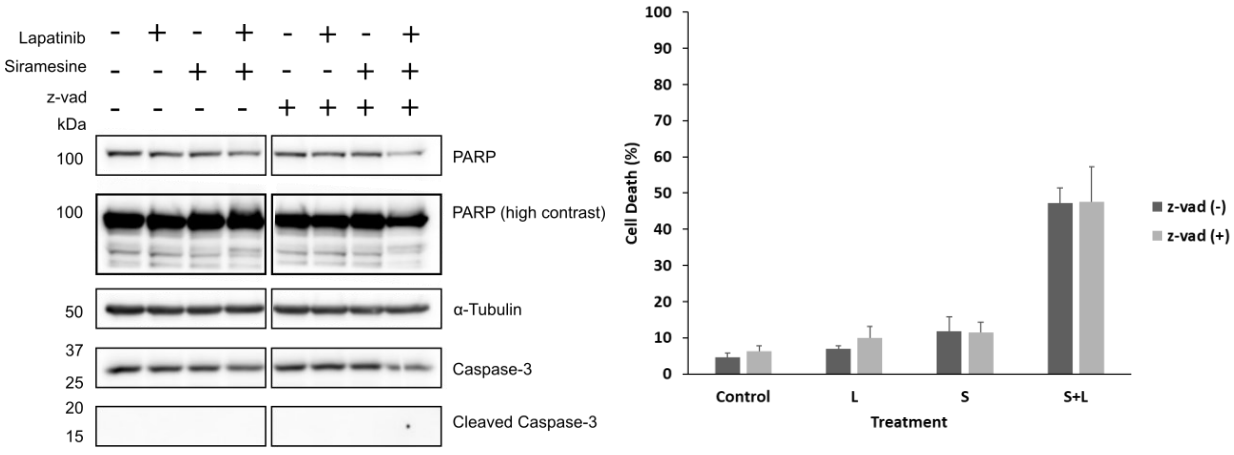

Figure 3.8. z-vad, an inhibitor of apoptosis, does not change the expression of apoptotic pathway proteins after 24 hour siramesine and lapatinib treatment in PC3 cells. A. Western blot of 5 x 10^5 PC3 cells treated with DMSO as a negative control, 0.5 µM lapatinib, 10 µM siramesine, or a combination of siramesine and lapatinib for 24 hours with or without the

addition of 10 μM z-vad for 1 hour prior to treatment. **B.** Trypan blue exclusion assay of PC3 cells after treatment. N=3 independent experiments.

3.4 Siramesine and lapatinib induce lysosome membrane permeabilization in advanced prostate cancer cells.

It has been shown that siramesine induces lysosome disruption in breast cancer cells and my results suggest that the drugs cause synergistic cell death in prostate cancer, so next I determined whether siramesine alone or in combination can cause lysosome disruption resulting in cell death in prostate cancer cells as the lysosome may be a potential target for combination treatments[99,177]. PC3 cells were treated with 10 μM siramesine, 0.5 μM lapatinib, or a combination of both for 4 hours before being washed, fixed, and stained with a fluorescent dye Lysotracker (Figure 3.9.). Lysotracker works by fluorescing when the pH is acidic, as it is a weak base that can diffuse across the lysosomal membrane but becomes protonated and fluoresces at low pH. Punctate fluorescence in cells indicates intact lysosomes, as shown in Figure 3.9B. The number of cells with weak or no staining were counted and divided by the total number of cells in each image to give the percentage of cells without intact lysosomes. From these results, the treatment of PC3 cells with siramesine and the combination decrease the number of intact acidic vesicles so that the number of cells with weak staining after the combination treatment is about 37% compared to the negative control with 10% (Figure 3.9A.). This suggests the combination treatment reduces acidic vesicles in PC3 cells, indicating lysosome membrane permeabilization.

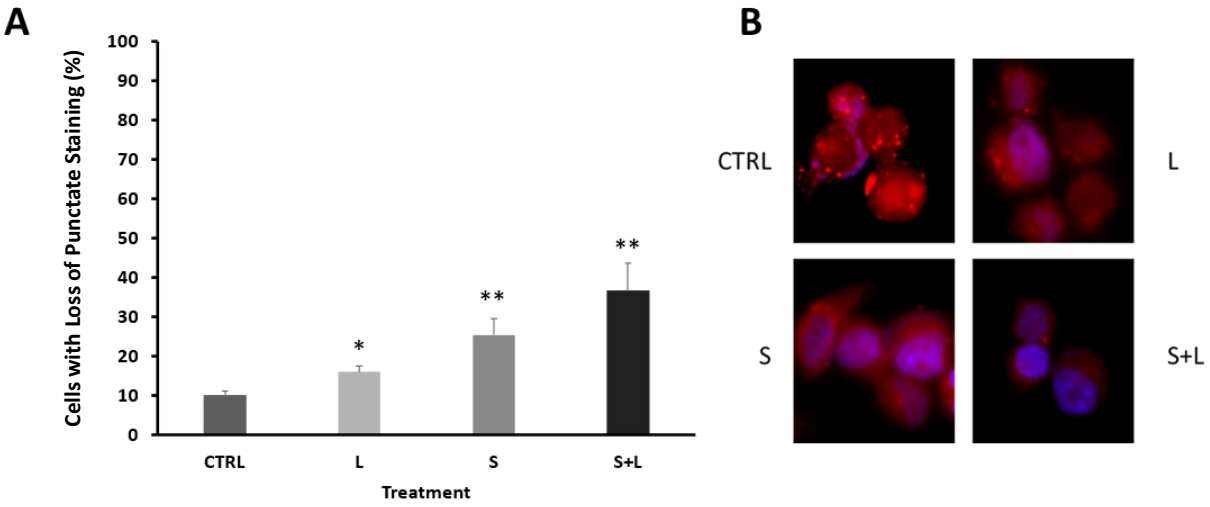

Figure 3.9. Siramesine and lapatinib treatment decreased lysotracker staining in PC3 cells. **A, B.** 3 x 10^5 PC3 cells were seeded per 60mm plate on glass coverslips and treated for 4 hours with DMSO as a negative control (CTRL), 0.5 µM lapatinib (L), 10 µM siramesine (S) or a combination of siramesine and lapatinib (S+L). Cells were stained for 30 mins at 37ºC in the dark with Lysotracker DND-99 and fixed for 20 minutes with paraformaldehyde at room temperature. Cells were mounted with media containing DAPI. Images were obtained by confocal microscopy using Cy3 (Lysotracker) and DAPI channels. **A.** The number of cells with no punctation and/or weak staining were counted and divided by the total number of cells per image. **B.** Confocal microscopy images of PC3 cells. $p<0.05$*, $p<0.01$**, $p< 0.001$***, $p< 0.0001$****. N=3 independent experiments.

To compare the effect of siramesine and lapatinib on lysosome disruption in another prostate cancer cell line I used LNCaP, an androgen sensitive prostate cancer cell line[212,214]. LNCaP cells were treated with 10 µM siramesine, 0.5 µM lapatinib, or a combination of both for

24 hours. I then determined the lysosome disruption using lysotracker and analyzed by flow cytometer. When LNCaP cells were treated with 0.5 µM lapatinib, 10 µM siramesine, or the combination treatment for 24 hours the loss of fluorescence did not change significantly at 6.0%, 6.7%, and 8.6% respectively when compared to the control (7.5%) (Figure 3.10.). Taken together, the androgen-sensitive LNCaP cells were resistant to siramesine and lapatinib treatment.

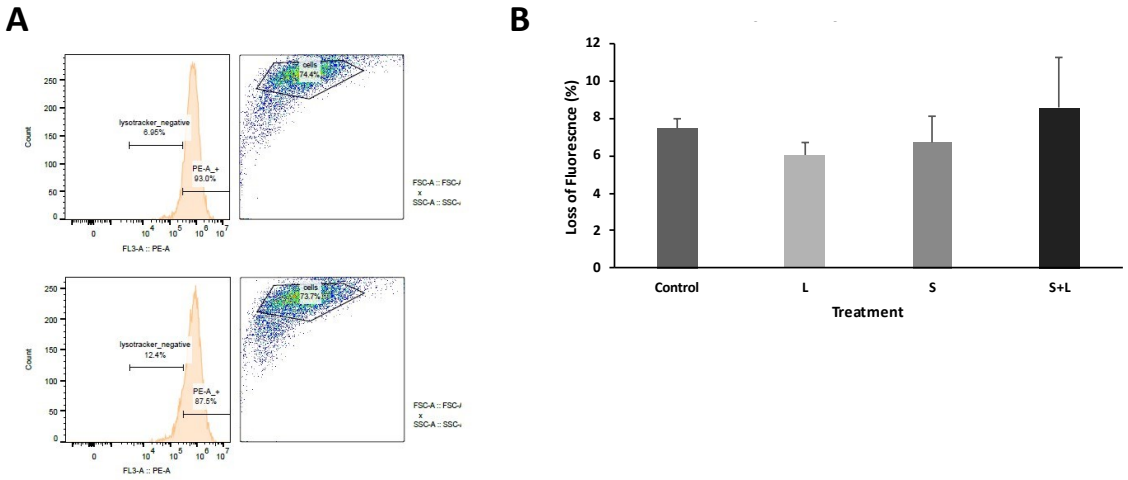

Figure 3.10. Siramesine and lapatinib treatment fails to reduce lysotracker staining in LNCaP cells. C, D, E. 5 x 10^5 LNCaP cells were seeded and treated with DMSO as a negative control (Control), 0.5 µM lapatinib (L), 10 µM siramesine (S) or a combination of siramesine and lapatinib (S+L) for 24 hours and stained with 100nM Lysotracker Red DND-99 for 1 hour at 37ºC in the dark. **C.** Gating for the flow cytometry assay on Lysotracker negative cells in the control (top) and combination (bottom). **D.** Flow cytometry assay on LNCaP cells after treatment. N=3 independent experiments.

3.5 Siramesine and lapatinib cause mitochondrial dysfunction and ROS production in prostate cancer cells leading to cell death.

It has been previously shown that siramesine and lapatinib increase ROS contributing to cell death[99,177]. In addition, previous literature has suggested that siramesine induces apoptotic cell death in PC3 prostate cancer cells, which could occur through caspase-independent apoptosis[196]. One driver for caspase-independent apoptosis is ROS[171,215]. I investigated whether increased ROS generation through siramesine and lapatinib is contributing to the death of these prostate cancer cells. I performed a flow cytometry assay using a stain that detects ROS such as super oxides and hydrogen peroxides known as Dihydroethidium (DHE) in PC3 cells treated for 24 hours with 10 μM of siramesine, 0.5 μM lapatinib, or the combination with or without α-tocopherol, an antioxidant[216,217]. Siramesine and the combination significantly elevated the level of ROS from about 10% in the control to about 20% and 40% respectively (Figure 3.11.). When the antioxidant α-tocopherol is added, cell death from the combination treatment decreased from 45.8% to 7.2%. This suggests that siramesine and lapatinib through their actions on the lysosome can induce cell death by mediating an increase of ROS in prostate cancer cells.

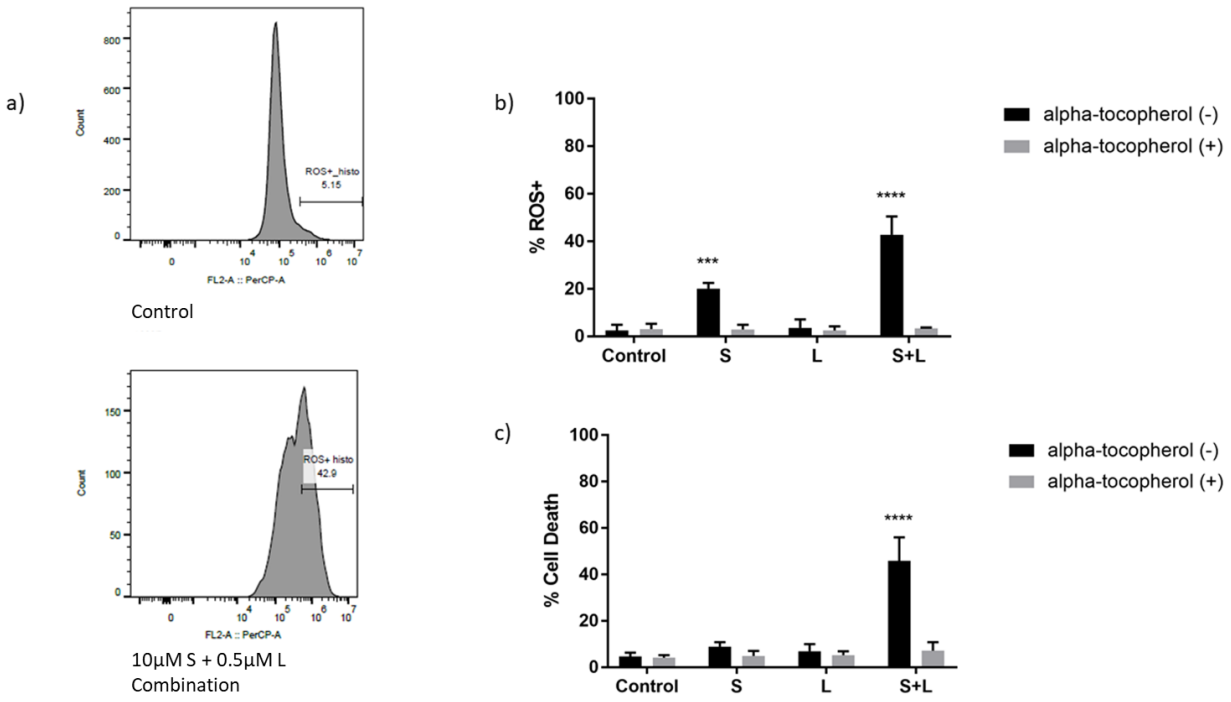

Figure 3.11. PC3 cells treated with siramesine and lapatinib increase ROS levels leading to cell death. A. Gating of the flow cytometry assay on DHE positive cells in the control (top) and combination (bottom) samples. **B.** Flow cytometry assay on 5 x 10^5 PC3 cells treated with DMSO as a negative control (Control), 0.5 µM lapatinib (L), 10 µM siramesine (S) or a combination of siramesine and lapatinib (S+L) for 24 hours with or without the addition of α-tocopherol for 1 hour prior to treatment. Cells were stained with DHE for 30 minutes at 37ºC in the dark. **C.** Trypan Blue cell death of PC3 cells treated with lapatinib, siramesine, or the combination of the two. $p<0.05$*, $p<0.01$**, $p< 0.001$***, $p< 0.0001$****. N=3 independent experiments.

One source of ROS is from the mitochondria and mitochondrial dysfunction contributes to cell death[118,177,218]. To determine if mitochondrial dysfunction might be occurring, I performed a western blot to determine the expression of MCL-1, a BCL-2 family member and anti-apoptotic protein that helps regulate mitochondrial function during cell death[219]. PC3 cells were treated with DMSO as a negative control, 0.5 μM lapatinib, 10 μM siramesine or a combination of siramesine and lapatinib for 24 hours and a western blot for MCL-1 was performed. The combination treatment decreased levels of MCL-1 consistently, with a densitometry of about 0.3 normalized to α-tubulin (Figure 3.12.). This indicates that mitochondria dysfunction is occurring.

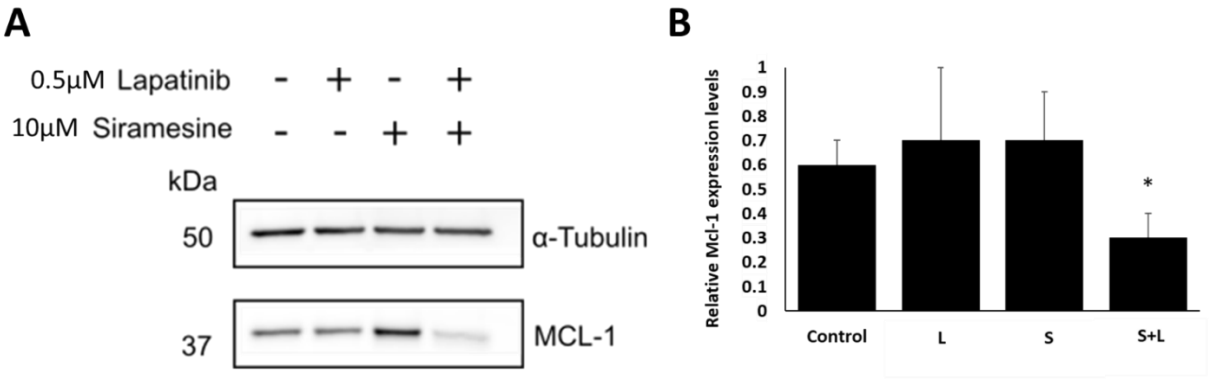

Figure 3.12. PC3 cells treated with siramesine and lapatinib decreased MCL1 expression. **A.** Western blot of 5 x 10^5 PC3 cells treated with DMSO as a negative control, 0.5 μM lapatinib, 10 μM siramesine or a combination of siramesine and lapatinib for 24 hours. **B.** Densitometry of MCL1. N=3 independent experiments.

Given that the previous results suggest mitochondrial dysfunction is occurring, I investigated whether this led to an increase in mitochondrial ROS produced and whether this

contributes to cell death in the prostate cancer cells. To determine mitochondrial generated ROS, I determined the levels of mitochondrial ROS using a flow cytometry assay with MitoSOX Red. MitoSOX Red is specific to ROS such as superoxide present in and produced by the mitochondria[220,221]. PC3 cells treated for 6, 24, and 48 hours with 10 μM of siramesine, 0.5 μM lapatinib, or the combination showed an increase in the number of MitoSOX Red positive cells (Figure 3.13.). At 6 hours the percentage of MitoSOX Red positive cells increased from 16.6% to 28.6% with lapatinib, 87.5% with siramesine, and 88.4% with the combination. Lapatinib and the combination had 34.6% and 61.9% MitoSOX Red positivity after 24 hours, and siramesine had approximately 10%. After 48 hours of treatment, the control has 18.3% of positive cells, while lapatinib, siramesine, and combination treatment increased it to 28.1%, 52.1%, and 78.2%, respectively. This correlated with the amount of cell death following treatment for L and L+S but not S. This indicates that ROS plays a significant role in siramesine and lapatinib induced cell death.

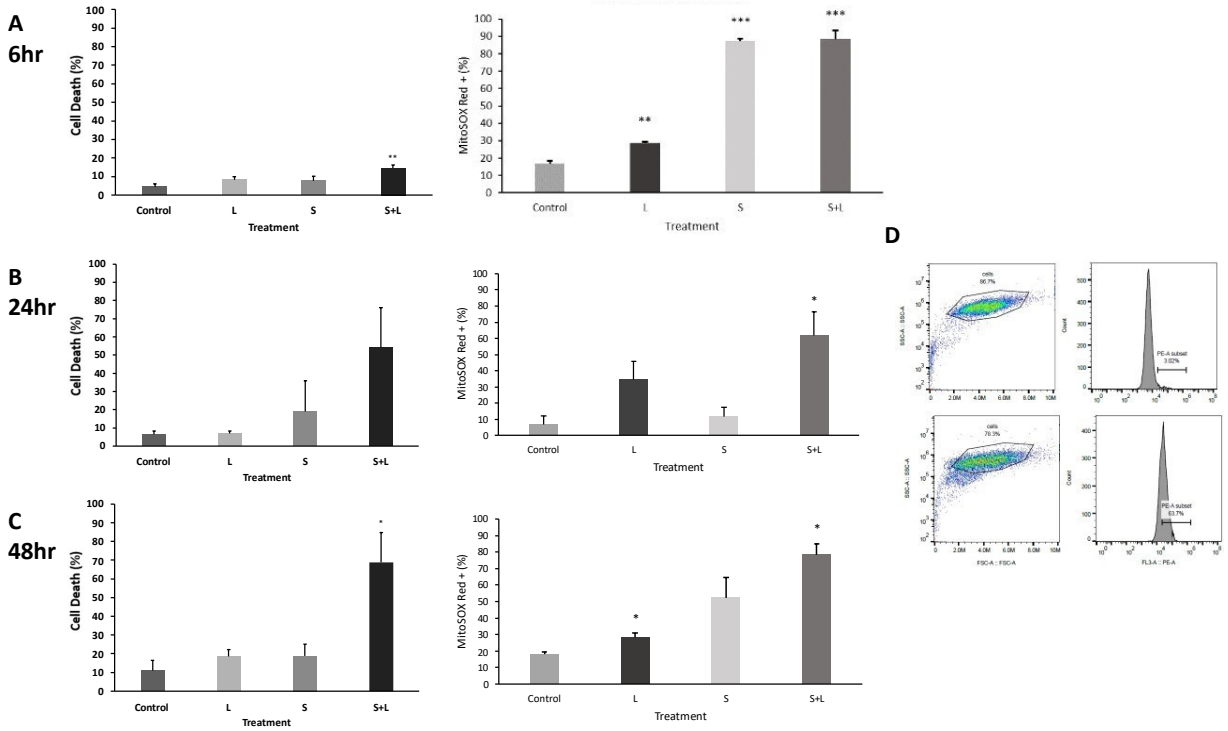

Figure 3.13. PC3 cells treated with siramesine and lapatinib increased mitochondrial ROS levels. A, B, C. 5 x 10^5 PC3 cells were seeded and treated with DMSO as a negative control (Control), 0.5 µM lapatinib (L), 10 µM siramesine (S) or a combination of siramesine and lapatinib (S+L) for 6 hours (A), 24 hours (B), or 48 hours (C). Cells were stained with 50 nM MitoSOX Red for 45 minutes at 37ºC in the dark and flow cytometry was performed. MitoSOX Red was detected using the PE channel. **D.** Gating of the flow cytometry assay on MitoSOX Red positive cells in the control (top) and combination (bottom) samples. p<0.05*, p<0.01**, p< 0.001***, p< 0.0001****. N=3 independent experiments.

3.6 Siramesine and lapatinib cause lysosome membrane permeabilization and the release of cathepsins from the lysosome but failed to result in BID cleavage.

As siramesine and lapatinib can induce LMP and the release of cathepsins from the lysosome, this could consequently result in increased reactive oxygen species (ROS) generation inside the cell and the mitochondria, which could be a factor involved in the cell death pathway [154,170]. To observe if the cathepsins released from the lysosome play a role in the mechanism for cell death initiated by siramesine and lapatinib treatment, I first performed an immunofluorescence experiment to determine if Cathepsin D, an enzyme localized to the lysosome specifically, is released from the lysosome after LMP. To compare the effects on prostate cells to a non-cancerous transformed cell line, I used the human embryonic kidney cell line 293 (HEK293) as a control, which is well characterized[222]. HEK293 (Figure 3.14.) and PC3 (Figure 3.15.) cells were treated with 10 μM siramesine, 0.5 μM lapatinib, or a combination of both for 4 hours before being washed, fixed, and stained with an antibody against Cathepsin D and an Alexa-488 fluorescently labelled secondary antibody. Lack of punctation and more diffuse staining indicates loss of intact lysosomes from disruption of the membrane and spillage of cathepsin D into the cytosol. Comparing the negative control to the combination of siramesine and lapatinib, there is an increase from about 4.4% to 43% for HEK293 cells, and from 7.4% to 40% for PC3 cells, with weak diffuse staining and therefore disrupted lysosomes (Figures 3.14A. and 3.15A.). This suggests the combination of siramesine and lapatinib is causing disruption to the lysosomal membrane, leading to lysosome membrane permeabilization and the release of cathepsin D into the cytosol.

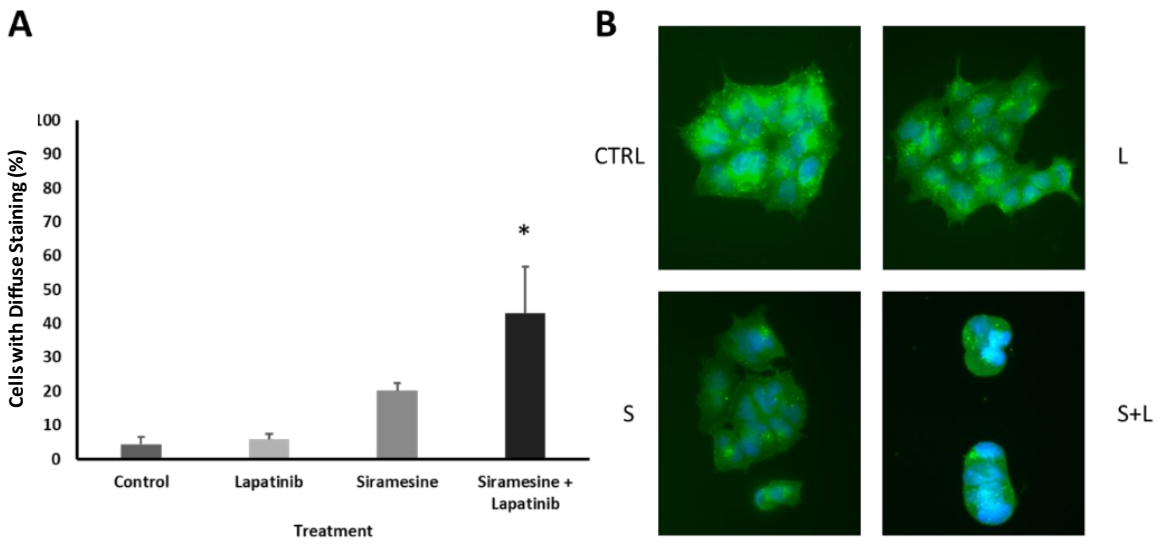

Figure 3.14. HEK293 cells treated with siramesine and lapatinib decreased cathepsin D punctate staining indicating disruption of lysosomes. 3 x 10^5 HEK293 cells were seeded per 60mm plate on glass coverslips and treated for 4 hours with DMSO as a negative control (CTRL), 0.5 µM lapatinib (L), 10 µM siramesine (S) or a combination of siramesine and lapatinib (S+L). Cells were fixed with 4% paraformaldehyde, then permeabilized with methanol and quenched with NH4Cl/PBS before blocking for 1 hour, incubating with a primary Cathepsin D antibody for 1 hour, and incubating in the dark for 1 hour with a secondary Alexa Fluor 488 antibody. Cells were mounted with media containing DAPI. **A.** The number of cells with no punctation and/or weak staining were counted and divided by the total number of cells per image. **B.** Confocal microscopy images of HEK293 cells after treatment. Images were obtained by confocal microscopy using FITC-50 (Cathepsin D) and DAPI-5 channels. $p<0.05$*, $p<0.01$**, $p< 0.001$***, $p< 0.0001$****. N=3 independent experiments.

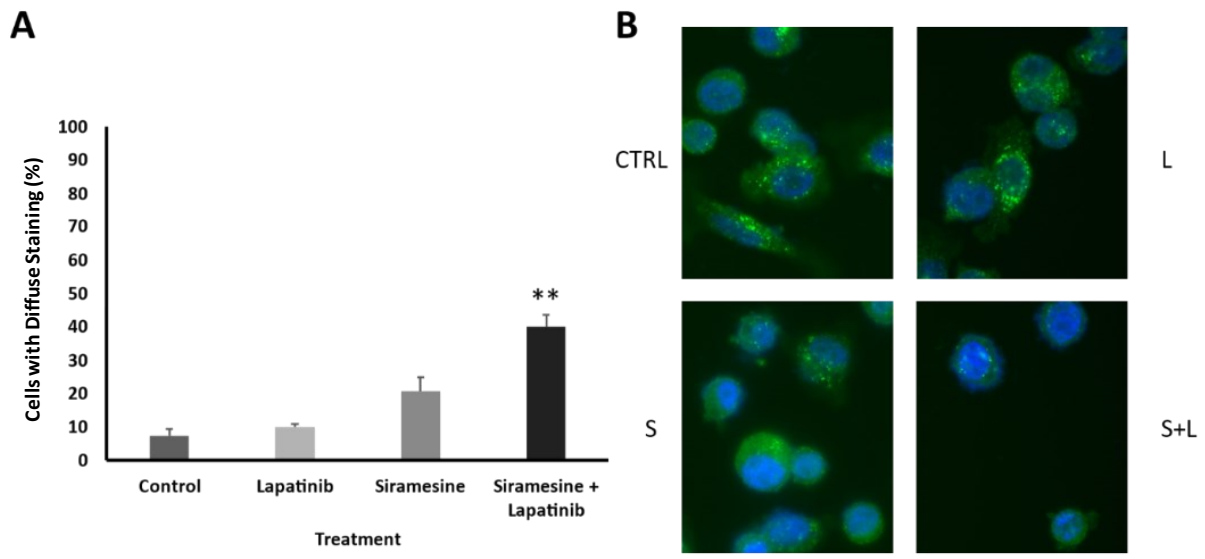

Figure 3.15. PC3 cells treated with siramesine and lapatinib decreased cathepsin D punctate staining indicating disruption of lysosomes. 3 x 10^5 PC3 cells were seeded per 60mm plate on glass coverslips and treated for 4 hours with DMSO as a negative control (CTRL), 0.5 µM lapatinib (L), 10 µM siramesine (S) or a combination of siramesine and lapatinib (S+L). Cells were fixed with 4% paraformaldehyde, then permeabilized with methanol and quenched with NH4Cl/PBS before blocking for 1 hour, incubating with a primary Cathepsin D antibody for 1 hour, and incubating in the dark for 1 hour with a secondary Alexa Fluor 488 antibody. Cells were mounted with media containing DAPI. **A.** The number of cells with no punctation and/or weak staining were counted and divided by the total number of cells per image. **B.** Confocal microscopy images of HEK293 cells after treatment. Images were obtained by confocal microscopy using FITC-50 (Cathepsin D) and DAPI-5 channels. $p<0.05$*, $p<0.01$**, $p< 0.001$***, $p< 0.0001$****. N=3 independent experiments.

To determine if the effects of siramesine and lapatinib-induced lysosome membrane permeabilization are leading to a caspase independent mechanism of cell death, I investigated the effect of the drugs on BID. BID is a BCL-2 family protein that when cleaved (tBID) and activated by caspases can interact with the mitochondrial proteins BAK and BAX to cause their conformational change resulting in pore formation in the mitochondrial membrane in the process of apoptosis[223,224]. Cathepsins have previously been shown to cleave BID in other types of cancer cells[154,224]. To determine whether cathepsin release leads to BID cleavage, I treated cells with the cathepsin inhibitor E-64[225]. A western blot was performed on PC3 cells treated with DMSO as a negative control, 0.5 μM lapatinib, 10 μM siramesine, or a combination of siramesine and lapatinib for 24 hours with or without the addition of 10 μM E-64, the cathepsin inhibitor, for 1 hour prior to treatment (Figures 3.16., 3.17.). In Figure 3.16., there is minimal cleavage of BID, and levels of BID expression do not change significantly from the untreated controls whether it was treated with E-64 or not. The densitometry of BID after the combination treatment without E-64 is about 1.5 with a high degree or variance relative to control. Addition of E-64 decreased the densitometry reading to ~0.6 in the combination treatment lanes. Neither siramesine nor lapatinib treatment caused a statistically significant difference in the densitometry for BID (Figure 3.16. C or D). In Figure 3.17., the PC3 cells show a lack of tBID and change in the expression of BID compared to the untreated control. There were no detectable cleaved BID bands (Figure 3.16. or 3.17.). The cathepsin inhibitor also has no effect on the amount of cell death, with the combination treatment resulting in 51.4% cell death without the inhibitor, and 46.5% with the inhibitor (Figure 3.17B.). Despite Cathepsin D being released from the lysosome after siramesine and lapatinib induced LMP, these results suggest the released cathepsins do not

cleave BID, and inhibiting the cathepsins does not influence the cell death observed after treatment. This indicates that cathepsin release from the lysosome failed to contribute to siramesine and lapatinib induced cell death.

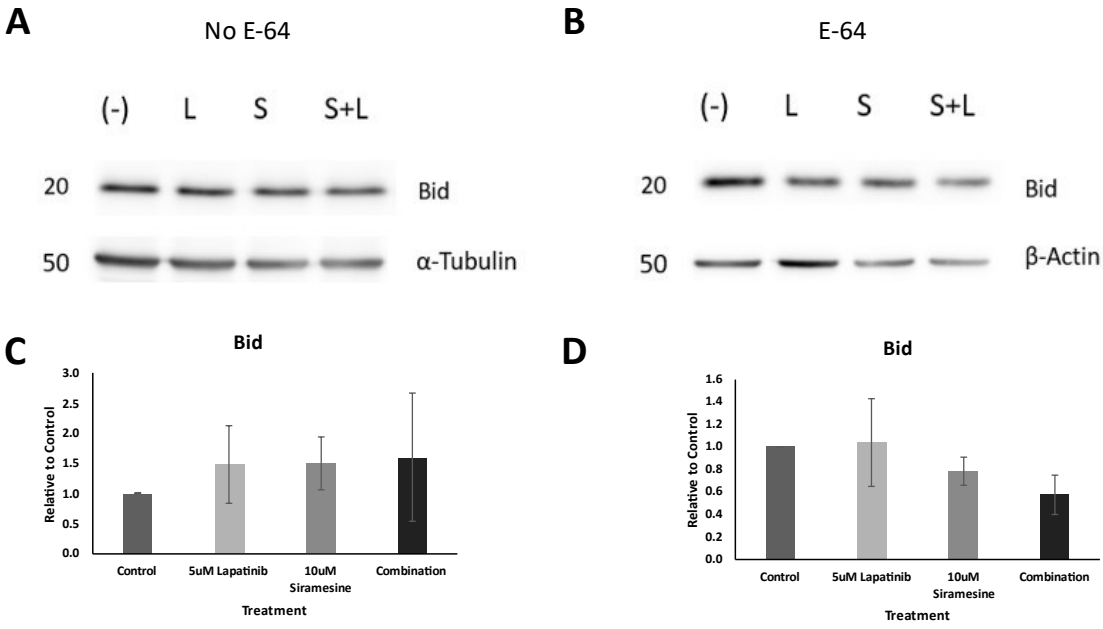

Figure 3.16. PC3 cells treated with siramesine and lapatinib failed to show cleavage of BID. **A, B.** Western blot of 5 x 10^5 PC3 cells treated with DMSO as a negative control, 0.5 µM lapatinib, 10 µM siramesine, or a combination of siramesine and lapatinib for 24 hours with (B) or without (A) the addition of 10 µM E-64 for 1 hour prior to treatment **C, D.** Densitometry of PC3 cells treated with (D) or without (C) E-64 relative to control. N=3 independent experiments.

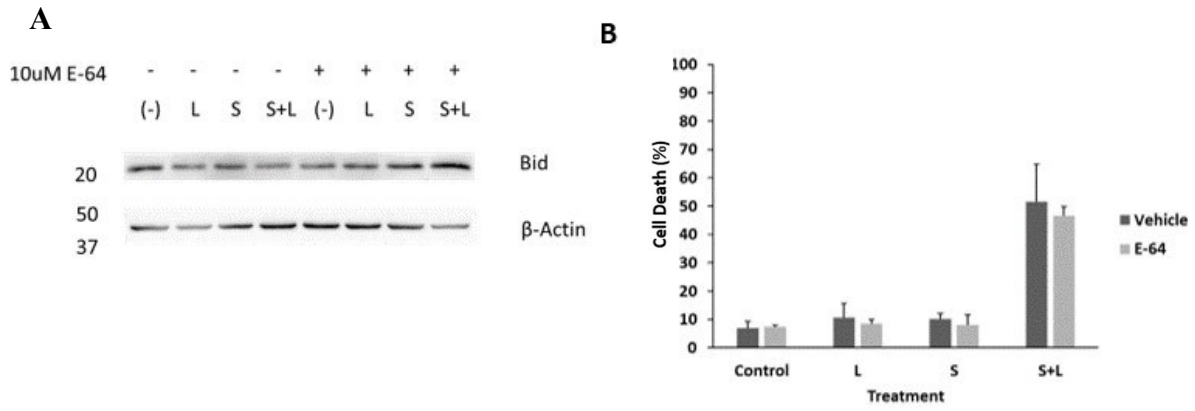

Figure 3.17. The cathepsin inhibitor E-64 fails to reduce cell death in PC3 cells treated with siramesine and lapatinib. A, B. Western blot of 5 x 10^5 PC3 cells treated with DMSO as a negative control, 0.5 μM lapatinib, 10 μM siramesine, or a combination of siramesine and lapatinib for 24 hours with (B) or without (A) the addition of 10 μM E-64 for 1 hour prior to treatment. **C.** Trypan Blue exclusion assay of PC3 cells after treatment. N=3 independent experiments.

3.7 Siramesine inhibits autophagy contributing to cell death when combined with lapatinib.

Autophagy is a process involving fusion of the lysosome to the autophagosome to form the autolysosome, with removing old and damaged organelles as one of its functions. It can have a pro- or anti-tumorigenic effect. To investigate whether siramesine inhibits or promotes autophagy, we evaluated autophagy flux. To measure the effect of siramesine treatment on autophagy flux, I performed a western blot after treating cells with siramesine and the autophagy inhibitor chloroquine. Chloroquine blocks fusion of the lysosome with the autophagosome, preventing the formation of the autolysosome[226]. This leads to the accumulation of autophagy marker proteins such as LC3II and p62. LC3II is also increased if autophagy flux is induced, as LC3I is converted to LC3II during the process of autophagy causing a conformation change that enables LC3II to move faster through the western blot gel. Under increased autophagy flux, combining siramesine and chloroquine will further increase the accumulation of LC3II and p62 protein levels compared to siramesine and chloroquine treatment alone.

Siramesine disrupts the lysosome membranes leading to cell death. Since autophagy requires lysosomes, I determined whether siramesine alone or in combination with lapatinib inhibits autophagy flux. HEK293 cells were treated with 0.5 μM lapatinib or 10 μM siramesine or in combination and 10uM of the autophagy inhibitor chloroquine was added 1 hour prior to treatment to validate and optimize the assay initially (Figure 3.18.). Chloroquine, being an autophagy inhibitor by preventing the fusion of the lysosome to the autophagosome, is expected to cause an increase in the amount of LC3II accumulated. Increasing autophagic flux, for example with starvation, along with the effects of chloroquine cause an even greater accumulation of LC3II. I determined that LC3II levels and ratio to LC3I increase for siramesine

and the combination treatment compared to the control in HEK293 cells, but when adding chloroquine in addition to siramesine, the levels of LC3II are not as significantly elevated as might be expected with increased autophagy flux (Figure 3.18A.,). For example, LC3II levels with the siramesine and lapatinib combination have an average density of 10.1 compared to the negative control and α-tubulin in HEK293 cells (Figure 3.18A.). This changes to 1.7 after adding chloroquine. There is also no further increase in LC3II levels in the combination compared to siramesine alone. When I investigated cell death, siramesine and lapatinib increased cell death from 8.7% in the negative control to 32% with siramesine alone, and 94% with the combination in HEK293 cells, both values being statistically significant (Figure 3.18B.). Adding chloroquine increased the cell death in the HEK293 cells from a baseline of 23% with chloroquine alone to 50% with lapatinib and chloroquine, and 48% with siramesine and chloroquine. When comparing the effects of adding chloroquine to siramesine, the difference is a statistically significant increase from 32% to 48% percent. This suggests that the damage to the lysosomes from the siramesine treatment prevents degradation of LC3 resulting in higher levels of LC3-II in autophagosomes in HEK293 cells, suggesting inhibition of autophagy flux, and that inhibition of autophagy by the chloroquine treatment fails to decrease cell death, which suggests that autophagy does not play a role in driving siramesine induced cell death in HEK293 cells.

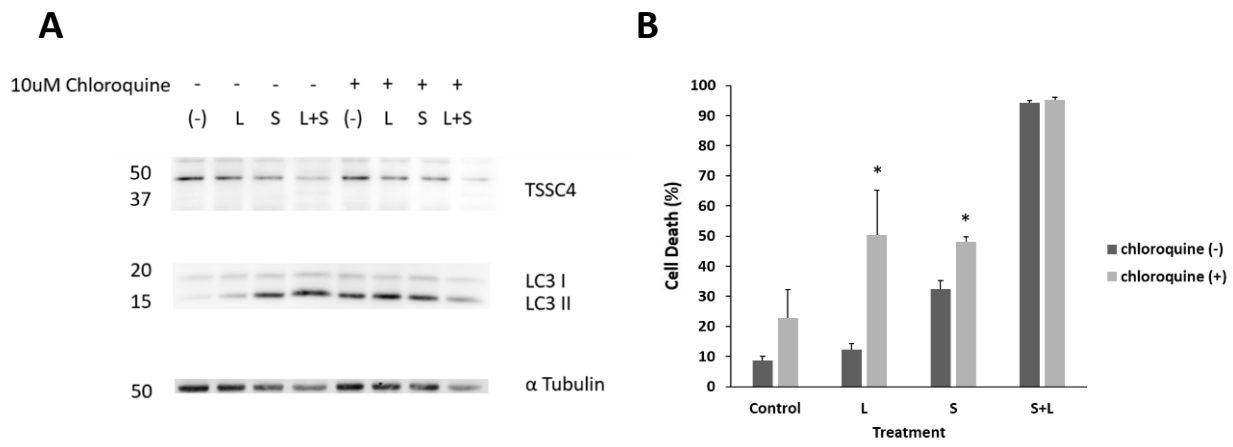

Figure 3.18. Siramesine increases LC3II expression in HEK293 cells and blocking autophagy with chloroquine increases cell death. A. Western blot and **B**. Trypan Blue exclusion assay of 5 x 10^5 HEK293 cells treated with DMSO as a negative control (-), 0.5 µM lapatinib (L), 10 µM siramesine (S) or a combination of siramesine and lapatinib (L+S) with or without 10 µM of chloroquine for 24 hours. N=3 independent experiments.

I also performed the chloroquine assay on PC3 cells (Figure 3.19). PC3 cells were treated with 0.5 µM lapatinib or 10 µM siramesine or in combination and 10uM of the autophagy inhibitor chloroquine was added 1 hour prior to treatment. Similarly to HEK293 cells, in PC3 cells I determined that LC3II levels and ratio to LC3I increase for siramesine and for the combination treatment compared to the control. There is also no further increase in LC3II levels in the combination compared to siramesine alone. However, when adding chloroquine in addition to siramesine, the levels of LC3II are not as significantly elevated as might be expected with increased autophagy flux. This suggests that the damage to the lysosomes from the siramesine treatment prevents degradation of LC3 resulting in higher levels of LC3-II in

autophagosomes in PC3 cells, suggesting inhibition of autophagy flux. When looking at cell death, the PC3 cell death is 10% in the negative control, which is increased to 15% with lapatinib, 13% with siramesine, and 67% with the lapatinib and siramesine combination (Figure 3.19.). Adding chloroquine to these cells results in 21% and 18% cell death when adding chloroquine to lapatinib and siramesine, respectively. The siramesine and lapatinib combination increases cell death when chloroquine is added, being 67% without chloroquine and 84% with chloroquine with no statistically significant difference between these measurements. This indicates that the inhibition of autophagy by the chloroquine treatment fails to decrease cell death, which suggests that autophagy does not play a role in driving siramesine induced cell death.

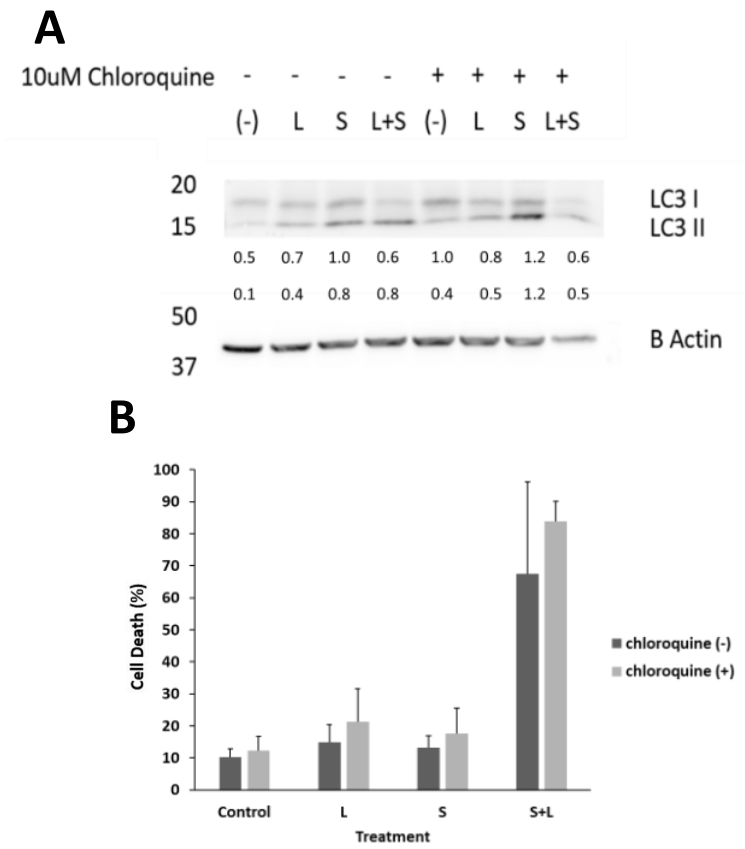

Figure 3.19. Siramesine increases LC3II expression in PC3 cells and blocking autophagy with chloroquine failed to further increased cell death. A. Western blot of 5 x 10^5 PC3 cells treated with DMSO as a negative control (-), 0.5 µM lapatinib (L), 10 µM siramesine (S) or a combination of siramesine and lapatinib (L+S) with or without 10 µM of chloroquine for 24 hours. **B**. Trypan Blue exclusion assay of PC3 cells after treatment. N=3 independent experiments.

This was also repeated in both cell lines with 10 µM of siramesine, 10 µM of chloroquine or in combination for 24 hours and I found a similar trend, as LC3II band density was about 11.9

with siramesine alone in PC3 cells, and 5.9 when chloroquine was added (Figure 3.20A.). In HEK293 cells, this was about 5.0 and 4.6 for siramesine alone and siramesine combined with chloroquine, respectively. This suggests that the damage to the lysosomes from the siramesine treatment prevents degradation of LC3 resulting in higher levels of LC3-II in autophagosomes.

In Figure 3.20., when comparing the cell death of HEK293 cells, siramesine alone had 70% cell death compared to the control which had 29%, and chloroquine and siramesine together had 55% cell death (Figure 3.20C.). The decrease in cell death when comparing the combination of siramesine and chloroquine to siramesine alone is not statistically significant. For PC3 cells, siramesine alone had 14% cell death compared to the control which had 7.6%, and chloroquine and siramesine together had 14% (Figure 3.20B.). Both siramesine alone and the siramesine chloroquine combination had similar cell death for the PC3 cells with no statistically significant difference between them. This indicates that autophagy does not play a role in driving siramesine induced cell death, as the inhibition of autophagy by the chloroquine treatment fails to decrease cell death.

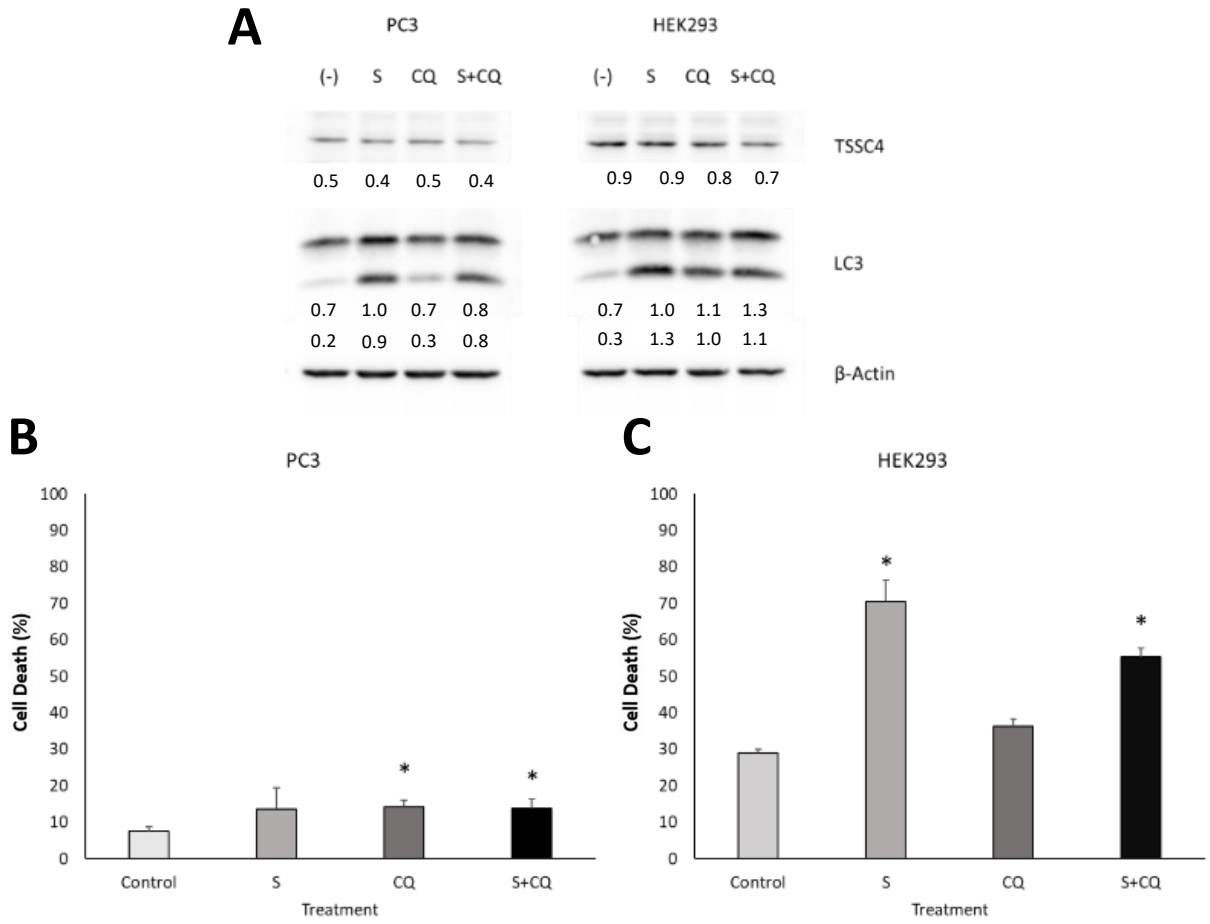

Figure 3.20. Siramesine increases LC3II expression in PC3 and HEK293 cells and blocking autophagy with chloroquine failed to further increased cell death. A. Western blot of 5 x 10^5 PC3 and HEK293 cells treated with DMSO as a negative control (-), 10 µM siramesine (S), 10 µM of chloroquine (CQ), or a combination of siramesine and chloroquine (S+CQ) for 24 hours. **B, C**. Trypan Blue exclusion assay for cell death on PC3 cells (B) and HEK293 cells (C) after treatment. N=3 independent experiments.

To further confirm whether autophagy is inhibited after siramesine treatment, p62 levels were determined by western blot after treatment. p62 cargoes molecules to the autophagosome and gets degraded by the autolysosome[227]. Using lysosome inhibitors such as chloroquine will prevent the formation of functional autolysosomes and the degradation of p62, so if there is an increase in autophagy flux, p62 after treatment with chloroquine will accumulate. PC3 cells were treated with 10 μM siramesine, without or without 20 μM chloroquine added 1 hour prior, and the cellular proteins were isolated and western blotted for p62 levels. Treatment with siramesine failed to decrease p62 levels and when siramesine is combined with 20μM chloroquine, p62 levels increased to about 1.1 with siramesine alone and to 1.7 with the siramesine chloroquine combination compared to the control after densitometry analysis (Figure 3.21.). This indicates the siramesine fails to induce autophagy in PC3 cells.

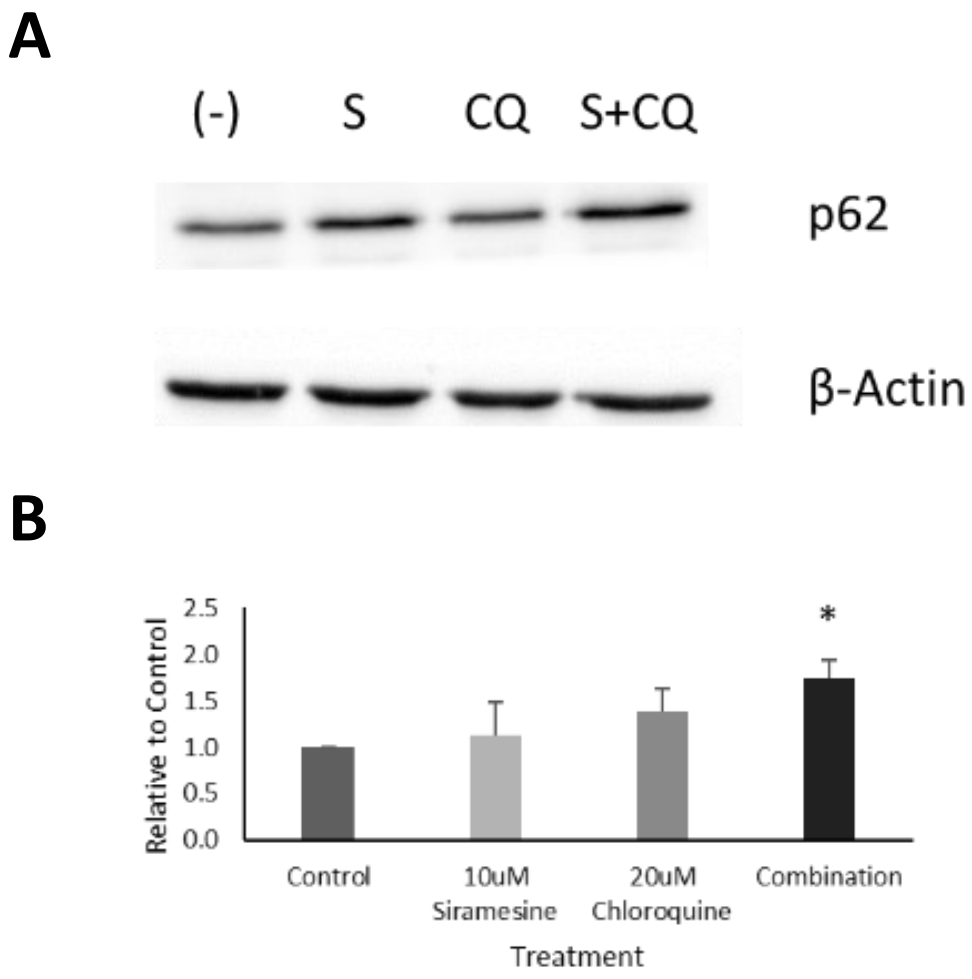

Figure 3.21. There is no decrease in p62 in PC3 cells treated with siramesine or chloroquine. A. Western blot of 5 x 10^5 PC3 cells treated with DMSO as a negative control (-), 10 μM siramesine (S), 20 μM chloroquine (CQ) or a combination of siramesine and chloroquine (S+CQ) for 24 hours. **B.** Densitometry of p62 in western blot relative to the negative control. N=3 independent experiments.

Starvation increases autophagy leading to cell survival in some cases and cell death in others[228]. To determine whether siramesine treatment increases starvation induced cell death, PC3 cells were treated with siramesine alone or in starvation conditions using serum-free media for 24 hours. I found that LC3II levels increased under normal and starved conditions compared to the control groups of each category, but the starvation condition failed to further increase LC3II levels (Figure 3.22B.). Average LC3II densitometry is about 3.6 with siramesine in normal conditions relative to the control, and in starvation with siramesine the density is about 2.7 with negligible statistical difference between these values. Furthermore, siramesine increased cell death from 7% in the untreated starvation condition to 50% under starvation and siramesine treatment, a statistically significant increase. This suggests that siramesine inhibits autophagic flux and further increases starvation induced cell death.

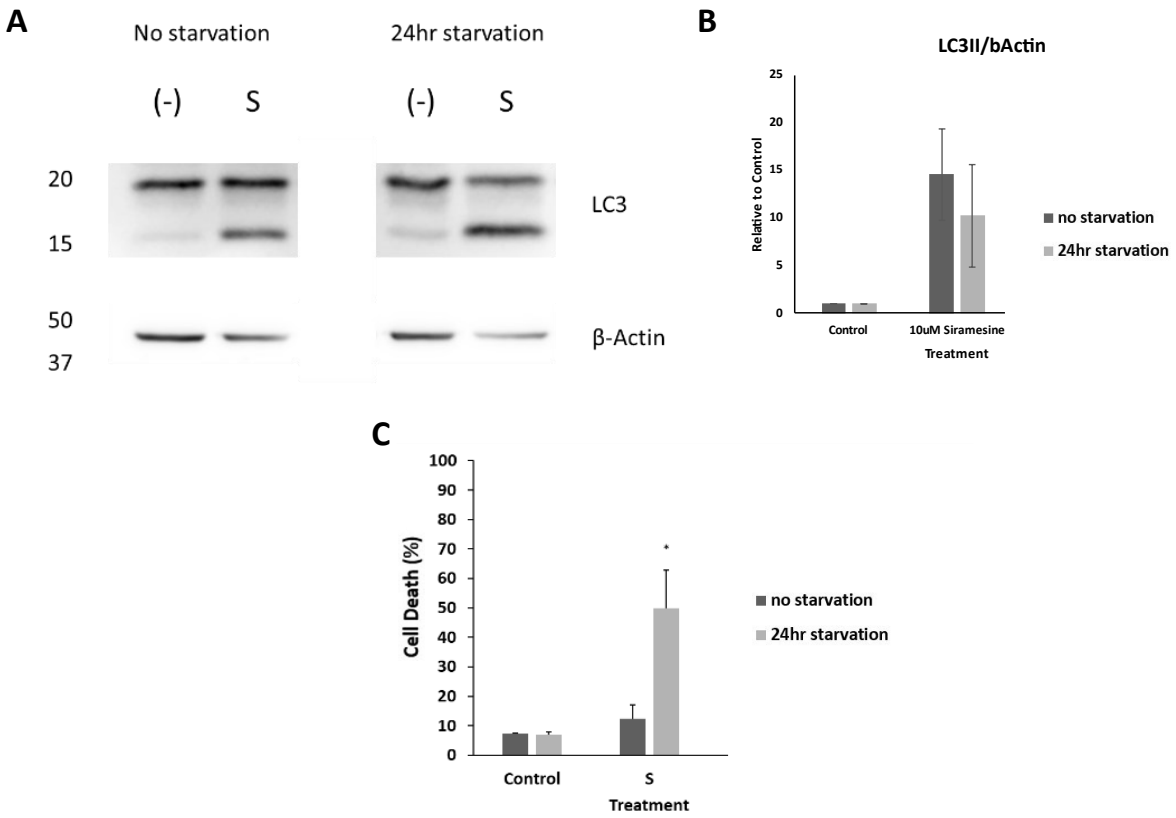

Figure 3.22. Starvation does not increase the amount of LC3II in PC3 cells treated with siramesine. A. Western blot, **B**. densitometry of LC3I, LC3II, and p62 compared to untreated control samples under 24 hour starvation or no starvation, and **C**. Trypan Blue exclusion assay for cell death of 5 x 10^5 PC3 cells treated with DMSO as a negative control (-), 10 µM siramesine (S), or 10 µM chloroquine (CQ) with or without starvation for 24 hours. N=3 independent experiments.

Chapter 4: Discussion

4.1 Discussion

Drug resistance is a major problem occurring in prostate cancer. In castration resistance in prostate cancer, treatment with ADT is ineffective requiring the need for alternative therapy strategies and drug combinations[229]. As prostate cancer cells are more sensitive to lysosome membrane permeabilization and have increased lysosome size and number of lysosomes compared to non-cancerous cells, targeting the lysosome is one strategy for overcoming drug resistance in advanced prostate cancers[105]. Combination therapy supports this strategy by affecting multiple pathways that can interplay and convergently affect the lysosome in cancer cells leading to various forms of cell death[230]. My results indicate that the lysosomotropic agent siramesine alone and in combination with the tyrosine kinase inhibitor lapatinib leads to synergistic cell death in the castration resistant p53 mutated PC3 prostate cancer cells.

Siramesine was initially developed as a drug for depression treatment due to its ability to inhibit sigma-2 receptors and does not have FDA approval as a cancer treatment, but research has shown that if repurposed as a lysosomotropic agent it can effectively cause cell death in a variety of cancer cell lines[99,177,194–196,218]. Siramesine has been demonstrated to kill breast, CLL and glioblastoma cells and the form of cell death varies by cancer type[99,156,177,231,232]. Among all the lysosomotropic agents tested, siramesine was demonstrated to have the most potent killing effect on prostate cancer PC3 cells, and when combined with lapatinib this effect is further increased[196]. Siramesine and lapatinib combination were able to increase ROS and induced cell death in PC3 cells that was attenuated by adding the antioxidant α-tocopherol. This indicates that

ROS contributes to prostate cancer cell death, which could result from the lysosome membrane's sensitivity to disruption by ROS because unlike other organelles, lysosomes lack enzymes like superoxide dismutase, catalase, or glutathione peroxidase that could act as antioxidants[105]. In addition, siramesine induced cell death involves mitochondrial ROS and loss of mitochondrial membrane potential. In other cell types such as breast cancer, leukemia, and glioblastoma cells, siramesine also increased ROS and treatment with antioxidants reduced siramesine induced cell death[99,156,177,194]. Thus, siramesine is an effective lysosome disrupting agent leading to cell death mediated by ROS.

Lysosome disruptors like siramesine can cause the lysosome content to release into the cytosol which can activate other intracellular signalling pathways such as release of cathepsins[162,233]. Cathepsins are proteases that are located within the lysosome[109]. Cathepsins leaked from LMP have been shown to cleave BID, causing an apoptotic cell death pathway activation as the cleaved BID cleaves BAX/BAK on the mitochondria, and connects lysosome disruption with mitochondrial dysfunction[118,234]. In other cancer types, cathepsins have been implicated in cell death resulting from treatment. For example, in CLL cells treated with valproic acid, cathepsin B is released and plays a role in cell death[235]. In contrast, siramesine induced release of cathepsin B in CLL cells fails to contribute to cell death[156]. My results indicate that siramesine and lapatinib treatment causes the release of cathepsin D into the cytosol of prostate cancer cells, but the cell death observed is independent of this given that inhibition of cathepsin function with E-64 does not decrease cell death. The treatments and subsequent cathepsin release also failed to cause significant BID cleavage. One possible explanation for this is the inactivation of cathepsins in the neutral pH of the cytosol[236]. However, other studies do show cathepsins

playing a role in prostate cancer cell growth and proliferation, such as work done by Park et al. in 2020 showing that knockdown of cathepsin A leads to inhibition of PC3 and Du145 cell proliferation and migration[237]. The extent and time of the release of cathepsins could also impact their ability to contribute to cell death. Taken together, cathepsins might not be essential to induce lysosome mediated cell death in prostate cancer cells.

Many lysosomotropic agents have been identified to induce cell death in cancer cells. Cationic amphiphilic drugs (CADs), incorporate into lysosomal membranes and neutralize the pH in the lysosome luminal space[197,198,238]. This leads to inhibition of enzyme activity such as cathepsins and lipases. There are over 30 different CADs that have shown cytotoxicity in cancer cells and demonstrate lysosome membrane permeabilization[197]. CAD antihistamines are effective at inducing lysosome-mediated cell death and patients taking antihistamines during chemotherapy showed reduced patient mortality rates. A study by Garcia et al. showed that clemastine, desipramine, and siramesine cause cell death in prostate cancer cell lines including PC3 cells after 24 hours of treatment[196]. Another lysosomotropic agent is tetrahydrocannabinol, the active component of Cannabis[239]. Tetrahydrocannabinol destabilizes lysosomes by inhibiting the enzyme dihydroceramide desaturase (DEGS1) leading to cell death. In a clinical trial, tetrahydrocannabinol treatment of glioblastoma patients indicated it could potentially increase survival[240]. Antibodies directed against CD20 have also shown lysosome disrupting activities in leukemia cells, but the mechanism is still unclear[241]. Drugs, such as antimalarial drugs, can also accumulate in lysosomes increasing ROS production leading to cell death[242]. Besides small-molecule drugs, nanoparticles can target the lysosome inducing LMP[243–245]. In addition, they can deliver chemotherapy or targeted therapy drugs to cancer cells. This is an attractive approach as I

demonstrated lapatinib and siramesine can induce synergistic apoptotic cell death and if targeted to cancer cells could overcome the issue of resistance while limiting toxicities on healthy cells. Further research is necessary to determine if lysosomotropic drugs will be effective in the clinical setting.

Lysosome-mediated cell death leads to different forms of programmed cell death. Previous research suggested this combination of siramesine and lapatinib induces apoptotic cell death as determined by an Annexin V assay in CLL cells, but in prostate cancer cells, I showed inhibiting caspases with z-vad fmk does not mitigate the amount of cell death[196]. In breast cancer cells, the combination of siramesine and lapatinib induced iron-dependent cell death called ferroptosis[99,177]. When cell death was examined at later time, it was shown breast cancer cells were dying from autophagy-mediated cell death[177]. Other lysosomotropic agents can trigger activation of NLRP3 inflammasomes leading to pyroptosis and could be regulated by the release of lysosomal cathepsins[183,246]. Based upon my results and other published reports, it seems the ability of lysosome disruption to induced different types of cell death depends upon the cellular context and needs to be further investigated.

Lysosome membrane disruption leading to cell death is regulated by the sphingolipid pathway[156,192,247]. Siramesine is an effective inhibitor of acid sphingomyelinase (aSMase) leading to LMP[156,192]. Indeed, I found that siramesine can effectively block the activity of acidic sphingomyelinase, an enzyme in the lysosome that breaks down sphingomyelin into ceramide in prostate cancer cells. Many other CADs can inhibit sphingomyelin phosphodiesterase (SMPD1) leading to LMP[192,199,248–250]. It has also been shown that siramesine induces cell death in CLL cells altering sphingosine levels and causing LMP[156]. Other researchers have found that in

glioma cells, the accumulation of sphingomyelin leads to cell death, and cancer cells are more sensitive to this compared to non-malignant cells[251]. The cancer cells also showed lower baseline levels of sphingomyelin. The balance of phospholipids in tumor cells as well as their lysosomal membranes is critical for the outcome of cancer cells, and disruption of this balance can lead to cell death[192,197,198,247]. In CLL cells, sphingosine levels are increased and when sphingosine was added to CLL cells, lysosome membrane permeabilization and cell death was observed[118]. Alterations in sphingolipid pathways have been described in many cancers[127,192]. This impacts cellular homeostasis and metastasis in cancer cells. Taken together, this suggests that targeting lysosomes will be an effective treatment in many types of cancers.

An alternative use for lysosomotropic agents like siramesine has the potential to enhance immunotherapy against prostate cancer, which has a relatively “cold” tumor environment that prevents the recruitment of immune cells and their anti-tumor actions[252]. Various clinical trials for immunotherapy options such as Sipuleucel-T, anti-PD1 or PD-L1 therapy, have shown varying levels of success with metastatic castration resistant prostate cancer, but using siramesine or other LMP inducing agents in combination with immunotherapy could be investigated to increase the effectiveness of these treatments[78–80]. It has been shown that ROS generation leading to lysosome membrane disruption can induce a form of cell death known as “immunogenic cell death,” which stimulates immune cells to mount a response against the dying cell[105]. Immunogenic cell death has 2 proposed mechanisms, one intrinsic and one extrinsic, and involves immune cells. Because this study was only done in cancer cell lines, determining if siramesine could cause immunogenic cell death would require an *in vivo* animal model or immune cell co-culture. Potentially the combination with siramesine can produce a "hot" tumor

microenvironment given that it causes ROS increase, LMP, and cell death resulting in the cell displaying dead cell markers and benefiting immunotherapies being used against advanced prostate cancer. This reflects work done by Fossel et al., where the prostate cancer cell line Du145 showed lysosome disruption and cell death after being treated with p-LDL resulting in increased ROS around the lysosome[253]. In another study, researchers showed activating xanthine oxidase with Alternol showed similar effects in prostate cancer cells but not in non-tumor cells[254]. In both studies, lysosome-induced immunogenic cell death was activated directly by the actions of the oxidation-related damage causing agents, and so combining siramesine is an avenue to further contribute to this form of cell death in cancer cells that are resistant to other forms of immunotherapy.

Autophagy plays a role in maintaining cellular homeostasis and is a process that involves the fusion of lysosomes with autophagosomes[114]. Previous literature shows autophagy can also contribute to both cell survival and cell death functions[115,116,129,255]. When basal autophagy is active, it promotes tumor cell survival by ensuring nutrient recycling in adverse cell conditions but increasing autophagy can become unsustainable resulting in cell death [129]. Given that the lysosome is involved in autophagy, targeting the lysosome with drugs like siramesine can disrupt autophagy. In a 2017 study by Ma et al., they found that in addition to ferroptosis, the combination of siramesine and lapatinib induces autophagic cell death in breast cancer cells at later times[177]. This correlated with increased autophagosomes after the combination treatment of siramesine and lapatinib. In prostate cancer cells, I showed that siramesine can inhibit autolysosome formation and increase autophagosomes without significantly increasing autophagic flux. Further work is required to determine the extent to which autophagy is

protective against the combination of siramesine and lapatinib for prostate cancer cells, and if blocking autophagy flux through the combination treatment blocks cell survival. Siramesine is not the only drug that is able to cause lysosome permeabilization leading to inhibition of autophagy. One type of LMP agent is chloroquine analogs that can target the lysosome, similar to how siramesine targets it to prevent autophagy and induce LMP[256]. In addition, these chloroquine derivatives block the process of autophagy, contributing to their cancer killing ability. Previous literature has shown that chloroquine analogs are able to cause apoptosis to occur in breast cancer, colon cancer, and glioblastomas alone or in combination with chemotherapy[256]. For example, the chloroquine derivative LYS05 can be used as single agent and can also be used with protein kinase inhibitors such as BRAF inhibitors to induce cell death[256,257]. However, some chloroquine derivatives result in various downsides. One such example is HCQ which has been given in combination therapy, and clinical trials treatment with HCQ has resulted in side effects such as neutropenia, thrombocytopenia, and sepsis[258]. Other drugs that act as lysosomotropic agents similarly to siramesine and chloroquine that induce both lysosome membrane permeabilization and inhibition of autophagy might be viable for clinical studies.

Lapatinib is a tyrosine kinase inhibitor that can inhibit EGFR (also known as HER1) and HER2 receptors[259]. EGFR is a receptor that interacts with epidermal growth factor and is often upregulated in cancers including prostate cancer, which is thought to contribute to prostate cancer acquiring resistance to androgen-based therapies[84]. EGF is also a necessary growth factor for prostate development[260]. HER2 is an EGFR family member that requires binding to EGFR or other family members to become activated[261,262]. When overexpressed it can homodimerize and

become activated. Overexpression of HER2 in breast cancer cells leads to invasion-promoting peripheral localization of lysosomes[131,263]. These EGFR family receptors could also inhibit autophagy flux preventing autophagy mediated cell death, which suggests an important role of lysosomes in their function[264]. The upregulation of both receptors has been implicated in promoting prostate cancer metastasis, as blocking their function prevents the growth of tumor xenografts in mice[260]. Unfortunately, EGFR inhibitors were not successful in clinical trials, but using lapatinib in combination with siramesine gave synergistic cell death in prostate cancer cells suggesting this might be a viable treatment strategy for this cancer[88,89,99,196,265,266]. Furthermore, expanding the combination of lysosome-disrupting agents to other targeted therapies such as antibodies or other kinase inhibitors could be an effective strategy to treat prostate cancers and will be the focus of future research.

4.2 Overall Conclusion

The combination of siramesine and lapatinib treatment in the prostate cancer cell line PC3 can cause lysosome membrane permeabilization leading to ROS production which is responsible for causing an apoptotic form of cell death independent of caspase activation. Caspase-independent apoptosis is additionally independent of the actions of cathepsins leaked during LMP. The combination treatment inhibits autophagic flux from progressing, which could prevent prostate cancer cell survival against starvation. Thus, targeting lysosome-mediated cell death in combination with targeted therapies could be an effective strategy to treat aggressive prostate cancer.

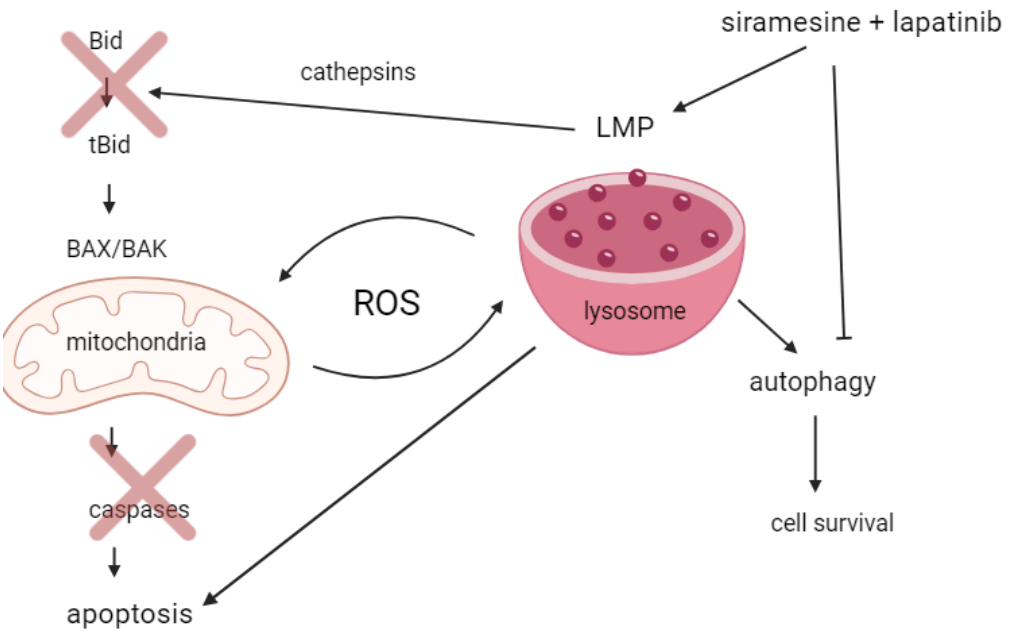

Figure 4.1. Proposed mechanism of action for the siramesine and lapatinib combination-induced cell death. Siramesine and lapatinib cause lysosome destabilization leading to LMP, cathepsin release, and ROS generation. However, there is no cleavage of BID by cathepsins. Instead, ROS contributes to a caspase-independent form of cell death. The drug combination also inhibits autophagy, which attenuates the pro-survival effect of autophagy. This figure is adapted from: Wang, F., Gómez-Sintes, R., & Boya, P. (2018).[153]

4.3 Future Directions

Utilizing lysosomotropic agents in combination with tyrosine kinase inhibitors is a potential strategy for overcoming drug resistance in advanced prostate cancers, but further work needs to be done to explore the therapeutic benefits of this combination. Siramesine and lapatinib showed synergistic cell death in prostate cancer cells, but the side effects for this combination in

a clinical setting are still unknown nor the mechanism of action for their synergy. Both drugs are not FDA-approved for use in prostate cancer but given that the combination resulted in prostate cancer cell death, drugs within similar categories such as other aSMase inhibitors that are FDA-approved can be tested to determine if the actions on aSMase by siramesine and EGFR or HER2 by lapatinib are what drive their cytotoxicity in prostate cancer cells. Combinations between other currently approved prostate cancer treatments including chemotherapy, hormone-based therapies, and radiotherapy with lysosomotropic agents and tyrosine kinase inhibitors can also be investigated to evaluate if this can prevent the progression of prostate cancer and emergence of castration resistance.

These results were obtained using *in vitro* cell lines including the castration-resistant advanced prostate cancer cell line PC3, the representative transformed cell line HEK293 and the non-malignant RWPE-1, but not an *in vivo* model. To more closely simulate the tumor microenvironment and potential impact of interactions with the immune system on the efficacy of the drug combination, the next steps would be to translate these experiments to an *in vivo* model, such as testing in mouse prostate cancer xenografts.

Previous literature has elucidated several links between the lysosome and mitochondria after lysosome membrane permeabilization. Despite studies that show cathepsins released from LMP lead to BID cleavage, subsequent BAX/BAK activation on the mitochondrial membrane, and apoptosis, the combination of siramesine and lapatinib resulted in cell death that was independent of the actions of the LMP-released cathepsins. Instead, the combination induced cell death was through an ROS-dependent caspase-independent mechanism. Mitochondrial membrane permeabilization (MMP) has been shown to result from LMP leading to caspase-

independent cell death, so future investigations can measure the mitochondrial membrane potential ($\Delta\psi_m$) to determine if MMP takes place after siramesine induces LMP. This can provide new insight into combinational treatments for prostate cancer, and their mechanism of action on the lysosome, the mitochondria, and in cell death.

References

1. Brenner, D. *et al.* Canadian Cancer Statistics 2023. *Canadian Cancer Statistics Advisory Committee in collaboration with the Canadian Cancer Society, Statistics Canada and the Public Health Agency of Canada.* (2023).

2. Gandaglia, G. *et al.* Epidemiology and Prevention of Prostate Cancer. *Eur Urol Oncol* **4**, 877–892 (2021).

3. Barsouk, A. *et al.* Epidemiology, Staging and Management of Prostate Cancer. *Medical Sciences* **8**, (2020).

4. Sekhoacha, M. *et al.* Prostate Cancer Review: Genetics, Diagnosis, Treatment Options, and Alternative Approaches. *Molecules* vol. 27 Preprint at https://doi.org/10.3390/molecules27175730 (2022).

5. Ellison, L. F. & Saint-Jacques, N. Five-year cancer survival by stage at diagnosis in Canada. *Health Rep* **34**, 3–15 (2023).

6. Cornford, P. *et al.* EAU-EANM-ESTRO-ESUR-SIOG Guidelines on Prostate Cancer. Part II—2020 Update: Treatment of Relapsing and Metastatic Prostate Cancer. *Eur Urol* **79**, 263–282 (2021).

7. Hanahan, D. & Weinberg, R. A. The Hallmarks of Cancer. *Cell* **100**, 57–70 (2000).

8. Hanahan, D. & Weinberg, R. A. Hallmarks of Cancer: The Next Generation. *Cell* **144**, 646–674 (2011).

9. Hanahan, D. Hallmarks of Cancer: New Dimensions. *Cancer Discov* **12**, 31–46 (2022).

10. Gurel, B. *et al.* NKX3.1 as a Marker of Prostatic Origin in Metastatic Tumors. *Surg Pathol* **34**, 1097–1105 (2010).

11. Lara Jr., P. N. *et al.* TMPRSS2-ERG Fusions Unexpectedly Identified in Men Initially Diagnosed With Nonprostatic Malignancies. *JCO Precis Oncol* **1**, (2017).

12. Guo, C. C. *et al.* TMPRSS2-ERG gene fusion in small cell carcinoma of the prostate. *Hum Pathol* **42**, 11–17 (2011).

13. Hubbard, G. K. *et al.* Combined MYC activation and Pten loss are sufficient to create genomic instability and lethal metastatic prostate cancer. *Cancer Res* **76**, 283–292 (2016).

14. Mcmenamin, M. E. *et al.* Loss of PTEN Expression in Paraffin-embedded Primary Prostate Cancer Correlates with High Gleason Score and Advanced Stage 1. *Cancer Res* **59**, 4291–4296 (1999).

15. Tomlins, S. A. *et al.* Role of the TMPRSS2-ERG gene fusion in prostate cancer. *Neoplasia* **10**, 177–188 (2008).

16. Gurel, B. *et al.* Nuclear MYC protein overexpression is an early alteration in human prostate carcinogenesis. *Modern Pathology* **21**, 1156–1167 (2008).

17. Graham, M. K. *et al.* Functional loss of ATRX and TERC activates Alternative Lengthening of Telomeres (ALT) in LAPC4 prostate cancer cells. *Molecular Cancer Research* **17**, 2480–2491 (2019).

18. Chen, W. S. *et al.* Novel Rb1-loss transcriptomic signature is associated with poor clinical outcomes across cancer types. *Clinical Cancer Research* **25**, 4290–4299 (2019).

19. Gerhardt, J. *et al.* FOXA1 promotes tumor progression in prostate cancer and represents a novel hallmark of castration-resistant prostate cancer. *American Journal of Pathology* **180**, 848–861 (2012).

20. Annala, M. *et al.* Frequent mutation of the FOXA1 untranslated region in prostate cancer. *Commun Biol* **1**, (2018).

21. Ding, Z. *et al.* SMAD4-dependent barrier constrains prostate cancer growth and metastatic progression. *Nature* **470**, 269–276 (2011).

22. Augello, M. A., Den, R. B. & Knudsen, K. E. AR function in promoting metastatic prostate cancer. *Cancer and Metastasis Reviews* vol. 33 399–411 Preprint at https://doi.org/10.1007/s10555-013-9471-3 (2014).

23. Zhang, D. T., Shi, J. G., Liu, Y. & Jiang, H. M. The prognostic value of Smad4 mRNA in patients with prostate cancer. *Tumor Biology* **35**, 3333–3337 (2014).

24. Taylor, R. A. *et al.* The influence of BRCA2 mutation on localized prostate cancer. *Nat Rev Urol* **16**, 281–290 (2019).

25. Fettke, H. *et al.* BRCA-deficient metastatic prostate cancer has an adverse prognosis and distinct genomic phenotype. *EBioMedicine* **95**, (2023).

26. Oh, M. *et al.* The association of BRCA1 and BRCA2 mutations with prostate cancer risk, frequency, and mortality: A meta-analysis. *Prostate* **79**, 880–895 (2019).

27. Castro, E. *et al.* Effect of BRCA Mutations on Metastatic Relapse and Cause-specific Survival after Radical Treatment for Localised Prostate Cancer. *Eur Urol* **68**, 186–193 (2015).

28. Narod, S. A. *et al.* Rapid progression of prostate cancer in men with a BRCA2 mutation. *Br J Cancer* **99**, 371–374 (2008).

29. Gregory, C. W. *et al.* A Mechanism for Androgen Receptor-mediated Prostate Cancer Recurrence after Androgen Deprivation Therapy. *Cancer Res* **61**, 4315–4319 (2001).

30. Aurilio, G. *et al.* Androgen receptor signaling pathway in prostate cancer: From genetics to clinical applications. *Cells* vol. 9 1–14 Preprint at https://doi.org/10.3390/cells9122653 (2020).

31. Lonergan, P. & Tindall, D. Androgen receptor signaling in prostate cancer development and progression. *J Carcinog* **10**, (2011).

32. Blessing, A. M. *et al.* Transcriptional regulation of core autophagy and lysosomal genes by the androgen receptor promotes prostate cancer progression. *Autophagy* **13**, 506–521 (2017).

33. Pisano, C. *et al.* Interactions between androgen receptor signaling and other molecular pathways in prostate cancer progression: Current and future clinical implications. *Crit Rev Oncol Hematol* **157**, (2021).

34. Brinkmann, A. O. *et al.* Mechanisms of androgen receptor activation and function. *Journal of Steroid Biochemistry and Molecular Biology* **69**, 307–313 (1999).

35. Grino, P. B., Griffin, J. E. & Wilson, J. D. Testosterone at High Concentrations Interacts with the Human Androgen Receptor Similarly to Dihydrotestosterone*. *Endocrinology* **126**, (1990).

36. Castoria, G. *et al.* Androgen-induced cell migration: Role of androgen receptor/filamin A association. *PLoS One* **6**, (2011).

37. Loy, C. J., Sim, K. S. & Yong, E. L. Filamin-A fragment localizes to the nucleus to regulate androgen receptor and coactivator functions. *PNAS* **100**, 4562–4567 (2003).

38. Egevad, L., Granfors, T., Karlberg, L., Bergh, A. & Stattin, P. Prognostic value of the Gleason score in prostate cancer. *BJU Int* **89**, 538–542 (2002).

39. Delahunt, B., Miller, R. J., Srigley, J. R., Evans, A. J. & Samaratunga, H. Gleason grading: Past, present and future. *Histopathology* vol. 60 75–86 Preprint at https://doi.org/10.1111/j.1365-2559.2011.04003.x (2012).

40. Gleason, D. F. Histologic Grading of Prostate Cancer: A Perspective. *Hum Pathol* **23**, (1992).

41. van den Bergh, R. C. N. *et al.* Outcomes of Men with Screen-Detected Prostate Cancer Eligible for Active Surveillance Who Were Managed Expectantly. *Eur Urol* **55**, 1–8 (2009).

42. Guijarro, A. *et al.* Influence of the location and number of metastases in the survival of metastatic prostatic cancer patients. *Actas Urol Esp* **41**, 226–233 (2017).

43. Mazzone, E. *et al.* Location of Metastases in Contemporary Prostate Cancer Patients Affects Cancer-Specific Mortality. *Clin Genitourin Cancer* **16**, 376-384.e1 (2018).

44. Jeger, J. L. Endosomes, lysosomes, and the role of endosomal and lysosomal biogenesis in cancer development. *Mol Biol Rep* **47**, 9801–9810 (2020).

45. De Nunzio, C., Presicce, F., Giacinti, S., Bassanelli, M. & Tubaro, A. Castration-resistance prostate cancer: what is the pipeline? *Minerva Urologica e nefrologica* **70**, 22–41 (2018).

46. Barata, P. C. & Sartor, A. O. Metastatic castration-sensitive prostate cancer: Abiraterone, docetaxel, or…. *Cancer* vol. 125 1777–1788 Preprint at https://doi.org/10.1002/cncr.32039 (2019).

47. Harris, W. P., Mostaghel, E. A., Nelson, P. S. & Montgomery, B. Androgen deprivation therapy: Progress in understanding mechanisms of resistance and optimizing androgen depletion. *Nat Clin Pract Urol* **6**, 76–85 (2009).

48. Cai, M. *et al.* Current therapy and drug resistance in metastatic castration-resistant prostate cancer. *Drug Resistance Updates* vol. 68 Preprint at https://doi.org/10.1016/j.drup.2023.100962 (2023).

49. Bhangal, G. *et al.* Expression of the multidrug resistance gene in human prostate cancer. *Urol Oncol* **5**, 118–121 (2000).

50. Krajewska, M. *et al.* Immunohistochemical Analysis of bcl-2, bax, bcl-X, and mcl-1 Expression in Prostate Cancers. *American Journal of Pathology* **148**, (1996).

51. Castilla, C. *et al.* Bcl-xL is overexpressed in hormone-resistant prostate cancer and promotes survival of LNCaP cells via interaction with proapoptotic Bak. *Endocrinology* **147**, 4960–4967 (2006).

52. Gao, J. *et al.* VISTA is an inhibitory immune checkpoint that is increased after ipilimumab therapy in patients with prostate cancer. *Nat Med* **23**, 551–555 (2017).

53. Mahajan, K. *et al.* ACK1/TNK2 Regulates Histone H4 Tyr88-phosphorylation and AR Gene Expression in Castration-Resistant Prostate Cancer. *Cancer Cell* **31**, 790-803.e8 (2017).

54. Macedo-Silva, C. *et al.* Epigenetic mechanisms underlying prostate cancer radioresistance. *Clin Epigenetics* **13**, (2021).

55. Pilling, A. B. & Hwang, C. Targeting prosurvival BCL2 signaling through Akt blockade sensitizes castration-resistant prostate cancer cells to enzalutamide. *Prostate* **79**, 1347–1359 (2019).

56. Zhang, Z. *et al.* Tumor Microenvironment-Derived NRG1 Promotes Antiandrogen Resistance in Prostate Cancer. *Cancer Cell* **38**, 279-296.e9 (2020).

57. Chang, K. H. *et al.* Dihydrotestosterone synthesis bypasses testosterone to drive castration-resistant prostate cancer. *Proc Natl Acad Sci U S A* **108**, 13728–13733 (2011).

58. Zoubeidi, A. *et al.* Cooperative interactions between androgen receptor (AR) and heat-shock protein 27 facilitate AR transcriptional activity. *Cancer Res* **67**, 10455–10465 (2007).

59. Deb, S. *et al.* Steroidogenesis in peripheral and transition zones of human prostate cancer tissue. *Int J Mol Sci* **22**, 1–16 (2021).

60. Thakur, M. K. *et al.* A phase II trial of ganetespib, a heat shock protein 90 Hsp90) inhibitor, in patients with docetaxel-pretreated metastatic castrate-resistant prostate cancer (CRPC)-a prostate cancer clinical trials consortium (PCCTC) study. *Invest New Drugs* **34**, 112–118 (2016).

61. Del Re, M. *et al.* The Detection of Androgen Receptor Splice Variant 7 in Plasma-derived Exosomal RNA Strongly Predicts Resistance to Hormonal Therapy in Metastatic Prostate Cancer Patients. *Eur Urol* **71**, 680–687 (2017).

62. Mitsiades, N. *et al.* Distinct patterns of dysregulated expression of enzymes involved in androgen synthesis and metabolism in metastatic prostate cancer tumors. *Cancer Res* **72**, 6142–6152 (2012).

63. Urbanucci, A. *et al.* Overexpression of androgen receptor enhances the binding of the receptor to the chromatin in prostate cancer. *Oncogene* **31**, 2153–2163 (2012).

64. Puhr, M. *et al.* PIAS1 is a determinant of poor survival and acts as a positive feedback regulator of AR signaling through enhanced AR stabilization in prostate cancer. *Oncogene* **35**, 2322–2332 (2016).

65. Puhr, M. *et al.* The glucocorticoid receptor is a key player for prostate cancer cell survival and a target for improved antiandrogen therapy. *Clinical Cancer Research* **24**, 927–938 (2018).

66. Krause, W. C., Shafi, A. A., Nakka, M. & Weigel, N. L. Androgen receptor and its splice variant, AR-V7, differentially regulate FOXA1 sensitive genes in LNCaP prostate cancer cells. *International Journal of Biochemistry and Cell Biology* **54**, 49–59 (2014).

67. Yang, Y. C. *et al.* Targeting androgen receptor activation function-1 with EPI to overcome resistance mechanisms in castration-resistant prostate cancer. *Clinical Cancer Research* **22**, 4466–4477 (2016).

68. Kim, E. H., Cao, D., Mahajan, N. P., Andriole, G. L. & Mahajan, K. ACK1–AR and AR–HOXB13 signaling axes: epigenetic regulation of lethal prostate cancers. *NAR Cancer* vol. 2 Preprint at https://doi.org/10.1093/narcan/zcaa018 (2020).

69. Watson, P. A., Arora, V. K. & Sawyers, C. L. Emerging mechanisms of resistance to androgen receptor inhibitors in prostate cancer. *Nat Rev Cancer* **15**, 701–711 (2015).

70. Veldscholte, J. *et al.* A Mutation in the Ligand Binding Domain of the Androgen Receptor of Human LNCaP Cells Affects Steroid Binding Characteristics and Response to Anti-Androgens. *Biochem Biophys Res Commun* **173**, 534–540 (1990).

71. Liu, H., Han, R., Li, J., Liu, H. & Zheng, L. Molecular mechanism of R-bicalutamide switching from androgen receptor antagonist to agonist induced by amino acid mutations using molecular dynamics simulations and free energy calculation. *J Comput Aided Mol Des* **30**, 1189–1200 (2016).

72. Bubendorf, L. *et al.* Survey of Gene Amplifications during Prostate Cancer Progression by High-Throughput Fluorescence in Situ Hybridization on Tissue Microarrays 1. *Cancer Res* **59**, 803–806 (1999).

73. Visakorpi, T. *et al.* In vivo amplification of the androgen receptor gene and progression of human prostate cancer. *Nat Genet* **9**, 401–406 (1995).

74. Schrader, A. J. *et al.* Enzalutamide in castration-resistant prostate cancer patients progressing after docetaxel and abiraterone. *Eur Urol* **65**, 30–36 (2014).

75. Ryan, C. J. *et al.* Persistent prostate-specific antigen expression after neoadjuvant androgen depletion: An early predictor of relapse or incomplete androgen suppression. *Urology* **68**, 834–839 (2006).

76. Jia, L. & Coetzee, G. A. Androgen receptor-dependent PSA expression in androgen-independent prostate cancer cells does not involve androgen receptor occupancy of the PSA locus. *Cancer Res* **65**, 8003–8008 (2005).

77. Saxena, P. *et al.* PSA regulates androgen receptor expression in prostate cancer cells. *Prostate* **72**, 769–776 (2012).

78. Kantoff, P. W. *et al.* Sipuleucel-T Immunotherapy for Castration-Resistant Prostate Cancer. *New England Journal of Medicine* **363**, 411–422 (2010).

79. Antonarakis, E. S. *et al.* Pembrolizumab for Treatment-Refractory Metastatic Castration-Resistant Prostate Cancer: Multicohort, Open-Label Phase II KEYNOTE-199 Study. *J Clin Oncol* **38**, 395–405 (2019).

80. Sharma, P. *et al.* Nivolumab Plus Ipilimumab for Metastatic Castration-Resistant Prostate Cancer: Preliminary Analysis of Patients in the CheckMate 650 Trial. *Cancer Cell* **38**, 489-499.e3 (2020).

81. Gunturi, A. & McDermott, D. F. Nivolumab for the treatment of cancer. *Expert Opin Investig Drugs* **24**, 253–260 (2015).

82. Di Lorenzo, G. *et al.* Expression of Epidermal Growth Factor Receptor Correlates with Disease Relapse and Progression to Androgen-independence in Human Prostate Cancer 1. *Clinical Cancer Research* **8**, 3438–3444 (2002).

83. Normanno, N. *et al.* Epidermal growth factor receptor (EGFR) signaling in cancer. *Gene* **366**, 2–16 (2006).

84. Peraldo-Neia, C. *et al.* Epidermal Growth Factor Receptor (EGFR) mutation analysis, gene expression profiling and EGFR protein expression in primary prostate cancer. *BMC Cancer* **11**, (2011).

85. Abreu-Martin, M. T., Chari, A., Palladino, A. A., Craft, N. A. & Sawyers, C. L. Mitogen-Activated Protein Kinase Kinase Kinase 1 Activates Androgen Receptor-Dependent Transcription and Apoptosis in Prostate Cancer. *Mol Cell Biol* **19**, 5143–5154 (1999).

86. Bunone, G., Briand, P.-A., Miksicek, R. J. & Picard, D. Activation of the unliganded estrogen receptor by EGF involves the MAP kinase pathway and direct phosphorylation. *EMBO J* **15**, 2174–2183 (1996).

87. Culig, Z. *et al.* Androgen Receptor Activation in Prostatic Tumor Cell Lines by Insulin-like Growth Factor-I, Keratinocyte Growth Factor, and Epidermal Growth Factor. *Cancer Res* **54**, 5474–5478 (1994).

88. Canil, C. M. *et al.* Randomized phase II study of two doses of gefitinib in hormone-refractory prostate cancer: A trial of the National Cancer Institute of Canada-Clinical Trials Group. *Journal of Clinical Oncology* **23**, 455–460 (2005).

89. Small, E. J. *et al.* A phase II trial of gefitinib in patients with non-metastatic hormone-refractory prostate cancer. *BJU Int* **100**, 765–769 (2007).

90. Tu, C.-Y. *et al.* Comparison of the effects of the three major tyrosine kinase inhibitors as first-line therapy for non-small-cell lung cancer harboring epidermal growth factor receptor mutations. *Oncotarget* **9**, 24237–24247 (2018).

91. Sirotnak, F. M., She, Y., Lee, F., Chen, J. & Scher, H. I. Studies with CWR22 Xenografts in Nude Mice Suggest That ZD1839 May Have a Role in the Treatment of Both Androgen-dependent and Androgen-independent Human Prostate Cancer 1. *Clinical Cancer Research* **8**, 3870–3876 (2002).

92. Sridhar, S. S. *et al.* A multicenter phase II clinical trial of Lapatinib (GW572016) in hormonally untreated advanced prostate cancer. *American Journal of Clinical Oncology: Cancer Clinical Trials* **33**, 609–613 (2010).

93. Ryan, Q. *et al.* FDA Drug Approval Summary: Lapatinib in Combination with Capecitabine for Previously Treated Metastatic Breast Cancer That Overexpresses HER-2. *Oncologist* **13**, 1114–1119 (2008).

94. Yuan, Y., Liu, X., Cai, Y. & Li, W. Lapatinib and lapatinib plus trastuzumab therapy versus trastuzumab therapy for HER2 positive breast cancer patients: an updated systematic review and meta-analysis. *Syst Rev* **11**, 264 (2022).

95. Whang, Y. E. *et al.* A phase II study of lapatinib, a dual EGFR and HER-2 tyrosine kinase inhibitor, in patients with castration-resistant prostate cancer. *Urologic Oncology: Seminars and Original Investigations* **31**, 82–86 (2013).

96. Liu, G. *et al.* Eastern Cooperative Oncology Group Phase II Trial of lapatinib in men with biochemically relapsed, androgen dependent prostate cancer1. *Urologic Oncology: Seminars and Original Investigations* **31**, 211–218 (2013).

97. Fonseca-Alves, C. E. *et al.* Lapatinib antitumor effect is associated with PI3K and MAPK pathway: An analysis in human and canine prostate cancer cells. *PLoS One* **19**, (2024).

98. Arai, S. *et al.* Tyrosine kinase inhibitors increase MCL1 degradation and in combination with BCLXL/BCL2 inhibitors drive prostate cancer apoptosis. *Clinical Cancer Research* **24**, 5458–5470 (2018).

99. Ma, S., Henson, E. S., Chen, Y. & Gibson, S. B. Ferroptosis is induced following siramesine and lapatinib treatment of breast cancer cells. *Cell Death Dis* **7**, (2016).

100. Dobbelstein, M. & Moll, U. Targeting tumour-supportive cellular machineries in anticancer drug development. *Nat Rev Drug Discov* **13**, 179–196 (2014).

101. Lübke, T., Lobel, P. & Sleat, D. E. Proteomics of the lysosome. *Biochim Biophys Acta Mol Cell Res* **1793**, 625–635 (2009).

102. Yim, W. W. Y. & Mizushima, N. Lysosome biology in autophagy. *Cell Discov* **6**, (2020).

103. Hämälistö, S. & Jäättelä, M. Lysosomes in cancer - living on the edge (of the cell). *Curr Opin Cell Biol* **39**, 69–76 (2016).

104. Shin, H. R. & Zoncu, R. The Lysosome at the Intersection of Cellular Growth and Destruction. *Dev Cell* **54**, 226–238 (2020).

105. Iulianna, T., Kuldeep, N. & Eric, F. The Achilles' heel of cancer: targeting tumors via lysosome-induced immunogenic cell death. *Cell Death Dis* **13**, (2022).

106. Hahm, E. R., Singh, K. B., Kim, S. H., Powolny, A. A. & Singh, S. V. The role of lysosome-associated membrane protein 2 in prostate cancer chemopreventive mechanisms of sulforaphane. *Cancer Prevention Research* **13**, 661–672 (2020).

107. Buratta, S. *et al.* Lysosomal exocytosis, exosome release and secretory autophagy: The autophagic- and endo-lysosomal systems go extracellular. *Int J Mol Sci* **21**, (2020).

108. Ji, S. *et al.* Targeted Enrichment of Enzyme-Instructed Assemblies in Cancer Cell Lysosomes Turns Immunologically Cold Tumors Hot. *Angewandte Chemie - International Edition* **60**, 26994–27004 (2021).

109. Turk, V., Turk, B., Guncar, G., Turk, D. & Kos, J. Lysosomal cathepsins: structure, role in antigen processing and presentation, and cancer. *Advan. Enzyme Regul* **42**, 285–303 (2002).

110. Delamarre, L., Pack, M., Chang, H., Mellman, I. & Trombetta, S. E. Differential Lysosomal Proteolysis in Antigen-Presenting Cells Determines Antigen Fate. *Science (1979)* **307**, 1630–1634 (2005).

111. Garg, S. *et al.* Lysosomal Trafficking, Antigen Presentation, and Microbial Killing Are Controlled by the Arf-like GTPase Arl8b. *Immunity* **35**, 182–193 (2011).

112. Chen, Y., Azad, M. B. & Gibson, S. B. Methods for detecting autophagy and determining autophagy-induced cell death. *Can J Physiol Pharmacol* **88**, 285–295 (2010).

113. Lee, Y. K. & Lee, J. A. Role of the mammalian ATG8/LC3 family in autophagy: Differential and compensatory roles in the spatiotemporal regulation of autophagy. *BMB Rep* **49**, 424–430 (2016).

114. Tanida Isei and Ueno, T. and K. E. LC3 and Autophagy. in *Autophagosome and Phagosome* (ed. Deretic, V.) 77–88 (Humana Press, Totowa, NJ, 2008). doi:10.1007/978-1-59745-157-4_4.

115. Kimmelman, A. C. & White, E. Autophagy and Tumor Metabolism. *Cell Metab* **25**, 1037–1043 (2017).

116. Kumar, S. *et al.* Autophagy and the lysosomal system in cancer. *Cells* **10**, (2021).

117. Cui, Z. *et al.* Structural basis for mTORC1-dependent regulation of the lysosomal and autophagic transcription factor TFEB. *bioRxiv* vol. 9 Preprint at https://doi.org/10.1101/2022.09.12.507619 (2022).

118. Dielschneider, R. F., Henson, E. S. & Gibson, S. B. Lysosomes as Oxidative Targets for Cancer Therapy. *Oxid Med Cell Longev* **2017**, (2017).

119. Watts, C. Lysosomes and lysosome-related organelles in immune responses. *FEBS Open Bio* **12**, 678–693 (2022).

120. Myerowitz, R., Puertollano, R. & Raben, N. Impaired autophagy: The collateral damage of lysosomal storage disorders. *EBioMedicine* **63**, (2021).

121. Ren, H. & Wang, G. Autophagy and lysosome storage disorders. in *Advances in Experimental Medicine and Biology* vol. 1207 87–102 (Springer, 2020).

122. Czibener, C. *et al.* Ca2+ and synaptotagmin VII-dependent delivery of lysosomal membrane to nascent phagosomes. *Journal of Cell Biology* **174**, 997–1007 (2006).

123. Tang, T. *et al.* The role of lysosomes in cancer development and progression. *Cell Biosci* **10**, (2020).

124. Gupta, S. *et al.* Lysosomal retargeting of Myoferlin mitigates membrane stress to enable pancreatic cancer growth. *Nat Cell Biol* **23**, 232–242 (2021).

125. Faubert, B., Solmonson, A. & DeBerardinis, R. J. Metabolic reprogramming and cancer progression. *Science* vol. 368 Preprint at https://doi.org/10.1126/science.aaw5473 (2020).

126. Racoma, I. O., Meisen, W. H., Wang, Q. E., Kaur, B. & Wani, A. A. Thymoquinone Inhibits Autophagy and Induces Cathepsin-Mediated, Caspase-Independent Cell Death in Glioblastoma Cells. *PLoS One* **8**, (2013).

127. Allemailem, K. S. *et al.* Novel approaches of dysregulating lysosome functions in cancer cells by specific drugs and its nanoformulations: A smart approach of modern therapeutics. *Int J Nanomedicine* **16**, 5065–5098 (2021).

128. Zhu, X. *et al.* TFEB Promotes Prostate Cancer Progression via Regulating ABCA2-Dependent Lysosomal Biogenesis. *Front Oncol* **11**, (2021).

129. White, E. & DiPaola, R. S. The double-edged sword of autophagy modulation in cancer. *Clinical Cancer Research* **15**, 5308–5316 (2009).

130. Santanam, U. *et al.* Atg7 cooperates with Pten loss to drive prostate cancer tumor growth. *Genes Dev* **30**, 399–407 (2016).

131. Rafn, B. *et al.* ErbB2-Driven Breast Cancer Cell Invasion Depends on a Complex Signaling Network Activating Myeloid Zinc Finger-1-Dependent Cathepsin B Expression. *Mol Cell* **45**, 764–776 (2012).

132. Zhitomirsky, B. & Assaraf, Y. G. Lysosomal sequestration of hydrophobic weak base chemotherapeutics triggers lysosomal biogenesis and lysosome-dependent cancer multidrug resistance. *Oncotarget* **6**, 1143–1156 (2014).

133. Levine, B. & Yuan, J. Autophagy in cell death: An innocent convict? *Journal of Clinical Investigation* **115**, 2679–2688 (2005).

134. Zhu, M. & Wang, X. Q. Regulation of mTORC1 by small GTPases in response to nutrients. *Journal of Nutrition* **150**, 1004–1011 (2020).

135. Nguyen, T. P., Frank, A. R. & Jewell, J. L. Amino acid and small GTPase regulation of mTORC1. *Cell Logist* **7**, e1378794 (2017).

136. Nakamura, S. & Yoshimori, T. New insights into autophagosome-lysosome fusion. *Journal of Cell Science* vol. 130 1209–1216 Preprint at https://doi.org/10.1242/jcs.196352 (2017).

137. Wang, Z. *et al.* The Vici Syndrome Protein EPG5 Is a Rab7 Effector that Determines the Fusion Specificity of Autophagosomes with Late Endosomes/Lysosomes. *Mol Cell* **63**, 781–795 (2016).

138. Tian, Y. *et al.* C. elegans Screen Identifies Autophagy Genes Specific to Multicellular Organisms. *Cell* **141**, 1042–1055 (2010).

139. McEwan, D. G. *et al.* PLEKHM1 regulates autophagosome-lysosome fusion through HOPS complex and LC3/GABARAP proteins. *Mol Cell* **57**, 39–54 (2015).

140. Gutierrez, M. G., Munafó, D. B., Berón, W. & Colombo, M. I. Rab7 is required for the normal progression of the autophagic pathway in mammalian cells. *J Cell Sci* **117**, 2687–2697 (2004).

141. Redza-Dutordoir, M. & Averill-Bates, D. A. Interactions between reactive oxygen species and autophagy: Special issue: Death mechanisms in cellular homeostasis. *Biochim Biophys Acta Mol Cell Res* **1868**, (2021).

142. Kim, J., Kundu, M., Viollet, B. & Guan, K. L. AMPK and mTOR regulate autophagy through direct phosphorylation of Ulk1. *Nat Cell Biol* **13**, 132–141 (2011).

143. Ganley, I. G. *et al.* ULK1·ATG13·FIP200 complex mediates mTOR signaling and is essential for autophagy. *Journal of Biological Chemistry* **284**, 12297–12305 (2009).

144. Jao, C. C., Ragusa, M. J., Stanley, R. E. & Hurley, J. H. A HORMA domain in Atg13 mediates PI 3-kinase recruitment in autophagy. *Proc Natl Acad Sci U S A* **110**, 5486–5491 (2013).

145. Suzuki, S. W. *et al.* Atg13 HORMA domain recruits Atg9 vesicles during autophagosome formation. *Proc Natl Acad Sci U S A* **112**, 3350–3355 (2015).

146. Tanida, I., Tanida-Miyake, E., Komatsu, M., Ueno, T. & Kominami, E. Human Apg3p/Aut1p homologue is an authentic E2 enzyme for multiple substrates, GATE-16, GABARAP, and MAP-LC3, and facilitates the conjugation of hApg12p to hApg5p. *Journal of Biological Chemistry* **277**, 13739–13744 (2002).

147. Kabeya, Y. *et al.* LC3, GABARAP and GATE16 localize to autophagosomal membrane depending on form-II formation. *J Cell Sci* **117**, 2805–2812 (2004).

148. Fujita, N. *et al.* The Atg16L complex specifies the site of LC3 lipidation for membrane biogenesis in autophagy. *Mol Biol Cell* **19**, 2092–2100 (2008).

149. Itakura, E., Kishi-Itakura, C. & Mizushima, N. The hairpin-type tail-anchored SNARE syntaxin 17 targets to autophagosomes for fusion with endosomes/lysosomes. *Cell* **151**, 1256–1269 (2012).

150. Jakobi, A. J. *et al.* Structural basis of p62/SQSTM1 helical filaments and their role in cellular cargo uptake. *Nat Commun* **11**, (2020).

151. Wurzer, B. *et al.* Oligomerization of p62 allows for selection of ubiquitinated cargo and isolation membrane during selective autophagy. *Elife* **4**, (2015).

152. Fennelly, C. & Amaravadi, R. K. Lysosomal biology in cancer. in *Methods in Molecular Biology* vol. 1594 293–308 (Humana Press Inc., 2017).

153. Wang, F., Gómez-Sintes, R. & Boya, P. Lysosomal membrane permeabilization and cell death. *Traffic* **19**, 918–931 (2018).

154. Boya, P. & Kroemer, G. Lysosomal membrane permeabilization in cell death. *Oncogene* **27**, 6434–6451 (2008).

155. Oberle, C. *et al.* Lysosomal membrane permeabilization and cathepsin release is a Bax/Bak-dependent, amplifying event of apoptosis in fibroblasts and monocytes. *Cell Death Differ* **17**, 1167–1178 (2010).

156. Dielschneider, R. F. *et al.* Lysosomotropic agents selectively target chronic lymphocytic leukemia cells due to altered sphingolipid metabolism. *Leukemia* **30**, 1290–1300 (2016).

157. Kashyap, D., Garg, V. K. & Goel, N. Intrinsic and extrinsic pathways of apoptosis: Role in cancer development and prognosis. in *Advances in Protein Chemistry and Structural Biology* vol. 125 73–120 (Academic Press Inc., 2021).

158. Wu, C. C. & Bratton, S. B. Regulation of the intrinsic apoptosis pathway by reactive oxygen species. *Antioxidants and Redox Signaling* vol. 19 546–558 Preprint at https://doi.org/10.1089/ars.2012.4905 (2013).

159. Dadsena, S., King, L. E. & García-Sáez, A. J. Apoptosis regulation at the mitochondria membrane level. *Biochimica et Biophysica Acta - Biomembranes* vol. 1863 Preprint at https://doi.org/10.1016/j.bbamem.2021.183716 (2021).

160. Feldstein, A. E. *et al.* Bax inhibition protects against free fatty acid-induced lysosomal permeabilization. *Am J Physiol Gastrointest Liver Physiol* **290**, 1339–1346 (2006).

161. Paris, C., Bertoglio, J. & Bréard, J. Lysosomal and mitochondrial pathways in miltefosine-induced apoptosis in U937 cells. *Apoptosis* **12**, 1257–1267 (2007).

162. Boya, P. *et al.* Lysosomal membrane permeabilization induces cell death in a mitochondrion-dependent fashion. *Journal of Experimental Medicine* **197**, 1323–1334 (2003).

163. Winterbourn, C. C. Are free radicals involved in thiol-based redox signaling? *Free Radic Biol Med* **80**, 164–170 (2015).

164. Mailloux, R. J. An update on mitochondrial reactive oxygen species production. *Antioxidants* **9**, (2020).

165. Guzy, R. D. *et al.* Mitochondrial complex III is required for hypoxia-induced ROS production and cellular oxygen sensing. *Cell Metab* **1**, 401–408 (2005).

166. Chandel, N. S. *et al.* Reactive oxygen species generated at mitochondrial Complex III stabilize hypoxia-inducible factor-1α during hypoxia: A mechanism of O2 sensing. *Journal of Biological Chemistry* **275**, 25130–25138 (2000).

167. Gibson, S. B. Investigating the role of reactive oxygen species in regulating autophagy. in *Methods in Enzymology* vol. 528 217–235 (Academic Press Inc., 2013).

168. Liou, G.-Y. & Storz, P. Reactive oxygen species in cancer. *Free Radic Res* **44**, 479–496 (2010).

169. Nakamura, H. & Takada, K. Reactive oxygen species in cancer: Current findings and future directions. *Cancer Sci* **112**, 3945–3952 (2021).

170. Dixon, S. J. & Stockwell, B. R. The role of iron and reactive oxygen species in cell death. *Nature Chemical Biology* vol. 10 9–17 Preprint at https://doi.org/10.1038/nchembio.1416 (2014).

171. Villalpando-Rodriguez, G. E. & Gibson, S. B. Reactive Oxygen Species (ROS) Regulates Different Types of Cell Death by Acting as a Rheostat. *Oxid Med Cell Longev* **2021**, (2021).

172. Galluzzi, L. *et al.* Molecular mechanisms of cell death: Recommendations of the Nomenclature Committee on Cell Death 2018. *Cell Death and Differentiation* vol. 25 486–541 Preprint at https://doi.org/10.1038/s41418-017-0012-4 (2018).

173. Brojatsch, J. *et al.* Distinct cathepsins control necrotic cell death mediated by pyroptosis inducers and lysosome-destabilizing agents. *Cell Cycle* **14**, 964–972 (2015).

174. Torii, S. *et al.* An essential role for functional lysosomes in ferroptosis of cancer cells. *Biochemical Journal* **473**, 769–777 (2016).

175. Su, Y. *et al.* Ferroptosis, a novel pharmacological mechanism of anti-cancer drugs. *Cancer Lett* **483**, 127–136 (2020).

176. Chen, Y. *et al.* Boosting ROS-Mediated Lysosomal Membrane Permeabilization for Cancer Ferroptosis Therapy. *Adv Healthc Mater* **12**, (2023).

177. Ma, S. *et al.* Ferroptosis and autophagy induced cell death occur independently after siramesine and lapatinib treatment in breast cancer cells. *PLoS One* **12**, (2017).

178. Lage, S. L. *et al.* Cytosolic flagellin-induced lysosomal pathway regulates inflammasome-dependent and -independent macrophage responses. *Proc Natl Acad Sci U S A* **110**, (2013).

179. Liu, X. *et al.* Inflammasome-activated gasdermin D causes pyroptosis by forming membrane pores. *Nature* **535**, 153–158 (2016).

180. Hotamisligil, G. S. Inflammation, metaflammation and immunometabolic disorders. *Nature* **542**, 177–185 (2017).

181. Pétrilli, V., Dostert, C., Muruve, D. A. & Tschopp, J. The inflammasome: a danger sensing complex triggering innate immunity. *Curr Opin Immunol* **19**, 615–622 (2007).

182. Bergsbaken, T., Fink, S. L. & Cookson, B. T. Pyroptosis: host cell death and inflammation. *Nat Rev Microbiol* **7**, 99–109 (2009).

183. Okada, M., Matsuzawa, A., Yoshimura, A. & Ichijo, H. The lysosome rupture-activated TAK1-JNK pathway regulates NLRP3 inflammasome activation. *Journal of Biological Chemistry* **289**, 32926–32936 (2014).

184. Goodall, M. L. *et al.* Development of potent autophagy inhibitors that sensitize oncogenic BRAF V600E mutant melanoma tumor cells to vemurafenib. *Autophagy* **10**, 1120–1136 (2014).

185. Boya, P. *et al.* Mitochondrial membrane permeabilization is a critical step of lysosome-initiated apoptosis induced by hydroxychloroquine. *Oncogene* **22**, 3927–3936 (2003).

186. Vogl, D. T. *et al.* Combined autophagy and proteasome inhibition - A phase 1 trial of hydroxychloroquine and bortezomib in patients with relapsed/refractory myeloma. *Autophagy* **10**, 1380–1390 (2014).

187. Wang, T. *et al.* Synthesis of Improved Lysomotropic Autophagy Inhibitors. *J Med Chem* **58**, 3025–3035 (2015).

188. Mahalingam, D. *et al.* Combined autophagy and HDAC inhibition: A phase I safety, tolerability, pharmacokinetic, and pharmacodynamic analysis of hydroxychloroquine in combination with the HDAC inhibitor vorinostat in patients with advanced solid tumors. *Autophagy* **10**, 1403–1414 (2014).

189. Goldberg, S. B. *et al.* A Phase I Study of Erlotinib and Hydroxychloroquine in Advanced Non–Small-Cell Lung Cancer. *Journal of Thoracic Oncology* **7**, 1602–1608 (2012).

190. Briceno, E., Reyes, S. & Sotelo, J. Therapy of glioblastoma multiforme improved by the antimutagenic chloroquine. *Neurosurg Focus* **14**, (2003).

191. Kolter, T. & Sandhoff, K. Lysosomal degradation of membrane lipids. *FEBS Lett* **584**, 1700–1712 (2010).

192. Petersen, N. H. T. *et al.* Transformation-Associated Changes in Sphingolipid Metabolism Sensitize Cells to Lysosomal Cell Death Induced by Inhibitors of Acid Sphingomyelinase. *Cancer Cell* **24**, 379–393 (2013).

193. Ostenfeld, M. S. *et al.* Anti-cancer agent siramesine is a lysosomotropic detergent that induces cytoprotective autophagosome accumulation. *Autophagy* **4**, 487–499 (2008).

194. Jensen, S. S., Petterson, S. A., Halle, B., Aaberg-Jessen, C. & Kristensen, B. W. Effects of the lysosomal destabilizing drug siramesine on glioblastoma in vitro and in vivo. *BMC Cancer* **17**, (2017).

195. Ostenfeld, M. S. *et al.* Effective tumor cell death by σ-2 receptor ligand siramesine involves lysosomal leakage and oxidative stress. *Cancer Res* **65**, 8975–8983 (2005).

196. Garcia, E. A., Bhatti, I., Henson, E. S. & Gibson, S. B. Prostate Cancer Cells Are Sensitive to Lysosomotropic Agent Siramesine through Generation Reactive Oxygen Species and in Combination with Tyrosine Kinase Inhibitors. *Cancers (Basel)* **14**, 5478 (2022).

197. Ellegaard, A. M. *et al.* Repurposing Cationic Amphiphilic Antihistamines for Cancer Treatment. *EBioMedicine* **9**, 130–139 (2016).

198. Ellegaard, A. M., Bach, P. & Jäättelä, M. Targeting Cancer Lysosomes with Good Old Cationic Amphiphilic Drugs. in *Reviews of Physiology, Biochemistry and Pharmacology* vol. 185 107–152 (Springer Science and Business Media Deutschland GmbH, 2023).

199. Hurwitz, R., Ferlinz, K. & Sandhoff, K. TheTricyclic Anfidepressanf Desipramine Causes Proteolytic Degradation of Lysosomal Sphingomyelinase in Human Fibroblasts. *Biol. Chem. Hoppe-Seyler* **375**, 447–450 (1994).

200. Yan, K. H. *et al.* Mefloquine exerts anticancer activity in prostate cancer cells via ROS-mediated modulation of Akt, ERK, JNK and AMPK signaling. *Oncol Lett* **5**, 1541–1545 (2013).

201. Chang, H. C. *et al.* Desipramine-induced apoptosis in human PC3 prostate cancer cells: Activation of JNK kinase and caspase-3 pathways and a protective role of [Ca2+]i elevation. *Toxicology* **250**, 9–14 (2008).

202. Wang, W. T. *et al.* Terfenadine induces anti-proliferative and apoptotic activities in human hormone-refractory prostate cancer through histamine receptor-independent Mcl-1 cleavage and Bak up-regulation. *Naunyn Schmiedebergs Arch Pharmacol* **387**, 33–45 (2014).

203. Huang, C. J. *et al.* Desipramine-induced Ca2+ movement and cytotoxicity in PC3 human prostate cancer cells. *Toxicology in Vitro* **21**, 449–456 (2007).

204. Pan, C. C. *et al.* Effect of nortriptyline on cytosolic Ca2+ regulation and viability in PC3 human prostate cancer cells. *Drug Dev Res* **71**, 323–330 (2010).

205. Chanas-Larue, A., Villalpando-Rodriguez, G. E., Henson, E. S., Johnston, J. B. & Gibson, S. B. Antihistamines are synergistic with Bruton's tyrosine kinase inhibiter ibrutinib mediated by lysosome disruption in chronic lymphocytic leukemia (CLL) cells. *Leuk Res* **96**, (2020).

206. Yan, K. H. *et al.* Mefloquine induces cell death in prostate cancer cells and provides a potential novel treatment strategy in vivo. *Oncol Lett* **5**, 1567–1571 (2013).

207. Öllinger, K. & Appelqvist, H. *Lysosomes Methods and Protocols*. vol. 1594 (2017).

208. Petersen, N. H. T. *et al.* Transformation-Associated Changes in Sphingolipid Metabolism Sensitize Cells to Lysosomal Cell Death Induced by Inhibitors of Acid Sphingomyelinase. *Cancer Cell* **24**, 379–393 (2013).

209. Geisslinger, F., Müller, M., Vollmar, A. M. & Bartel, K. Targeting Lysosomes in Cancer as Promising Strategy to Overcome Chemoresistance—A Mini Review. *Frontiers in Oncology* vol. 10 Preprint at https://doi.org/10.3389/fonc.2020.01156 (2020).

210. Chou, T.-C. & Talalay, P. Quantitative Analysis of Dose-Effect Relationships: The Combined Effects of Multiple Drugs or Enzyme Inhibitors. *Adv Enzyme Regul* **22**, 27–55 (1984).

211. Sobel, R. E. & Sadar, M. D. Cell lines used in prostate cancer research: A compendium of old and new lines - Part 2. *Journal of Urology* **173**, 360–372 (2005).

212. Lee, C. *et al.* Regulation of Proliferation and Production of Prostate-Specific Antigen in Androgen-Sensitive Prostatic Cancer Cells, LNCaP, by Dihydrotestosterone*. *Endocrinology* **138**, 796–803 (1995).

213. Sobel, R. E. & Sadar, M. D. Cell lines used in prostate cancer research: A compendium of old and new lines - Part 1. *Journal of Urology* **173**, 342–359 (2005).

214. Elshazly, A. M. & Gewirtz, D. A. Making the Case for Autophagy Inhibition as a Therapeutic Strategy in Combination with Androgen-Targeted Therapies in Prostate Cancer. *Cancers (Basel)* **15**, 5029 (2023).

215. Lorenzo, H. K., Susin, S. A., Penninger, J. & Kroemer, G. Apoptosis inducing factor (AIF): a phylogenetically old, caspase-independent effector of cell death. *Cell Death Differ* **6**, 516–524 (1999).

216. Wang Qilong and Zou, M.-H. Measurement of Reactive Oxygen Species (ROS) and Mitochondrial ROS in AMPK Knockout Mice Blood Vessels. in *AMPK: Methods and Protocols* (ed. Neumann Dietbert and Viollet, B.) 507–517 (Springer New York, New York, NY, 2018). doi:10.1007/978-1-4939-7598-3_32.

217. Nusret Engin, K. Alpha-tocopherol: looking beyond an antioxidant. *Mol Vis* **15**, 855–860 (2009).

218. Hafner Ĉesen, M., Repnik, U., Turk, V. & Turk, B. Siramesine triggers cell death through destabilisation of mitochondria, but not lysosomes. *Cell Death Dis* **4**, (2013).

219. Craig, R. W. MCL1 provides a window on the role of the BCL2 family in cell proliferation, differentiation and tumorigenesis. *Leukemia* **16**, 444–454 (2002).

220. Berliner, L. & Parinandii, N. *Biological Magnetic Resonance 34 - Measuring Oxidants and Oxidative Stress in Biological Systems*. vol. 34 (2020).

221. Kauffman, M. *et al.* MitoSOX-Based Flow Cytometry for Detecting Mitochondrial ROS. *Reactive Oxygen Species (Apex)* vol. 2 361–370 Preprint at https://doi.org/10.20455/ros.2016.865 (2016).

222. Thomas, P. & Smart, T. G. HEK293 cell line: A vehicle for the expression of recombinant proteins. *J Pharmacol Toxicol Methods* **51**, 187–200 (2005).

223. Dadsena, S., King, L. E. & García-Sáez, A. J. Apoptosis regulation at the mitochondria membrane level. *Biochimica et Biophysica Acta - Biomembranes* vol. 1863 Preprint at https://doi.org/10.1016/j.bbamem.2021.183716 (2021).

224. Soond, S. M., Kozhevnikova, M. V., Savvateeva, L. V., Townsend, P. A. & Zamyatnin, A. A. Intrinsically connected: Therapeutically targeting the cathepsin proteases and the bcl-2 family of protein substrates as co-regulators of apoptosis. *International Journal of Molecular Sciences* vol. 22 Preprint at https://doi.org/10.3390/ijms22094669 (2021).

225. Saudenova, M. *et al.* Behind every smile there's teeth: Cathepsin B's function in health and disease with a kidney view. *Biochim Biophys Acta Mol Cell Res* **1869**, (2022).

226. Mauthe, M. *et al.* Chloroquine inhibits autophagic flux by decreasing autophagosome-lysosome fusion. *Autophagy* **14**, 1435–1455 (2018).

227. Hennig, P. *et al.* The Pathways Underlying the Multiple Roles of p62 in Inflammation and Cancer. *Biomedicines* **9**, 707 (2021).

228. Chen, Y. & Gibson, S. B. Three dimensions of autophagy in regulating tumor growth: cell survival/death, cell proliferation, and tumor dormancy. *Biochim Biophys Acta Mol Basis Dis* **1867**, (2021).

229. Buck, S. A. J., Koolen, S. L. W., Mathijssen, R. H. J., de Wit, R. & van Soest, R. J. Cross-resistance and drug sequence in prostate cancer. *Drug Resistance Updates* **56**, (2021).

230. Mokhtari, R. B. *et al.* Combination therapy in combating cancer SYSTEMATIC REVIEW: COMBINATION THERAPY IN COMBATING CANCER BACKGROUND. **8**, 38022–38043 (2017).

231. Jensen, S. S., Petterson, S. A., Halle, B., Aaberg-Jessen, C. & Kristensen, B. W. Effects of the lysosomal destabilizing drug siramesine on glioblastoma in vitro and in vivo. *BMC Cancer* **17**, (2017).

232. Cash, T. P. *et al.* Induction of lysosome membrane permeabilization as a therapeutic strategy to target pancreatic cancer stem cells. *Cancers (Basel)* **12**, 1790 (2020).

233. Zdolsek, J., Zhang, H., Roberg, K., Brunk, U. & Sies, H. H2o2-mediated damage to lysosomal membranes of j-774 cells. *Free Radic Res* **18**, 71–85 (1993).

234. Droga-Mazovec, G. *et al.* Cysteine cathepsins trigger caspase-dependent cell death through cleavage of bid and antiapoptotic Bcl-2 homologues. *Journal of Biological Chemistry* **283**, 19140–19150 (2008).

235. Yoon, J. Y. *et al.* Synergistic apoptotic response between valproic acid and fludarabine in chronic lymphocytic leukaemia (CLL) cells involves the lysosomal protease cathepsin B. *Blood Cancer J* **3**, (2013).

236. Bieth, J. G. *et al.* Regulation of the Activity of Lysosomal Cysteine Proteinases by pH-lnduced Inactivation and/or Endogenous Protein Inhibitors, Cystatins. *Biol. Chem. Hoppe-Seyler* **376**, 225–230 (1995).

237. Park, S. *et al.* Suppression of cathepsin a inhibits growth, migration, and invasion by inhibiting the p38 MAPK signaling pathway in prostate cancer. *Arch Biochem Biophys* **688**, (2020).

238. Halliwell, W. H. Cationic Amphiphilic Drug-Induced Phospholipidosis. *Toxicol Pathol* **25**, 53–59 (1997).

239. Hernández-Tiedra, S. *et al.* Dihydroceramide accumulation mediates cytotoxic autophagy of cancer cells via autolysosome destabilization. *Autophagy* **12**, 2213–2229 (2016).

240. Guzmán, M. *et al.* A pilot clinical study of Δ9-tetrahydrocannabinol in patients with recurrent glioblastoma multiforme. *Br J Cancer* **95**, 197–203 (2006).

241. Ivanov, A. *et al.* Monoclonal antibodies directed to CD20 and HLA-DR can elicit homotypic adhesion followed by lysosome-mediated cell death in human lymphoma and leukemia cells. *Journal of Clinical Investigation* **119**, 2143–2159 (2009).

242. Das, S., Dielschneider, R., Chanas-LaRue, A., Johnston, J. B. & Gibson, S. B. Antimalarial drugs trigger lysosome-mediated cell death in chronic lymphocytic leukemia (CLL) cells. *Leuk Res* **70**, 79–86 (2018).

243. Wang, J. *et al.* Silica nanoparticles induce autophagy dysfunction via lysosomal impairment and inhibition of autophagosome degradation in hepatocytes. *Int J Nanomedicine* **12**, 809–825 (2017).

244. Sabella, S. *et al.* A general mechanism for intracellular toxicity of metal-containing nanoparticles. *Nanoscale* **6**, 7052–7061 (2014).

245. Ding, L. *et al.* Intracellular Fate of Nanoparticles with Polydopamine Surface Engineering and a Novel Strategy for Exocytosis-Inhibiting, Lysosome Impairment-Based Cancer Therapy. *Nano Lett* **17**, 6790–6801 (2017).

246. Bruchard, M. *et al.* Chemotherapy-triggered cathepsin B release in myeloid-derived suppressor cells activates the Nlrp3 inflammasome and promotes tumor growth. *Nat Med* **19**, 57–64 (2013).

247. Petersen, N. H. T., Kirkegaard, T., Olsen, O. D. & Jäättelä, M. Connecting Hsp70, sphingolipid metabolism and lysosomal stability. *Cell Cycle* **9**, 2305–2309 (2010).

248. Yoshida, Y. *et al.* Reduction of Acid Sphingomyelinase Activity in Human Fibroblasts Induced by AY-9944 and Other Cationic Amphiphilic Drugs. *J. Biochem* **98**, 1669–1679 (1985).

249. Kornhuber, J. *et al.* Identification of new functional inhibitors of acid sphingomyelinase using a structure-property-activity relation model. *J Med Chem* **51**, 219–237 (2008).

250. Alakoskela, J. M., Vitovič, P. & Kinnunen, P. K. J. Screening for the drug-phospholipid interaction: Correlation to phospholipidosis. *ChemMedChem* **4**, 1224–1251 (2009).

251. Barceló-Coblijn, G. *et al.* Sphingomyelin and sphingomyelin synthase (SMS) in the malignant transformation of glioma cells and in 2-hydroxyoleic acid therapy. *PNAS* **108**, 19569–19574 (2011).

252. Stultz, J. & Fong, L. How to turn up the heat on the cold immune microenvironment of metastatic prostate cancer. *Prostate Cancer Prostatic Dis* **24**, 697–717 (2021).

253. Fossel, E. T., Zanella, C. L., Fletcher, J. G. & Hui, K. K. S. Cell Death Induced by Peroxidized Low-Density Lipoprotein: Endopepsis1. *Cancer Res* **54**, 1240–124 (1994).

254. Xu, H. *et al.* Xanthine oxidase-mediated oxidative stress promotes cancer cell-specific apoptosis. *Free Radic Biol Med* **139**, 70–79 (2019).

255. Bao, J., Liu, B. & Wu, C. The prospects of therapeutic potential and drug development targeting autophagy in cancer. in *Advances in Experimental Medicine and Biology* vol. 1207 663–679 (Springer, 2020).

256. Al-Bari, M. A. A. Co-targeting of lysosome and mitophagy in cancer stem cells with chloroquine analogues and antibiotics. *J Cell Mol Med* **24**, 11667–11679 (2020).

257. DeVorkin, L. *et al.* Autophagy inhibition enhances sunitinib efficacy in clear cell ovarian carcinoma. *Molecular Cancer Research* **15**, 250–258 (2017).

258. Rosenfeld, M. R. *et al.* A phase I/II trial of hydroxychloroquine in conjunction with radiation therapy and concurrent and adjuvant temozolomide in patients with newly diagnosed glioblastoma multiforme. *Autophagy* **10**, 1359–1368 (2014).

259. Medina, P. & Goodin, S. Lapatinib: A Dual Inhibitor of Human Epidermal Growth Factor Receptor Tyrosine Kinases. *Clin Ther* **30**, (2008).

260. Day, K. C. *et al.* HER2 and EGFR overexpression support metastatic progression of prostate cancer to bone. *Cancer Res* **77**, 74–85 (2017).

261. Rubin, I. & Yarden, Y. The basic biology of HER2. *Annals of Oncology* vol. 12 S3–S8 Preprint at (2001).

262. Schechter, A. L. *et al.* The neu oncogene: an erb-B-related gene encoding a 185,000-Mr tumour antigen. *Nature* **312**, 513–516 (1984).

263. Hao, M. *et al.* Autophagy Blockade Limits HER2+ Breast Cancer Tumorigenesis by Perturbing HER2 Trafficking and Promoting Release Via Small Extracellular Vesicles. *Dev Cell* **56**, 341-355.e5 (2021).

264. Henson, E., Chen, Y. & Gibson, S. EGFR family members' regulation of autophagy is at a crossroads of cell survival and death in cancer. *Cancers (Basel)* **9**, (2017).

265. Gravis, G. *et al.* Results from a monocentric phase II trial of erlotinib in patients with metastatic prostate cancer. *Annals of Oncology* **19**, 1624–1628 (2008).

266. Nabhan, C. *et al.* Erlotinib Has Moderate Single-agent Activity in Chemotherapy-naïve Castration-resistant Prostate Cancer: Final Results of a Phase II Trial. *Urology* **74**, 665–671 (2009).